UNIVERSITÀ DEGLI STUDI DI PADOVA

Dipartimento di Fisica e Astronomia "Galileo Galilei"

Master's Degree in Physics

Final Dissertation

The Bispectrum of Axion Perturbations

Thesis supervisor

Prof. Nicola Bartolo

Thesis co-supervisors

Prof. Sabino Matarrese

Dr. Valentina Danieli

Candidate

Chaima Baztami

Academic Year 2024/2025

Mein Amt ist, im ausgeprägten Einmaligen
das Ewige zu gestalten und zu zeigen.

- *Bäume*, Hermann Hesse

Contents

1 Inflation **4**
- 1.1 The Expanding Universe . . . 4
  - 1.1.1 The FLRW metric . . . 4
  - 1.1.2 The Friedmann Equations . . . 5
  - 1.1.3 Cosmological Horizon . . . 7
  - 1.1.4 Hubble Radius . . . 8
- 1.2 Loose Ends of The Hot Big Bang Model . . . 9
  - 1.2.1 The Horizon Problem . . . 9
  - 1.2.2 Flatness Problem . . . 11
  - 1.2.3 Unwanted relics . . . 13
- 1.3 Inflation: The Basics . . . 14
  - 1.3.1 The Inflaton Field . . . 14
  - 1.3.2 Slow-Roll Dynamics . . . 15
  - 1.3.3 Reheating . . . 17
  - 1.3.4 From Quantum Fluctuations to Density Perturbations . . . 18

2 Axion Evolution **20**
- 2.1 Cosmological Setting . . . 20
- 2.2 Axion Evolution . . . 20
- 2.3 Background Evolution . . . 22
- 2.4 First Order Fluctuations . . . 25
  - 2.4.1 Bogoliubov Transformations . . . 27
  - 2.4.2 Mode Functions Evolution . . . 28
- 2.5 Second Order Fluctuations . . . 30

3 Axion Bispectrum **31**
- 3.1 Unveiling The Quantumness . . . 31
- 3.2 Axion Field Bispectrum . . . 32
  - 3.2.1 Quantum Bispectrum . . . 32
  - 3.2.2 Classical Bispectrum . . . 34
- 3.3 Axion Energy Density Bispectrum . . . 40
- 3.4 Field Dynamics Bispectrum . . . 43

4 Conclusions **51**

Abstract

Inflation traces the wealth of structures in the Universe back to quantum fluctuations of the inflaton, the scalar field driving the accelerated expansion during inflation. Compelling as this may be, cosmological data are just as consistent with classical primordial fluctuations. This might be explained by the inflationary mechanism itself: the rapid expansion of the Universe squeezed the inflaton fluctuations. At the level of free fields, squeezed quantum states are observationally indistinguishable from classical probability distributions, so whether interactions remove the ambiguity is a question worth exploring. An ideal setup for this purpose is that of axion-like particles in the early Universe. In this thesis, we consider axions from the misalignment mechanism and explore the possibility that the bispectrum of axion fluctuations may encode information about their quantum nature. We find that the quantum bispectrum is enhanced in the squeezed configuration and always larger near the axion potential maximum, regardless of the geometry of the wave vectors. We also find that the classical bispectrum does not differ from the quantum one due to the absence of time derivatives in the axion self-interactions.

Introduction

According to the standard cosmological model, the Universe underwent a period of quasi-exponential expansion in its early stages, known as inflation. The inflationary paradigm proved very successful in overcoming the drawbacks of the Hot Big Bang model, solving several puzzles of the latter, such as the horizon problem. It also provides a compelling explanation for the origin of cosmic structures: quantum fluctuations of the scalar field driving inflation, the inflaton, were exponentially stretched. These microscopic fluctuations turned macroscopic by the expansion of the Universe provided the seeds for structure formation. However, while inflation assigns a quantum origin to the initial perturbations, the temperature fluctuations we observe in the Cosmic Microwave Background (CMB) are classical. Thus, if the fluctuations started as quantum, some mechanism must have caused their "classicalization". Whether observable traces of the quantum origin remain is an open question. Inflation does offer a possible explanation: the rapid expansion of the Universe puts the fluctuations in a squeezed state, a special quantum state for which the uncertainty in one variable is arbitrarily small. By the uncertainty principle, the conjugate variable has a proportionately large uncertainty, making the state highly quantum. Even so, the quantumness is not observable because the expectation values of physical quantities on a Gaussian squeezed state are indistinguishable from a statistical average of a stochastic distribution. Therefore, fluctuations of free fields appear classical, even though ideas have been put forth to overcome this, such as designing a Bell experiment to perform on the CMB (more details can be found in [3] and [22] - [24]). A natural question then is whether the distinction becomes observationally less challenging for interacting fields. In particular, this thesis considers a self-interacting field in the early Universe.

There is an obstacle to the preservation of quantum features: decoherence through interactions with the environment. Decoherence refers to the loss of quantum superposition and the ensuing properties as the system becomes coupled to the environment, which in the cosmological context coincides with the primordial plasma (for more on this topic, the interested reader can refer to [4] - [7], [10], [17], [20], [21] and [25]). In this respect, axions from the misalignment mechanism coupled to the plasma only through gravitational interactions represent an interesting case study because they could evade decoherence. Indeed, the misalignment mechanism is a non-thermal production mechanism and, as such, does not require the axion to be in thermal equilibrium with the primordial plasma. Axions are produced from an initial displacement of the field from the minimum of its potential. Moreover, since the axion potential is periodic, it allows for self-interactions. These, however, switch off in the late Universe, when the axion settles stably in its minimum. This is a further advantage of considering axions: the fact that they behave as free particles in the asymptotic future allows one to rely on the Bogoliubov formalism to compute the evolution of the fluctuations. We will consider the scenario where the Peccei-Quinn symmetry is broken before inflation, as opposed to during thermal evolution of the Universe. In the first case, computing the axion field evolution is simpler because inflation smooths the field leaving only small-amplitude fluctuations that can be studied within perturbation theory.

This thesis builds upon [9], which analyses the effects of self-interactions on the squeezing of axion fluctuations at the background level, and pursues the ideas presented in [12]. The latter work explores the possibility of distinguishing between quantum and classical fluctuations by means of the three-point function, or bispectrum in Fourier space. The quantum bispectrum is associated with the creation of virtual particles from the vacuum, a concept with no classical counterpart. Classical fluctuations are local variations of the particle density due to the presence of physical particles whose evolution is governed by causal physics. Hence, the creation of particles in the final state implies the decay

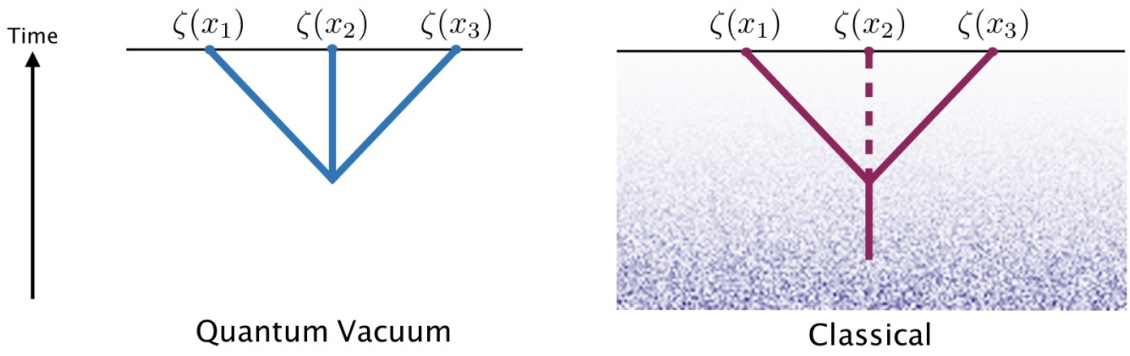

Figure 1: Pictorial representation of the processes producing the bispectrum signal in the quantum and classical case. *Left:* Particle creation from the vacuum. *Right*: 2-body decay of a physical particle. Picture taken from [12].

of a particle in the initial state, as illustrated in Figure 1. These processes manifest as poles in the bispectrum. It should be pointed out that only the absence of these poles provides univocal information: their presence can be accounted for by both classical fluctuations and highly excited quantum states. However, only quantum vacuum fluctuations can explain their absence. We pursue this idea by computing the bispectrum of axion fluctuations in a quantum and classical set-up.
The thesis is organized in three main chapters. In the first one, we review the inflationary paradigm: we consider how it addresses the shortcomings of the Hot Big Bang model, its main features and the connection it draws between primordial density perturbations and quantum fluctuations. The second chapter is devoted to analyzing the evolution of the axion field. We first decompose the field into a homogeneous background and a perturbation, then compute their evolution for different initial displacement angles by numerically solving the respective equations of motion. The perturbation must include contributions up to second order to yield a non-vanishing bispectrum, since that is the order at which non-Gaussianity first appears. The third chapter constitutes the core of the thesis and is where we compute the bispectrum of axion perturbations. We first outline the idea presented in [12] of using higher-order correlators to probe the quantum nature of the fluctuations. We then proceed to compute the bispectrum of the axion field fluctuations in both the quantum and the classical set-up. Finally, we turn to the bispectrum of the axion energy density perturbations.

Chapter 1

Inflation

This first chapter introduces basic concepts and definitions from the study of the early universe that are necessary to discuss the topics of the thesis and briefly reviews the inflationary paradigm. Both these essential notions and the much broader subject of inflationary cosmology are discussed extensively in many textbooks. In particular, this chapter draws mainly from [11], [14] and [16].

1.1 The Expanding Universe

1.1.1 The FLRW metric

The most successful theory of gravity at present is Einstein's general relativity, praised not only for the impressive number of tests it passed with flying colors but also for its sheer beauty. Despite being the weakest force in nature, gravity quite literally shapes the universe. In fact, according to general relativity, time and space are woven into the same fabric, forming the backdrop of any physical process. This fabric responds to the presence of a body that exerts gravity by bending around it. Thus, Einstein's theory relates the geometry of spacetime to its matter and energy content, investing the former with a new physical meaning. The geometry of spacetime is encoded in the metric tensor $g_{\mu\nu}$, usually defined via the invariant line element:

$$ds^2 = g_{\mu\nu} dx^\mu dx^\nu. \tag{1.1}$$

The metric tensor describing our Universe must capture two important features which are firmly grounded in observations: 1) the Universe is undergoing an accelerated expansion and 2) it appears *homogeneous* and *isotropic* on sufficiently large scales. This latter point is known as the *cosmological principle* and implies that the Universe looks the same from all points (homogeneity) and in all directions (isotropy), *at the appropriate length scales*. Such distances are much larger than the size of the Solar System, which clearly does not appear homogeneous and isotropic. In fact, the validity of the cosmological principle requires distances of the order of hundreds of Mpc, with $1\,\mathrm{Mpc} \approx 3 \times 10^{16}\,\mathrm{m}$, which is far larger than even the diameter of our galaxy, the Milky Way (about 30 kpc). In terms of mathematical symmetries, homogeneity and isotropy correspond to invariance under spatial translations and rotations, respectively. The most generic metric tensor compatible with this picture is the Friedmann-Lemaître-Robertson-Walker (FLRW) metric:

$$ds^2 = -dt^2 + a^2(t) \left[\frac{dr^2}{1 - \kappa r^2} + r^2 d\Omega^2 \right], \tag{1.2}$$

where $d\Omega^2 = d\theta^2 + \sin^2(\theta) d\phi^2$. The coordinates (r, θ, ϕ) are referred to as *comoving coordinates* and t, the *cosmic time*, is the proper time measured by an observer at rest in the comoving frame, i.e. an observer for whom $dr = d\Omega = 0$. The comoving coordinates are called so because they do not change in time and the stretching of physical distances due to the expansion is encoded in the scale factor $a(t)$, so that $r_{phys}(t) = a(t) r_{com}$. Finally, the curvature κ is related to the geometry of the Universe:

upon appropriately rescaling the coordinates, κ takes on one of three possible values, $-1, 0$ or 1. The first possibility corresponds to the geometry of a hyperboloid, where the internal angles of a triangle add up to less than 180°. For $\kappa = 0$ we recover the familiar Euclidean geometry, where they add up to exactly 180°, and the last logical possibility, a sum greater than 180°, is the case $\kappa = 1$, which can be modeled by a sphere. Clearly, in all of these instances, the constant t sections of (1.2) are homogeneous and isotropic. Throughout this thesis, we will always consider $\kappa = 0$, which is also supported by a large body of observations. We will see that accounting for the apparent flatness of the Universe is one of the successes of inflation. As suggested by the denominator $1 - \kappa r^2$, r is dimensionless in this parameterization of the line element, while the scale factor carries units of length.

1.1.2 The Friedmann Equations

The equations that govern the dynamics of the expanding universe can be derived using the machinery of general relativity. The latter is based on the Einstein field equations:

$$R_{\mu\nu} - \frac{1}{2} g_{\mu\nu} R = 8\pi G T_{\mu\nu}. \tag{1.3}$$

$R_{\mu\nu}$ is the Ricci tensor and is obtained from the Riemann tensor $R^{\lambda}{}_{\sigma\mu\nu}$ by contracting the first and third indices, $R_{\mu\nu} = R^{\rho}{}_{\mu\rho\nu}$. The Riemann tensor is in turn given by:

$$R^{\lambda}{}_{\sigma\mu\nu} = \partial_\mu \Gamma^{\lambda}{}_{\sigma\nu} - \partial_\nu \Gamma^{\lambda}{}_{\sigma\mu} + \Gamma^{\lambda}{}_{\mu\rho}\Gamma^{\lambda}{}_{\nu\sigma} - \Gamma^{\lambda}{}_{\nu\rho}\Gamma^{\lambda}{}_{\mu\sigma}. \tag{1.4}$$

Here, $\Gamma^{\mu}{}_{\nu\lambda}$ are the Christoffel symbols, built out of the metric tensor according to:

$$\Gamma^{\mu}{}_{\nu\lambda} = \frac{1}{2} g^{\mu\rho} \left(\frac{\partial g_{\rho\nu}}{\partial x^\lambda} + \frac{\partial g_{\rho\lambda}}{\partial x^\nu} + \frac{\partial g_{\nu\lambda}}{\partial x^\rho} \right). \tag{1.5}$$

$R = R^{\mu}{}_{\mu}$ is the Ricci scalar, G Newton's constant and $T_{\mu\nu}$ is the energy-momentum tensor describing the sources of gravity. The left-hand side of (1.3) is often written as a single tensor, $G_{\mu\nu}$, known as the Einstein tensor. $G_{\mu\nu}$ satisfies the Bianchi identity, i.e. its covariant derivative vanishes, $\nabla_\mu G^{\mu\nu} = 0$, which, via Einstein's equations, is equivalent to the continuity equation for the energy-momentum tensor, $\nabla_\mu T^{\mu\nu} = 0$. The Einstein equations can be derived by applying the variational principle with respect to the metric to the action $S_{TOT} = S_{EH} + S_m$, where

$$S_{EH} = \int d^4x \sqrt{-g} \frac{R}{16\pi G} \tag{1.6}$$

is the Einstein-Hilbert action accounting for gravity and g is the determinant of the metric tensor. The factor $\sqrt{-g}$ ensures general covariance of the integral measure. S_m instead is the action accounting for all sources of matter and radiation:

$$S_m = \int d^4x \sqrt{-g} \mathcal{L}_m, \tag{1.7}$$

where $\mathcal{L}_m$ is the corresponding Lagrangian density.
To make use of the Einstein equations we must find an appropriate expression for $T_{\mu\nu}$ given the properties of our Universe. By the cosmological principle, the off-diagonal components of the stress-energy tensor must be vanishing, and the spatial diagonal components must be equal. The simplest form for $T_{\mu\nu}$ compatible with these requirements is that of a perfect fluid having density ρ and pressure p:

$$T^{\mu}{}_{\nu} = \mathrm{diag}(-\rho, p, p, p), \tag{1.8}$$

The 00 and the ij components of the Einstein equations with (1.8) as stress-energy tensor yield:

$$H^2 = \frac{8\pi G}{3} \rho, \tag{1.9}$$

$$\frac{\ddot{a}}{a} = -\frac{4\pi G}{3} (\rho + 3p) \tag{1.10}$$

respectively. These are known as the *Friedmann equations*. Here, the dot indicates a derivative with respect to cosmic time and the Hubble parameter $H \equiv \dot{a}/a$ measures the expansion rate of the Universe. From the continuity equation, we have:

$$\dot{\rho} + 3H(\rho + p) = 0. \tag{1.11}$$

The two Friedmann equations and (1.11) are not independent. In fact, differentiating (1.9) with respect to cosmic time and using $\dot{\rho} = -3H(\rho + p)$, we recover (1.10). Therefore, we have only two independent equations to solve for three unknowns: $a(t)$, $\rho(t)$ and $p(t)$. To close the system, we introduce an additional relation connecting the density and the pressure, known as *equation of state*. The simplest parametrization for this relation is $p = w\rho$, with w constant. Hence, (1.11) becomes:

$$\mathrm{d}(\ln \rho) = -3\mathrm{d}(\ln a)\,(1 + w)\,, \tag{1.12}$$

whose solution is:

$$\frac{\rho}{\rho_*} = \left(\frac{a}{a_*}\right)^{-3(1+w)}. \tag{1.13}$$

The $*$ corresponds to some reference time. The value of w varies depending on the nature of the fluid: $w = 0$ is the equation of state for so-called pressureless matter, i.e. a fluid whose pressure is negligible compared to its energy density. In this case, ρ decreases with a^3, the same factor by which volumes increase due to the expansion of the Universe. In other words, the energy per unit volume is diluted as the volume grows. This is the case of non-relativistic matter. $w = 1/3$ describes a fluid of relativistic particles. In this case, $\rho \propto a^{-4}$ because, in addition to the dilution effect, the energy is red-shifted a a^{-1}. An interesting case is that of $w = -1$, which leads to a constant energy density. This is the equation of state of a *cosmological constant* and is interesting in relation to the so-called *dark energy*, the component driving the current accelerated expansion of the Universe. In fact, the simplest realization of dark energy is a cosmological constant. The field equations (1.3) predict either an expanding or a contracting universe. In order to recover a static universe, Einstein added by hand a cosmological constant Λ:

$$R_{\mu\nu} - \frac{1}{2}g_{\mu\nu}R = 8\pi G T_{\mu\nu} + \Lambda g_{\mu\nu}. \tag{1.14}$$

In Einstein's understanding, the negative pressure ($w = -1$ implies $p < 0$) exerted by this component would balance the pull of gravity and this poise of forces would prevent the Universe from expanding or contracting. Notice that, in the vacuum, $T_{\mu\nu}$ vanishes and the Einstein equations read:

$$R_{\mu\nu} - \frac{1}{2}g_{\mu\nu}R = \Lambda g_{\mu\nu}. \tag{1.15}$$

from which we see that $\Lambda g_{\mu\nu}$ can be likened to an energy-momentum tensor of the vacuum and Λ to an energy of the vacuum. The cosmological constant appears also in Quantum Field Theory, which indeed predicts its presence, but with an energy density far exceeding the measured one. In fact, a vacuum energy as large as that allowed by QFT would be strongly at variance with the existence of cosmic structures because it would cause too rapid an expansion for them to form. The Friedmann equations in the presence of a cosmological constant read:

$$H^2 = \frac{8\pi G}{3}\rho + \frac{\Lambda}{3}, \tag{1.16}$$

$$\frac{\ddot{a}}{a} = -\frac{4\pi G}{3}(\rho + 3p) + \frac{\Lambda}{3}. \tag{1.17}$$

Given the scalings we found and the fact that $a(t)$ decreases going back in time, it is clear that radiation dominates the energy content of the Universe early on. As the Universe evolves, radiation is superseded by matter as the dominant component of the cosmic fluid, while dark energy, with its constant density, is negligible in the early Universe but bound to impose itself on both matter and

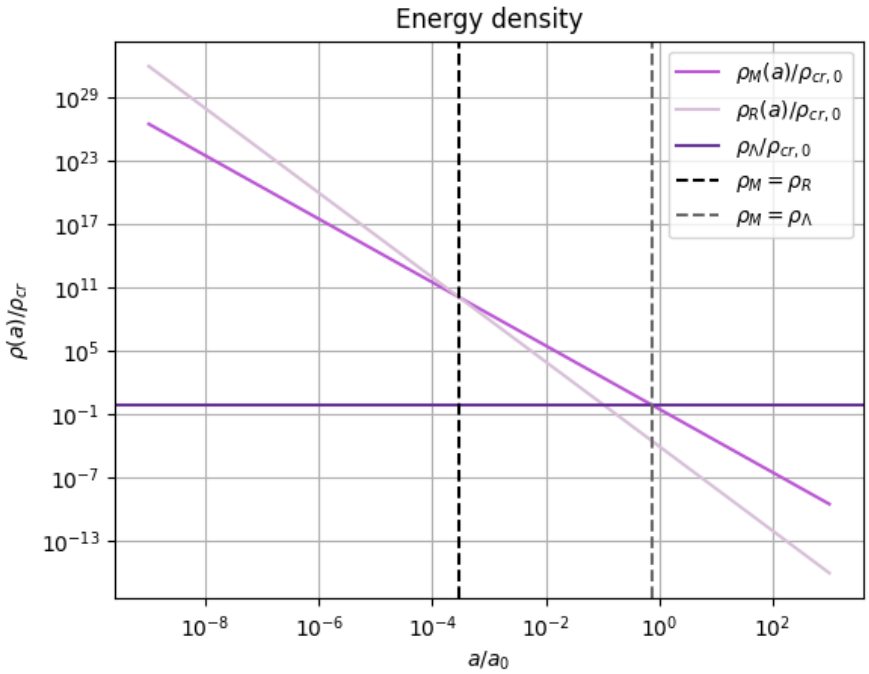

Figure 1.1: Time evolution of the energy densities of radiation, non-relativistic matter and dark energy in terms of the scale factor normalized to its currents value. The densities have been divided by the critical density today. The critical density is the total energy density of a geometrically flat universe. The vertical lines indicate the times when the energy density of non-relativistic matter was equal to that of radiation (black line) and that of dark energy (gray line). The values of measured quantities necessary for this figure were taken from [1].

radiation as they red-shift. In fact, dark energy is by far the dominant component of the current Universe and, even though it seems to behave as a cosmological constant, the question of what makes it up remains fully open. The time evolution of the energy density for radiation, pressureless matter and dark energy is shown in Figure 1.1. Notice how recent dark energy domination is.
Once $\rho(a)$ is known, (1.9) can be used to solve for $a(t)$. For $w \neq -1$, we have:

$$a(t) = a_* \left(\frac{t}{t_*}\right)^{\frac{2}{3(1+w)}}, \tag{1.18}$$

while $w = -1$ yields an exponential growth of the scale factor, $a(t) \propto e^{Ht}$, with H constant.

1.1.3 Cosmological Horizon

How distant can a source be for its light to have had enough time to reach us in the lifetime of the Universe? The answer to this question is known as *cosmological horizon*, the maximum distance over which two systems are in causal contact with each other. To derive it, consider a photon emitted by some source and let the position of the latter coincide with the origin of our coordinates. Notice that we are free to choose any point as origin because of homogeneity. Moreover, if the photon can propagate unperturbed, it will follow a purely radial trajectory. This is because the photon starts at $r = 0$ and for any straight line passing through the origin, both θ and ϕ are constant. In other words, the null geodesics $ds^2 = 0$ are radial trajectories. Which direction we choose is also arbitrary by isotropy. Thus, we have:

$$dt = \pm a(t) f(r) dr, \tag{1.19}$$

where:

$$f(r) = \frac{1}{\sqrt{1 - \kappa r^2}}. \tag{1.20}$$

The appropriate sign to choose is + because the radial coordinate of the photon is increasing. Hence, if the photon is received at time t and has traveled a comoving distance r from the origin, we have:

$$\int_0^t \frac{dt'}{a(t')} = \int_0^r dr' f(r'). \tag{1.21}$$

Since r' is a comoving coordinate, the physical cosmological horizon is given by:

$$d_H(t) = a(t) \int_0^t \frac{dt'}{a(t')} = a(t) l, \tag{1.22}$$

where l is the comoving horizon. Notice that $d_H(t)$ might not be finite. In fact, from (1.18) we have:

$$d_H(t) = t^{\frac{2}{3(1+w)}} \int_0^t dt' (t')^{\frac{-2}{3(1+w)}}, \tag{1.23}$$

but the improper integral $\int_0^c dx x^{-\alpha}$ converges only if $\alpha < 1$. Hence, the convergence of $d_H(t)$ requires $w > -1/3$, in which case:

$$d_H(t) = \frac{3(1+w)}{1+3w} t. \tag{1.24}$$

When finite, the cosmological horizon is also referred to as *particle horizon.*

1.1.4 Hubble Radius

Another distance one can define in cosmology is the *Hubble radius*, given by:

$$R_C(t) = \frac{1}{H(t)}, \tag{1.25}$$

which can be related to the horizon $d_H(t)$ using (1.18):

$$R_C(t) = \frac{3}{2}(1+w)t = \frac{1+3w}{2} d_H(t). \tag{1.26}$$

The inverse of the Hubble parameter, $\tau_H = 1/H$, is known as *Hubble time* and represents the characteristic timescale of the expansion. Over a Hubble time, the scale factor roughly doubles. In fact, for $w \neq -1$, (1.18) yields $\tau_H = \frac{3(1+w)}{2} t$, so that:

$$a(t+\tau_H) = a\left(\frac{(5+3w)t}{2}\right) = a(t)\left(\frac{5+3w}{2}\right)^{\frac{2}{3(1+w)}}. \tag{1.27}$$

Thus, if $w = 0$ $a(t)$ increases by a factor 1.8 over a Hubble time, if $w = 1/3$ by a factor $\sqrt{3}$. In the case of a cosmological constant, $a(t) \propto \exp(Ht)$ and the scale factor increases by a factor e after a time $1/H$. Notice that the Hubble radius corresponds to the maximum distance of a source whose light can reach us over a Hubble time, whereas in defining the cosmological horizon we considered the entire age of the Universe. Therefore, even though the particle horizon and the Hubble radius are related and are often used interchangeably, they are conceptually different. When the word horizon is used in relation to the range of causal physics, the Hubble radius is usually meant. As for the cosmological horizon, we can define a *comoving Hubble radius*, given by:

$$r_H(t) = \frac{R_C(t)}{a(t)} = \frac{1}{\dot{a}(t)} = \frac{1}{a(t)H(t)}, \tag{1.28}$$

which we can also relate to the comoving horizon:

$$\frac{d_H(t)}{a(t)} = \int_0^t \frac{dt'}{a(t')} = \int_0^a d\ln a' \frac{1}{\dot{a}'} = \int_0^a d\ln a' r_H. \tag{1.29}$$

The comoving horizon is the logarithmic integral of the comoving Hubble radius.

1.2 Loose Ends of The Hot Big Bang Model

In hindsight, one of the most compelling features of inflation is that it may provide an explanation for the primordial density perturbations at the origin of cosmic structures. Historically, however, this is not the question inflation was introduced to address. The Hot Big Bang Model is able to account for the evolution of the Universe from as early as fractions of a second after the Big Bang to today. Perhaps its most celebrated success is primordial nucleosynthesis. We know that the nuclear activity of stars alone cannot explain the observed abundances of light nuclei, such as deuterium and helium-4. Big Bang nucleosynthesis (BBN) refers to an early period of light nuclei formation, between 0.01 and 100 seconds after the Big Bang, and predicts abundances for these light elements that agree really well with the observations. Thus, the Hot Big Bang model is a rather successful framework in itself, but there are features of the Universe that require finely tuned initial conditions to be explained within this framework, hinting at the possibility of a more encompassing theory. Inflation was put forth by Alan Guth in the 1980's [13] precisely to address these shortcomings. In this section, we present the puzzles that motivated the introduction of inflation and how they are solved.

1.2.1 The Horizon Problem

We begin by discussing the so-called *horizon problem*. To elucidate why this is a puzzle, let us first notice that the Hubble radius we defined in the previous section, $r_H(t)$, is an increasing function of time if $\ddot{a} < 0$:

$$\dot{r}_H(t) = \frac{-\ddot{a}(t)}{\dot{a}^2(t)}. \tag{1.30}$$

From (1.10), we see that a decelerating expansion requires $w > -1/3$. Hence, in a universe containing only non-relativistic matter and radiation, r_H would grow in time, so that larger and larger scales become accessible for causal connections. Notice that the cosmological constant instead yields $\ddot{a} > 0$. As we have already mentioned, the cosmological constant is a possible, although problematic, realization of dark energy, the component responsible for the current accelerated expansion of the Universe. However, dark energy only came to dominate the dynamics of the Universe in its most recent evolution and is not relevant for the horizon problem. This is because the horizon problem really strikes one as a problem when considering the *Cosmic Microwave Background* (CMB). The early Universe contained an extremely hot and dense plasma in which particles were kept coupled to each other by frequent interactions. As the expansion of the Universe progressed, the temperature and density gradually dropped, and the various particle species present decoupled from the plasma in different stages. In particular, when photons and electrons decoupled, the latter, along with protons, were able to form the first neutral hydrogen atoms (this is known as *recombination*) and the photons became free to propagate through the Universe. In fact, until then the Universe had been opaque and no radiation from earlier times can be directly observed today. These photons make up the CMB. Every observer is reached from all directions by a flux of photons emanating from a thin surface, known as *last scattering surface*, centered on the observer and located at about $6000\,h^{-1}\,\mathrm{Mpc}$, with $h = H_0/(100\,\mathrm{km\,s^{-1}Mpc^{-1}})$. This is the distance covered by a photon that started propagating at recombination and reaches the observer today. The CMB displays an almost perfect black-body spectrum peaked at a temperature of about 2.7 K first measured by FIRAS in the early nineties as part of the COBE mission. In Figure 1.2, the FIRAS data are compared with an actual 2.7 K black-body spectrum. Impressively, the error bars had to be multiplied by 400 to make them visible, which really conveys how closely the data track the black-body curve. What is puzzling about the CMB is the near exact isotropy of its temperature: the peak temperature of the black-body is the same in all directions up to fluctuations of one part in 10^5. It is by no means surprising for systems in contact with each other to thermalise to the same temperature, but CMB photons last scattered off electrons when the Universe was about 300,000 years old (it is 14 billion years old today!) and have not interacted ever since. In particular, the distance between CMB photons reaching the observer from opposite directions of the sky, known as the *quadrupole scale*, is comparable to the horizon today. Thus, the Universe has simply not existed long enough for these photons to interact and reach the same temperature. Since the properties of the CMB reflect those of the early universe, asking why is the CMB temperature

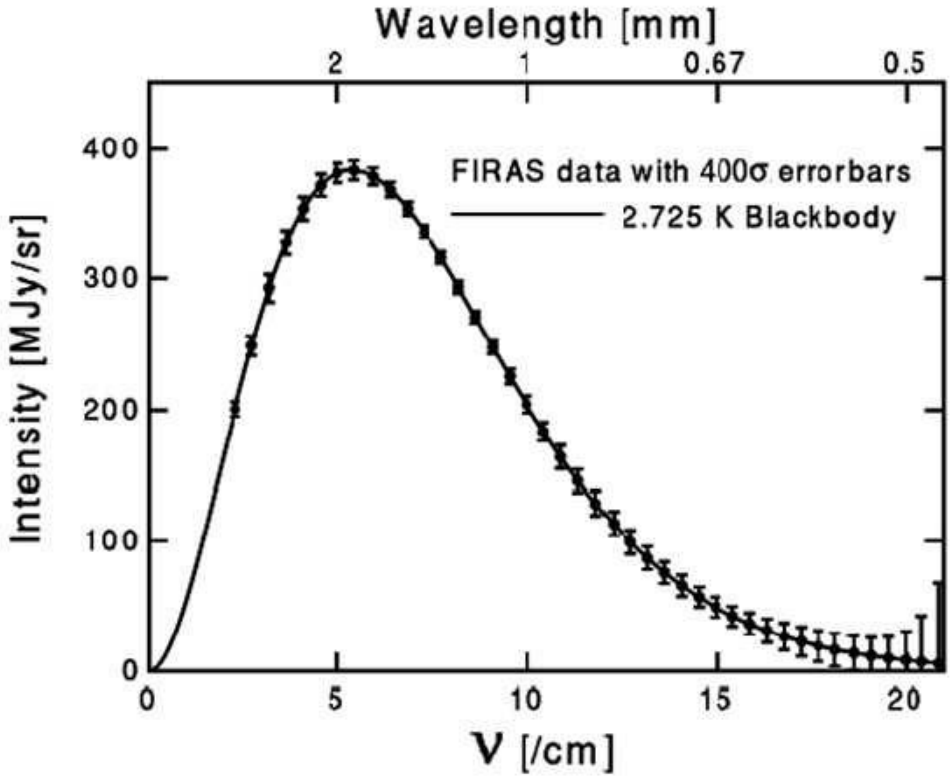

Figure 1.2: CMB measurements collected by the FIRAS instrument as part of the COBE mission, launched in 1989. The error bars were multiplied by 400 to make them visible. Picture taken from [29].

so uniform is equivalent to asking why is the Universe so homogeneous and isotropic. Of course, one could postulate these features as initial conditions, but, as we will see, inflation actually provides a dynamical explanation for the smoothness of the Universe on large scales. Inflation is an early period of accelerated expansion during which the scale factor grew exponentially in time. Since during inflation $\ddot{a} > 0$, $\dot{r}_H < 0$. The scales r_H crosses while decreasing become temporarily larger than the range of causal interactions until r_H crosses them again after inflation, when it resumes growing. At that point, they re-enter the causal patch. The quadrupole scale is re-entering the horizon today, as it is comparable to the size of the observable universe. If inflation happened under the appropriate conditions, the quadrupole scale was smaller than the horizon at the beginning of inflation, placing two photons from opposite directions of the CMB sky in causal contact at that time. This would explain the isotropy of the CMB. The natural question then is: how much expansion is required to solve the horizon problem? For an order of magnitude estimate, let us assume that the Universe has been radiation-dominated since the end of inflation. Then, $H \propto a^{-2}$ and:

$$a_0^2 H_0 = a_f^2 H_f, \tag{1.31}$$

where the left-hand is evaluated today and the right-hand side at the end of inflation. The energy of the radiation-dominated plasma is determined by its temperature, and, since the energy red-shifts as a^{-1}, we have $T \propto a^{-1}$, or:

$$a_0 T_0 = a_f T_f. \tag{1.32}$$

Thus:

$$\frac{a_0 H_0}{a_f H_f} = \frac{a_f}{a_0} = \frac{T_0}{T_f}. \tag{1.33}$$

For T_0 we take the CMB temperature $T_{\rm CMB} \approx 2.7\,{\rm K} \approx 10^{-4}\,{\rm eV}$, while a typical energy scale for inflation is $T_f \approx 10^{15}\,{\rm GeV}$. Hence, the comoving Hubble radius today is 28 orders of magnitude larger than what it was at the end of inflation. For inflation to solve the horizon problem, the largest scales accessible to observations today must have been within the horizon when the Universe began to

expand. The simplest realization of inflation is a so-called de-Sitter expansion, in which the Hubble parameter is taken to be constant:

$$a(t) = a_f e^{H_f(t-t_f)}, \tag{1.34}$$

with $t < t_f$. To solve the horizon problem, we require that the Hubble radius today is smaller than the radius at the beginning of inflation:

$$\frac{a_0 H_0}{a_i H_f} > 1, \tag{1.35}$$

where a_i is the scale factor at the beginning of inflation and we are using the fact that H is constant all throughout inflation in a de-Sitter expansion, so that $H_i = H_f$. From what we found before, $a_0 H_0 \approx 10^{-28} a_f H_f$, leading to $a_f/a_i > 10^{28}$. Since the growth of the scale factor is exponential, this result is usually expressed in terms of the number of e-folds, $\ln(a_f/a_i)$. For inflation to solve the horizon problem, it must have lasted more than $\ln(10^{28}) \approx 64$ e-folds. Let us close with a visual rendition of how inflation solves the horizon problem. We first introduce the following variable:

$$d\chi = \frac{1}{\sqrt{1-\kappa r^2}} dr, \tag{1.36}$$

and the conformal time $d\tau = dt/a(t)$, in terms of which the FLRW metric line element reads:

$$ds^2 = a^2(\tau)\left[-d\tau^2 + d\chi^2 + r^2(\chi) d\Omega^2\right], \tag{1.37}$$

with $r(\chi)$ given by:

$$\begin{cases} \sinh\chi & \kappa = -1 \\ \chi & \kappa = 0 \\ \sin\chi & \kappa = 1. \end{cases} \tag{1.38}$$

This way, for $\kappa = 0$, (1.37) is a conformal transformation of the Minkowski metric tensor. As we have already observed, the null geodesics correspond to $d\tau = \pm d\chi$, i.e. lines of slope $\pm$ in the (χ, τ) plane. A visualization of the problem is shown in Figure 1.3: the green lines are null geodesics, P and Q are points on the last scattering surface, and the two dashed horizontal lines correspond to $\tau = 0$ and today. The standard cosmological model places the Big Bang at $\tau = 0$, so that, if P and Q are sufficiently apart, the photons never had time to interact. In fact, following their geodesics back in time, they cross the Big Bang singularity before intersecting. Instead, with inflation, the singularity is pushed to $-\infty$, allowing a time in the past during which the photons at P and Q were in causal contact.

1.2.2 Flatness Problem

The next loose end of the Big Bang model to discuss is the flatness problem. The starting point is the first Friedmann equation for generic κ :

$$H^2 = \frac{8}{3}\pi G\rho - \frac{\kappa}{a^2}. \tag{1.39}$$

The energy densities of radiation and non-relativistic matter scale as a^{-4} and a^{-3} respectively, so, while the curvature term is negligible at early times, it eventually dominates later on. To better understand this, we divide the first Friedmann equation by H^2 and define the critical density $\rho_{\rm cr} \equiv 3H^2(t)/M_{\rm Pl}^2$, where $M_{\rm Pl} = \sqrt{8\pi G}$ is the reduced Planck mass. We have:

$$\frac{\rho(t)}{\rho_{\rm cr}(t)} - 1 = \frac{\kappa}{H^2(t)a^2(t)} = \kappa r_H^2(t). \tag{1.40}$$

The ratio $\Omega \equiv \rho/\rho_{\rm cr}$ is known as *density parameter*. An analogous parameter is defined also for the curvature term:

$$\Omega_\kappa = -\frac{\kappa}{a^2 H^2}, \tag{1.41}$$

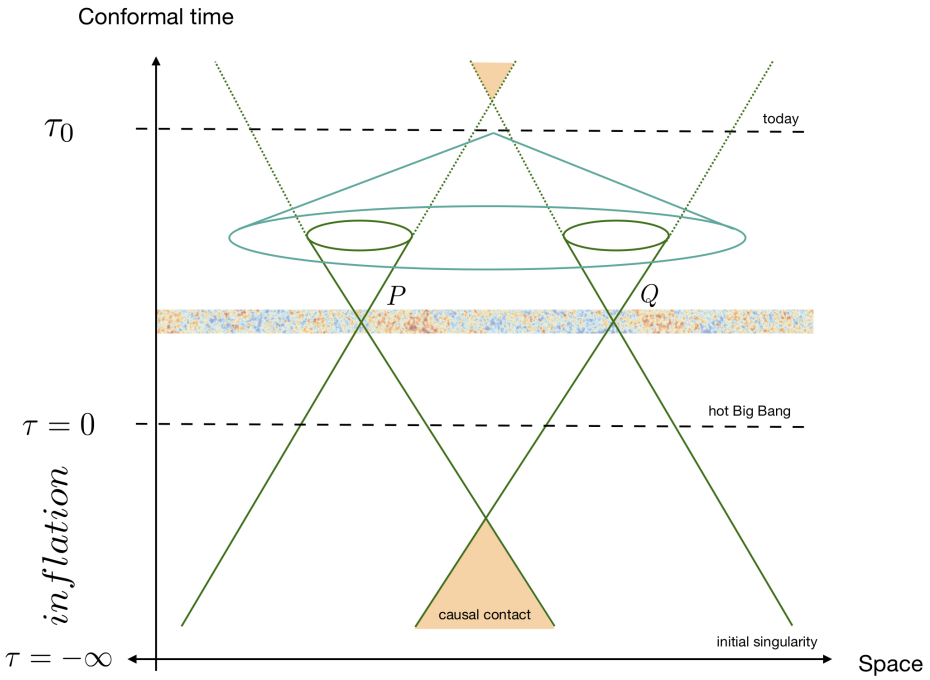

Figure 1.3: Depiction of the inflationary solution to the horizon problem. P and Q are points on the last scattering surface, chosen so that they are causally disconnected today. By moving the singularity to $\tau = -\infty$, inflation allows a time in the past when photons at P and Q were in causal contact. Picture taken from [27].

so that $\Omega + \Omega_\kappa = 1$. Notice that the critical density is the value of ρ for which the Universe has $\kappa = 0$. If $\rho > \rho_{\rm cr}$, the curvature is positive, while $\rho < \rho_{\rm cr}$ leads to $\kappa < 0$. As we have seen, the comoving Hubble radius grows in time if the Universe contains only radiation and pressureless matter. Thus, even if the curvature term is negligible at early times and Ω is close to 1, the growth of r_H is bound to drive the density parameter away from 1, provided $\kappa \neq 0$. We know from cosmological data that today $|\Omega(t_0) - 1| < 10^{-3}$, so this number must have been even smaller back in time. Once again, we could just assume that the density parameter was initially so close to unity that over the entire lifetime of the Universe only a small departure of 10^{-3} from 1 was possible. How close to $\Omega = 1$ must the initial condition be? Let us consider times in the past and attempt to estimate how small $|\Omega_\kappa(t)| = |\Omega(t) - 1|$ was based on its current value. Now, equation (1.18) for the time dependence of the scale factor was derived neglecting the curvature term. Since we are interested in the value of $\Omega_\kappa(t)$ at early times, when the energy density dominates the right-hand side of the Friedmann equation (1.9), we can take (1.18) to hold. A further approximation we make is to consider the present-day Universe as matter dominated, neglecting the fairly recent transition to dark energy domination. During matter domination, $H \propto a^{-3/2}$, so that:

$$a(t)H(t) = a_0 H_0 \left(\frac{a_0}{a(t)}\right)^{1/2}, \tag{1.42}$$

where the subscript 0 indicates that a and H are evaluated today and t is some time during matter domination. We take $t = t_{\rm eq}$, the time of equality between the energy density of radiation and that of pressureless matter, which marks the end of radiation domination. The ratio $a_0/a_{\rm eq}$ can be expressed in terms of the redshift z, defined as:

$$1 + z_{\rm eq} = \frac{\nu(t_{\rm eq})}{\nu(t_0)}, \tag{1.43}$$

where $\nu(t)$ is the frequency. If we imagine a photon emitted at the time of equality with frequency $\nu(t_{\rm eq})$, an observer receiving it today would measure a frequency $\nu(t_0) < \nu(t_{\rm eq})$ because the photon propagated through an expanding Universe. Since the wavelength is stretched by a factor $a(t)$, the

frequency of the photon decreases by the same factor, $\nu(t) \propto a^{-1}(t)$. Therefore:

$$\frac{\nu(t_{\rm eq})}{\nu(t_0)} = \frac{a(t_0)}{a(t_{\rm eq})}. \tag{1.44}$$

$\Omega_\kappa(t_{eq})$ is then:

$$\frac{-\kappa}{(a(t_{\rm eq})H(t_{\rm eq}))^2} = \Omega_\kappa(t_0)(1+z_{\rm eq})^{-1}, \tag{1.45}$$

from which we see that $|\Omega_\kappa|$ is further suppressed by a factor $(1+z_{\rm eq})^{-1} \approx 1/3330$ at the time of matter-radiation equality. Before $t_{\rm eq}$ the Universe was dominated by the relativistic component of ρ, so to extrapolate Ω_κ to even earlier times we use:

$$a(t)H(t) = a(t_{\rm eq})H(t_{\rm eq})\left(\frac{a_{\rm eq}}{a(t)}\right). \tag{1.46}$$

Now t is a time before matter-radiation equality and we have leveraged the fact that during radiation domination $H \propto a^{-2}$. This leads to:

$$\frac{-\kappa}{(a(t)H(t))^2} = \Omega_\kappa(t_{\rm eq})\left(\frac{a(t_{\rm eq})}{a(t)}\right)^{-2}. \tag{1.47}$$

As we did in the previous section, we trade a for T since we are in radiation domination. The temperature of the plasma at equality was $T_{\rm eq} \approx 1\,{\rm eV}$ and if we extrapolate Ω_κ back to Big Bang nucleosynthesis, $T_{\rm eq}$ must be compared with $T_{\rm BBN} \approx 1\,{\rm MeV}$. Thus, $|\Omega_\kappa|$ is further suppressed by a factor 10^{-12}. We asked how close the initial condition must be to $\Omega = 1$ to explain the smallness of Ω_κ today and the answer is uncomfortably fine-tuned. Once again, inflation removes the need of unlikely initial conditions by providing a dynamical explanation for the current state of the Universe. Since $|\Omega_\kappa| = \kappa r_H^2$ and the Hubble radius decreases during inflation, $|\Omega_\kappa|$ will be smaller at the end of inflation compared to its value at the beginning. To appreciate how effective this suppression can be, let us assume that $|\Omega_\kappa|$ was an order one number when the Universe started to expand. If inflation begins at time t_i and ends at t_f, we have:

$$a_i = a_f e^{H_{inf}(t_i - t_f)}, \tag{1.48}$$

where we are assuming again a de-Sitter expansion with constant Hubble parameter H_{inf}. The curvature density parameter at the end of inflation is then:

$$\frac{\kappa}{(a_f H_{inf})^2} = \frac{\kappa}{(a_i H_{inf})^2} e^{2H_{inf}(t_i - t_f)} \approx e^{2H_{\rm inf}(t_i - t_f)}, \tag{1.49}$$

where in the last step we used our assumption of Ω_κ being close to unity at t_i to approximate it with 1. The remaining term is simply $(a_i/a_f)^2$. In the previous section, we found that inflation can solve the horizon problem only if $a_f/a_i > 10^{28}$, which for $|\Omega_\kappa|$ implies:

$$\frac{\kappa}{(a_f H_{inf})^2} = \left(\frac{a_i}{a_f}\right)^2 < 10^{-56}. \tag{1.50}$$

which is very small indeed. So if inflation lasts a sufficient number of e-folds to solve the horizon problem, it can also explain why we measure such a small Ω_κ today, or, equivalently, why the total energy density of the Universe is so close to the critical density. Even if Ω_κ is initially non-negligible, inflation suppresses it exponentially and even if in the post-inflationary universe Ω evolves away from 1, inflation will have driven it so close to unity that we still measure a very small Ω_κ to this day.

1.2.3 Unwanted relics

The last shortcoming of the Hot Big Bang model we briefly mention was also one of the main motivations for inflation and arises in the context of unified gauge theories. These involve the spontaneous breaking of a gauge group into a smaller symmetry group, in analogy with the electroweak phase

transition of the Standard Model. A symmetry is said to be spontaneously broken when the system transitions to a minimum that violates the symmetry, but the Lagrangian of the theory still satisfies it. In the case of the Standard Model, the symmetry group of the unified electroweak sector, $SU(2)_L \times U(1)_Y$, breaks into the symmetry group of electromagnetism, $U(1)_{\text{em}}$, when the Higgs boson settles in one of the infinitely many minima of its potential (the famous Mexican hat potential). In grand unified theories, spontaneous symmetry breaking is associated with the production of *magnetic monopoles*. These are very massive particles that would easily dominate the energy content of the Universe, leading to a density parameter $\Omega(t_0)$ much larger than 1. Magnetic monopoles are only one example of a larger variety of stable, massive particles predicted by extensions of the Standard Model that are easily produced in the early universe and should survive to dominate the energy density today. Since their existence is at variance with observations, they are referred to as *unwanted relics*. We cannot rely on annihilation processes to deplete their density because the expansion of the Universe makes it progressively harder for particles and antiparticles to find each other and annihilate. Instead, inflation is able to dilute their density very efficiently, so that even if they are produced their contribution to Ω today is not in conflict with observations (provided they are produced before inflation).

1.3 Inflation: The Basics

In the previous sections we presented the major shortcomings of the Hot Big Bang model and saw how they are solved by a period of accelerated expansion in the early stages of the Universe. To be more precise, the key requirement is that the Hubble radius decreases in time. We now turn to the question of how such a period can be achieved. As we will see in the upcoming sections, a simple scalar field satisfying certain properties can realize inflation by providing an almost constant energy density.

1.3.1 The Inflaton Field

We begin by considering the Lagrangian density of a scalar field ϕ:

$$\mathcal{L} = -\frac{1}{2} g^{\mu\nu} \partial_\mu \phi \partial_\nu \phi - V(\phi). \tag{1.51}$$

The associated energy-momentum tensor can be computed by varying the action $S = \int d^4x \mathcal{L}$ with respect to the metric:

$$T_{\mu\nu} = -\frac{2}{\sqrt{-g}} \frac{\delta S}{\delta g_{\mu\nu}}, \tag{1.52}$$

where $g_{\mu\nu}$ in our case is the FLRW metric with $\kappa = 0$. Assuming the Lagrangian density does not depend on derivatives of the metric, from varying the action we have:

$$T^{\mu\nu} = \frac{-2}{\sqrt{-g}} \left[\frac{\delta(\sqrt{-g})}{\delta g_{\mu\nu}} \mathcal{L} + \sqrt{-g} \frac{\partial \mathcal{L}}{\partial g_{\mu\nu}} \right]. \tag{1.53}$$

A useful matrix property to compute the variation of $\sqrt{-g}$ is $\text{Tr}[\ln A] = \ln[\det A]$, which allows us to write:

$$-g = \det g = e^{\ln \det g} = e^{Tr \ln g}. \tag{1.54}$$

Notice that we are omitting the tensor indices of the metric. Thus:

$$\frac{\delta \det g}{\delta g_{\mu\nu}} = e^{Tr \ln g} g^{\mu\nu} = \det g \, g^{\mu\nu}. \tag{1.55}$$

Using (1.55), the energy-momentum tensor reads:

$$T_{\mu\nu} = \partial_\mu \phi \partial_\nu \phi - g_{\mu\nu} \mathcal{L}. \tag{1.56}$$

Next, we decompose ϕ into a homogeneous background field $\bar{\phi}(t)$ and a fluctuation $\delta\phi(t,\vec{x})$. Let us consider the background first. Since $\bar{\phi}$ is homogeneous, the energy density and the pressure are simply given by:

$$\bar{\rho} = \frac{1}{2}\dot{\bar{\phi}}^2 + V, \tag{1.57}$$

$$\bar{p} = \frac{1}{2}\dot{\bar{\phi}}^2 - V, \tag{1.58}$$

where the dot indicates a derivative with respect to cosmic time. By comparing (1.57) and (1.58), we see that ϕ can mimic a cosmological constant if $\dot{\phi}^2 << V(\phi)$. The specific form of V is model dependent, but to achieve $\bar{p} \approx -\bar{\rho}$ the potential must be sufficiently flat. The condition $\dot{\phi}^2 << V(\phi)$ defines the so-called *slow-roll* regime. Notice that even if initially the kinetic term is not negligible, the slow-roll condition will eventually become valid, as long as the potential is sufficiently flat. In fact, suppose that initially $\dot{\phi}^2 >> V(\phi)$. The equation of state then is $w = 1$, which translates into a severe dilution of the energy density, $\rho \propto a^{-3(1+w)} = a^{-6}$. Thus, if the potential is flat enough to keep the field rolling, the latter will eventually enter a slow-roll regime. This is a desirable feature because it makes $\dot{\phi}^2 << V(\phi)$ a general condition. In other words, slow-roll is an attractor solution. The scalar field driving inflation is known as *inflaton*.
The equation of motion for the inflaton can be derived as usual from the Euler-Lagrange equations applied to (1.51):

$$\frac{\partial(\sqrt{-g}\mathcal{L})}{\partial\phi} - \partial_\mu \frac{\partial(\sqrt{-g}\mathcal{L})}{\partial(\partial_\mu\phi)} = 0. \tag{1.59}$$

The result is:

$$\ddot{\phi} + 3H\dot{\phi} - \frac{\nabla^2\phi}{a^2} + \frac{dV}{d\phi} = 0. \tag{1.60}$$

Since the dynamics of the background is responsible for inflation, we devote the next section to analyzing it and better characterizing the slow-roll regime.

1.3.2 Slow-Roll Dynamics

At the background level, (1.60) reads:

$$\ddot{\bar{\phi}} + 3H\dot{\bar{\phi}} + \left.\frac{dV}{d\phi}\right|_{\phi=\bar{\phi}} = 0. \tag{1.61}$$

As we have seen, $\bar{\phi}$ can mimic a cosmological constant and therefore drive a quasi-exponential expansion of the Universe if the potential is sufficiently flat. This requirement leads to the so-called *slow-roll conditions*, the first of which we have already inferred:

$$\dot{\bar{\phi}}^2 << V(\phi). \tag{1.62}$$

The second slow-roll condition is given by:

$$\ddot{\bar{\phi}} << 3H\dot{\bar{\phi}}. \tag{1.63}$$

Equation (1.60) is reminiscent of a problem in classical mechanics involving a body subject to a force $F \propto -dV/d\phi$ and a friction term $3H\dot{\bar{\phi}}$. Thus, the second slow-roll condition requires the acceleration of the field to be small compared to the friction term, or equivalently, the force and friction terms must be comparable. Notice that during inflation $\bar{\phi}$ dominates the energy budget of the Universe because relativistic species and pressureless matter red-shift as a^{-4} and a^{-3} respectively, so they are suppressed by the exponential growth of the scale factor. The same applies to the curvature term, κ/a^2. Hence, the first Friedmann equation reduces to:

$$H^2 = \frac{8\pi G}{3}\left[\frac{1}{2}\dot{\bar{\phi}}^2 + V\right]. \tag{1.64}$$

Finally, using the first slow-roll condition in the Friedmann equation (1.64) and the second condition in (1.61), we find:

$$\begin{cases} H^2 \approx \frac{8\pi G}{3} V(\bar{\phi}) \\ 3H\dot{\bar{\phi}} \approx -\frac{dV}{d\bar{\phi}}, \end{cases} \tag{1.65}$$

summarizing the dynamics of the slow-roll regime. For a more quantitative description, it is useful to introduce the *slow-roll parameters*:

$$\epsilon = -\frac{\dot{H}}{H^2}, \tag{1.66}$$

$$\eta = -\frac{\ddot{\bar{\phi}}}{H\dot{\bar{\phi}}}. \tag{1.67}$$

Let us attempt to gain a better sense of how these parameters are related to the slow-roll conditions by assuming the latter hold and verifying what they imply for ϵ and η. From differentiating (1.64) with respect to t, we have:

$$2H\dot{H} = \frac{8\pi G}{3}(\ddot{\bar{\phi}} + V'(\bar{\phi}))\dot{\bar{\phi}} = -8\pi G H \dot{\bar{\phi}}^2, \tag{1.68}$$

where for brevity we use a prime $'$ to denote the derivative with respect to ϕ at the background level and the last equality follows from the equation of motion (1.61). This allows us to write ϵ as:

$$\epsilon = -\frac{\dot{H}}{H^2} = 4\pi G \frac{\dot{\bar{\phi}}^2}{H^2} \approx \frac{3}{2}\frac{\dot{\bar{\phi}}^2}{V(\bar{\phi})}. \tag{1.69}$$

Notice that we used the first slow-roll condition in the last equality. Hence, ϵ measures the ratio between the kinetic term and the potential and as a result must be small. This latter fact could have been inferred already from the definition of ϵ: the ratio $-\dot{H}/H^2$ can be interpreted as measuring the rate of change of the Hubble parameter. Since inflation involves a quasi-exponential growth of the scale factor and $H = \frac{\dot{a}}{a}$, H must change slowly during inflation. Another suggestive way of recasting ϵ relates it to the slope of the potential:

$$\epsilon \approx \frac{1}{16\pi G}\left(\frac{V'}{V}\right)^2, \tag{1.70}$$

which follows from (1.69) using $3H\dot{\bar{\phi}} \approx -V'$. That the slow-roll conditions imply $\eta << 1$ is more evident. More interesting is its connection with the second derivative of the potential. Notice that ϵ in turn was proportional to V'. In fact, one can define even more parameters like ϵ and η related to higher derivatives of the potential which prove useful when navigating models and comparing predictions with data. For η we have:

$$\eta = \frac{1}{H\dot{\bar{\phi}}}\left(-\frac{V^{"}\dot{\bar{\phi}}}{3H} + \frac{-\epsilon}{3}V'\right), \tag{1.71}$$

where we used $\dot{\bar{\phi}} \approx -\dot{V}/(3H)$. Since the second slow-roll condition implies $V'/(3H\dot{\bar{\phi}}) \approx 1$, we find:

$$\eta = \frac{1}{8\pi G}\frac{V^{"}}{V} - \epsilon. \tag{1.72}$$

Once again, $\eta << 1$ and $\epsilon << 1$ imply $V^{"} << V$, i.e. a flat potential. As a closing remark, $\epsilon << 1$ is enough to achieve the equation of state $w \approx -1$ but the additional requirement of a slowly changing field velocity $\dot{\bar{\phi}}$, which is encoded in $\eta << 1$, ensures inflation lasts enough e-folds to solve the Big Bang puzzles.

1.3.3 Reheating

In the previous sections, we saw how a scalar field endowed with a sufficiently flat potential can realize inflation. Clearly though, inflation must end at some point: we do not want to solve the puzzles of the Big Bang model at the cost of spoiling its successes (or denying our existence). In particular, the aftermath of inflation must be a radiation dominated universe, as described by the standard cosmological model. We have already mentioned that one of the most celebrated successes of the Big Bang model is primordial nucleosynthesis, which took place at $T_{\rm BBN} \approx 1\,\text{MeV}$. Thus, by the time the Universe reaches this temperature, it must already contain a plasma of thermalized particles. Moreover, the exponential growth of $a(t)$ during inflation will have diluted all particle species present before the expansion, so the task of populating the plasma with Stardard Model (SM) particles falls on the inflaton itself. The mechanism by which the energy density of the inflaton is transferred to the thermal bath is known as *reheating*. Inflation ends when the first slow-roll condition ceases to hold and $\epsilon = 1$. This happens when the inflaton has rolled to the region where V begins to slope downward toward the minimum and is no longer flat. At this point, the inflaton rolls to the minimum and starts to oscillate around it. However, this motion is also subject to the friction term $3H\dot{\phi}$ whose effect is to dampen the oscillations, reducing their amplitude. At the same time, the inflaton is decaying into SM particles. Let us briefly derive a few equations to better understand how this could play out. The description we provide below is merely a putting into formulae of the qualitative picture we have outlined in words up to here but it is enough to capture the basic idea of reheating. More details can be found in [2].

To account for the decays, we introduce a new term in the inflaton equation of motion:

$$\ddot{\phi} + 3H\dot{\phi} + V' = -\Gamma_\phi \dot{\phi}, \tag{1.73}$$

where Γ_ϕ is the inflaton decay width. Next, we multiply (1.73) by $\dot{\phi}$:

$$\frac{d}{dt}\left(\frac{\dot{\phi}}{2} + V\right) + 3H\dot{\phi}^2 + \Gamma_\phi \dot{\phi}^2 = 0. \tag{1.74}$$

Now, the inflaton oscillations are subject to a friction force, but if the period of the oscillations is much smaller than the damping time, each oscillation is effectively harmonic and we can use the virial theorem. The latter states that the average of the kinetic energy over a period of the oscillations is equal to the average of the potential, $\langle \frac{\dot{\phi}^2}{2} \rangle = \langle V \rangle$. Here, the angled brackets denote an average. Thus, approximating $2\dot{\phi} \approx \frac{\dot{\phi}^2}{2} + V = \bar{\rho}$, the inflaton equation becomes:

$$\frac{d\bar{\rho}}{dt} + 3H\bar{\rho} = -\Gamma_\phi \bar{\rho}. \tag{1.75}$$

Notice that the virial theorem also implies $\langle p \rangle = 0$. If the right-hand of (1.75) were 0, $\bar{\rho}$ would red-shift as a^{-3}, like the energy density of non-relativistic matter, but since the inflaton is decaying the energy in the comoving volume is not conserved. In particular, the decays add an exponential suppression to the usual a^{-3} dilution:

$$\bar{\rho}(t) = \bar{\rho}(t_{osc}) \left(\frac{a(t_{osc})}{a(t)}\right)^3 \exp\left[-\Gamma_\phi (t - t_{osc})\right], \tag{1.76}$$

where t_{osc} denotes the time at which the oscillations begin. If $t - t_{osc} << \Gamma_\phi^{-1}$, i.e. for time intervals over which the inflaton is stable, the exponential factor is negligible.

Up to this point, we have considered only the evolution of the inflaton, so let us now turn to the thermal bath. The inflaton decays are injecting heat in the plasma, so, by the first law of thermodynamics, $\delta Q = dU + pdV$, we have:

$$\delta Q = d(\rho_R a^3) + p_R d(a^3) = \Gamma_\phi (\bar{\rho} a^3) dt. \tag{1.77}$$

In fact, $\bar{\rho}a^3$ is the energy injection for a single decay and $\Gamma_\phi dt$ is the number of decays in the interval dt. Moreover, we are considering a unitary comoving volume, so $V = a^3$ in physical coordinates and

the corresponding energy variation of the thermal bath is $d(\rho_R a^3)$. Using the equation of state for radiation, $p_R = \rho_R/3$, and performing the derivatives, we find:

$$\frac{d\rho_R}{dt} + 4H\rho_R = \Gamma_\phi \bar{\rho}. \tag{1.78}$$

Notice that the decay term $\Gamma_\phi \bar{\rho}$ is sourcing the energy density of the thermal bath and depleting that of the inflaton, so it appears with opposite signs in the respective equations. A detailed analysis of the reheating phase requires solving the system of coupled Boltzmann equations given by (1.75) and (1.78), but we will stop at this essential picture.

1.3.4 From Quantum Fluctuations to Density Perturbations

Inflation is able to explain both why the CMB sky is nearly isotropic and why it is not perfectly isotropic. We have already answered the first question when we discussed the horizon problem. During inflation, the Hubble radius decreases, so that even a region the size of our observable universe could have been causally connected at the beginning of inflation if the expansion lasted long enough. In this section, we outline how the inflationary paradigm can also answer the second question.
The fluctuations of the CMB temperature reflect the tiny perturbations in the matter density at the time of photon decoupling. In fact, before their release, CMB photons were tightly coupled to the thermal bath, which prevented over-densities from growing further. The picture to keep in mind is the following: local over-densities attract the matter component to which photons are coupled, i.e. the baryons, into potential wells. Photons gather around the over-densities too, following the baryons, but they also exert an increasing radiation pressure as they are compressed in the potential wells. Eventually, the pressure causes the bundle of photons and baryons to rebound, preventing the collapse. This dynamic sets off pressure waves through the plasma that determine a very interesting feature of the CMB spectrum, known as *baryon acoustic oscillations*. We will not consider this effect further; we only point out, that after photon decoupling the in-fall of matter in the potential wells could finally progress into a gravitational collapse leading to the formation of cosmic structures. There remains the question of how these initial density perturbations came to be. The inflationary answer involves quantum fluctuations of the inflaton field. Let us see how the connection is drawn. First, we define the *curvature perturbation on uniform energy density hypersurfaces* ζ, given by:

$$\zeta = -\Phi - H\frac{\delta\rho}{\dot{\rho}}. \tag{1.79}$$

Here, ρ refers to a generic source of energy density and Φ is the spatial part of the scalar metric perturbation. In fact, metric perturbations are unavoidable in the context of inflation. Early on, the inflaton ϕ dominates the energy-momentum tensor of the Universe, so fluctuations $\delta\phi$ are bound to induce perturbations of the metric via the Einstein equations. The perturbed metric in turn will affect the evolution of the inflaton. We only mention in passing that a key prediction of inflation is the presence of a stochastic gravitational wave background due precisely to these perturbations of the metric. The coupling between metric and field perturbations is studied through gauge-invariant quantities that are built out of both types of fluctuations. The curvature perturbation ζ is an example. An important property of ζ is that it remains constant on super-horizon scales, so it allows one to connect the inflaton fluctuations with observables at later times. To see an example, we choose the spatial flatness gauge, where $\Phi = 0$, i.e. the spatial part of the metric is unperturbed. Consider a mode k that re-enters the horizon during radiation domination at time $t(k)_{\rm in}$ and let $t(k)_{\rm out}$ be the time when it left the horizon during inflation. The reader can refer to Figure 1.4. The time of horizon crossing depends on the mode, so in this sense $t_{\rm in}$ and $t_{\rm out}$ are functions of k. We have:

$$\zeta|_{t(k)_{\rm out}} = \zeta|_{t(k)_{\rm in}}\,. \tag{1.80}$$

The curvature perturbation at $t(k)_{\rm out}$ is $-H\frac{\delta\phi}{\dot{\phi}}$, while at $t(k)_{in}$ the relevant energy density is that of radiation, $\rho = \rho_R$. Thus, $\dot{\rho}_R \propto -4a^{-5}\dot{a} \propto -4\rho_R H$. Finally, we have:

$$-H\frac{\delta\phi}{\dot{\phi}}\bigg|_{t(k)_{\rm out}} = \frac{1}{4}\frac{\delta\rho_R}{\rho_R} = \frac{\delta T}{T}\bigg|_{t(k)_{\rm in}}, \tag{1.81}$$

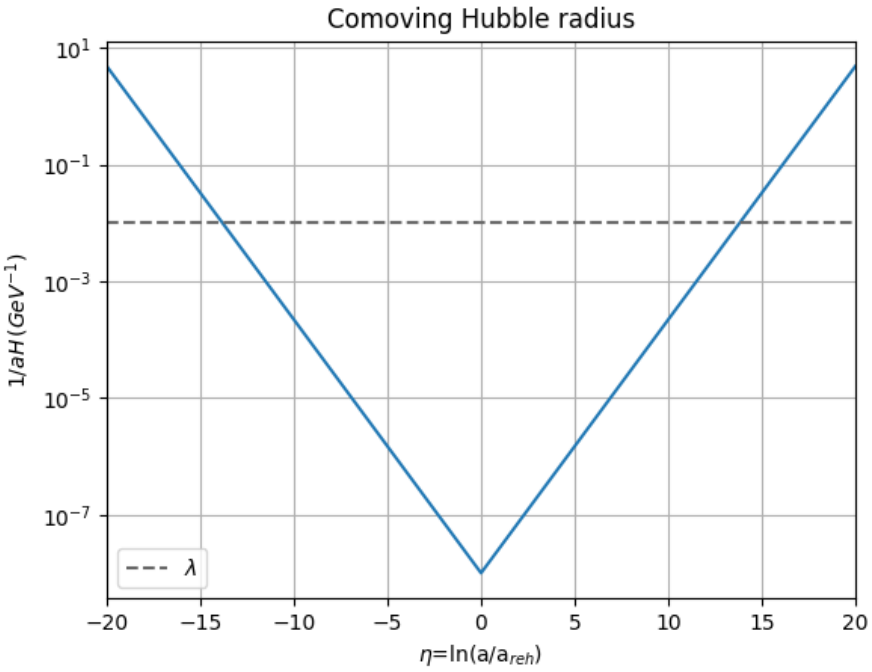

Figure 1.4: Comoving Hubble radius as a function of $\eta = \ln\left(\frac{a}{a_{\rm reh}}\right)$. The evolution shown encompasses inflation, modeled as a de Sitter expansion, and the subsequent radiation dominated epoch up to $\eta = 20$. Reheating is assumed to occur instantaneously. The dashed line corresponds to the mode $k = 100\,\text{GeV}$.

where, in the last equality, we used the fact that $\rho_R \propto T^4$. As anticipated, the temperature fluctuations of the thermal bath, the same fluctuations imprinted in the CMB sky, are related to quantum fluctuations of the inflaton field.

Chapter 2

Axion Evolution

2.1 Cosmological Setting

In this chapter, we study the evolution of the axion field. We assume that inflation unfolds as a de Sitter expansion and that reheating occurs instantaneously, ushering in a period of radiation domination followed by a matter-dominated epoch. The underlying metric is the flat FRW metric, $ds^2 = -dt^2 + a^2(t)d\vec{x}\cdot d\vec{x}$, where t is the cosmic time. For ease of calculation, we will often adopt the time variable $\eta = \ln(a/a_{\rm reh})$, which is related to the cosmic time via the Hubble parameter according to:

$$H = \frac{1}{a}\frac{da}{dt} = \frac{d\ln a}{dt} = \frac{d\eta}{dt}. \tag{2.1}$$

The FRW line element becomes $ds^2 = -(d\eta/H)^2 + e^{2\eta}d\vec{x}\cdot d\vec{x}$. The Hubble rate in terms of η reads:

$$\begin{cases} H_{\rm inf} & \eta \leq \eta_{\rm reh} \\ H_{\rm inf}e^{-2\eta} & \eta > \eta_{\rm reh}, \end{cases} \tag{2.2}$$

where $H_{\rm inf}$ is the energy scale of inflation and $e^{\eta_{\rm reh}}$ is the value of the scale factor at reheating. The time evolution of the Hubble parameter is displayed in Fig.2.1. We also assume that the Peccei-Quinn (PQ) symmetry is broken before inflation, which implies that the symmetry-breaking scale f must be greater than the inflation scale $H_{\rm inf}$. Moreover, to ensure that the symmetry is not restored during reheating, f must also be greater than the reheating temperature $T_{\rm reh}$. Since for the case of instantaneous reheating $T_{\rm reh} \approx \sqrt{M_{\rm Pl}H_{\rm inf}} > H_{\rm inf}$, $f > T_{\rm reh}$ is enough to meet our requirements.

2.2 Axion Evolution

We will consider axions from the misalignment mechanism subject to the potential:

$$V(\phi) = m^2 f^2 \left[1 - \cos\left(\frac{\phi}{f}\right)\right], \tag{2.3}$$

where $\phi = \phi(t, \vec{x})$ is the axion field and m its mass, which we assume to be constant. As we do not commit to any specific axion bearing model in this thesis, we refer the reader to [19] for a review on axions and their relevance for cosmology.
The axion field can be split into a homogeneous background $\bar{\phi}(t)$ and a perturbation $\delta\phi(t, \vec{x})$. For our purposes, $\delta\phi(t, \vec{x})$ entails a first order perturbation and a second order one, $\delta\phi^{(1)}(t, \vec{x})$ and $\delta\phi^{(2)}(t, \vec{x})$ respectively, so that $\delta\phi(t, \vec{x}) = \delta\phi^{(1)}(t, \vec{x}) + \delta\phi^{(2)}(t, \vec{x})$. A scalar field in an expanding universe obeys the following equation:

$$\ddot{\phi} + 3H\dot{\phi} - \frac{\nabla^2\phi}{a^2} + \frac{dV}{d\phi} = 0, \tag{2.4}$$

where the dot indicates a derivative with respect to cosmic time and we have omitted the dependence of ϕ on the space-time coordinates $(t, \vec{x})$ for the sake of brevity. Equation (2.4) can be derived from

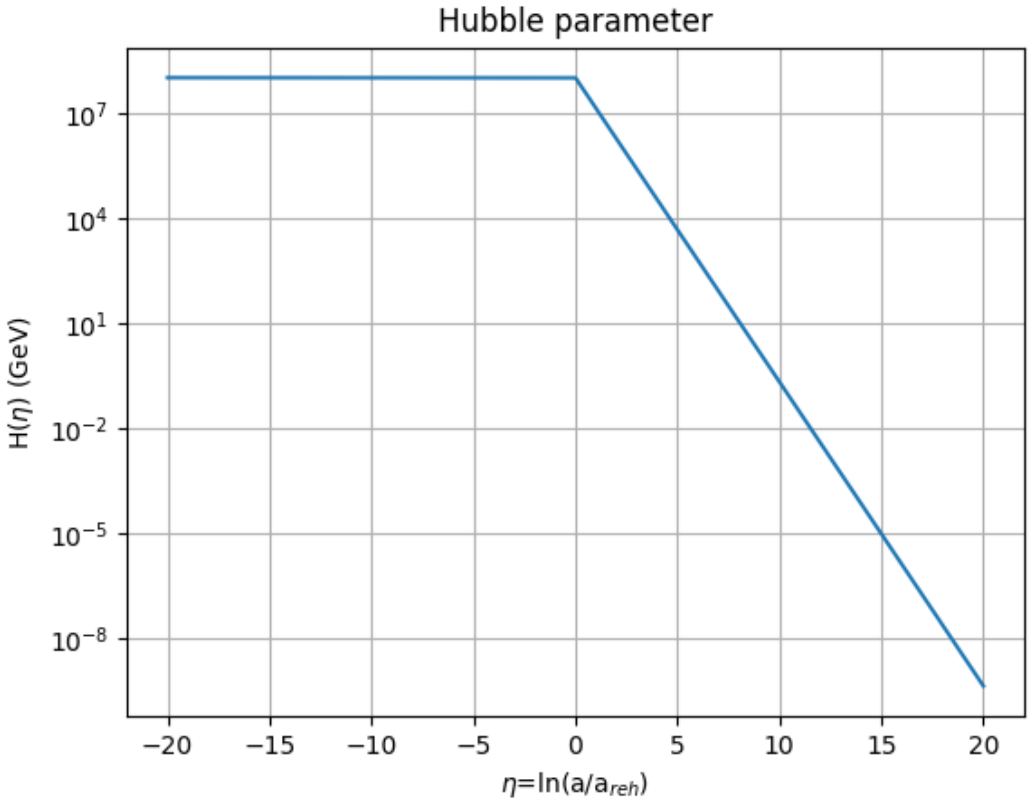

Figure 2.1: Time evolution of the Hubble parameter as a function of $\eta = \ln a/a_{\rm reh}$.

the Lagrangian density $\mathcal{L} = -\frac{1}{2}\partial_\mu\phi\partial^\mu\phi - V(\phi)$. In fact, for a generic metric and Lagrangian density $\mathcal{L}$ involving a scalar field ϕ, the least action principle yields the Euler-Lagrange equation:

$$\frac{\partial(\sqrt{-g}\mathcal{L})}{\partial\phi} - \partial_\mu\left(\frac{\partial(\sqrt{-g}\mathcal{L})}{\partial(\partial_\mu\phi)}\right) = 0, \tag{2.5}$$

where $\sqrt{-g}$ is the determinant of the metric tensor. Specializing to the FRW metric and the $\mathcal{L}$ of our problem, $\sqrt{-g} = a^3(t)$ and the two terms of the Euler-Lagrange equation read:

$$\frac{\partial(\sqrt{-g}\mathcal{L})}{\partial\phi} = -a^3\frac{dV}{d\phi}, \tag{2.6}$$

$$\partial_\mu\left(\frac{\partial(\sqrt{-g}\mathcal{L})}{\partial(\partial_\mu\phi)}\right) = 3a^2\dot{a}\dot{\phi} + a^3\ddot{\phi} - a\delta^{ij}\partial_i\partial_j\phi. \tag{2.7}$$

Finally, by dividing the difference between equations (2.6) and (2.7) by a^3 we recover (2.4).
Let us now expand the first derivative of V about the homogeneous background:

$$\frac{dV}{d\phi} = m^2 f\sin\left(\frac{\bar{\phi}}{f}\right) + m^2\cos\left(\frac{\bar{\phi}}{f}\right)(\delta\phi^{(1)} + \delta\phi^{(2)}) - \frac{m^2}{f}\sin\left(\frac{\bar{\phi}}{f}\right)\frac{1}{2}(\delta\phi^{(1)} + \delta\phi^{(2)})^2 + ... \tag{2.8}$$

Substituting this expansion and the decomposition $\phi(t,\vec{x}) = \bar{\phi}(t) + \delta\phi^{(1)}(t,\vec{x}) + \delta\phi^{(2)}(t,\vec{x})$ into equation (2.4) yields:

$$\ddot{\bar{\phi}} + 3H\dot{\bar{\phi}} + m^2 f\sin\left(\frac{\bar{\phi}}{f}\right) = 0 \tag{2.9}$$

for the evolution of the background, and:

$$\delta\ddot{\phi}^{(1)} + 3H\delta\dot{\phi}^{(1)} - \frac{\nabla^2\delta\phi^{(1)}}{a^2} + m^2\cos\left(\frac{\bar{\phi}}{f}\right)\delta\phi^{(1)} = 0, \tag{2.10}$$

$$\delta\ddot{\phi}^{(2)} + 3H\delta\dot{\phi}^{(2)} - \frac{\nabla^2\delta\phi^{(2)}}{a^2} + m^2\cos\left(\frac{\bar{\phi}}{f}\right)\delta\phi^{(2)} = \frac{m^2}{f}\sin\left(\frac{\bar{\phi}}{f}\right)\frac{\left(\delta\phi^{(1)}\right)^2}{2} \tag{2.11}$$

for the first and second-order perturbations. In the next section, we begin our analysis of the axion field evolution by first solving the background equation.

2.3 Background Evolution

Since the symmetry-breaking scale f is a free parameter, a more convenient variable to track the background evolution is the displacement angle $\theta = \bar{\phi}/f$. This way, f does not appear explicitly. Dividing equation (2.9) by f we find:

$$\ddot{\theta} + 3H\dot{\theta} + m^2\sin(\theta) = 0. \tag{2.12}$$

Trading t for η as time variable, the equation becomes:

$$\theta'' + \left(3 + \frac{H'}{H}\right)\theta' + \frac{m^2}{H^2}\sin(\theta) = 0, \tag{2.13}$$

where the prime denotes a derivative with respect to η. Equation (2.9) resembles that of a damped oscillator. The expansion of the Universe contributes to the friction term via the Hubble parameter. Hence, the background evolution will be determined by the competition between the Hubble friction and the oscillatory term proportional to the mass. In particular, since the Hubble rate decreases in time, we can expect it to dominate early on, causing the field to remain stuck near its initial value. After the Hubble parameter becomes comparable to the mass, the field enters a regime of damped oscillations. We have solved equation (2.13) numerically for different initial field values and the results are displayed in Figure 2.2 and Figure 2.3. As we can see, the exact time at which the oscillations appear, as well as their amplitude, are affected by the initial conditions. An initial field value closer to the maximum of the potential delays the onset of the oscillations and enhances their amplitude. For the sake of the numerical calculation, the axion mass was set to $m = 100\,\text{GeV}$, which is decidedly too large for a viable axion dark matter candidate, but allows us to gain a qualitative understanding of the axion evolution while keeping the numerical computation feasible. Instead, f and H_{inf} were set to $f = 10^{10}\,\text{GeV}$ and $H_{\text{inf}} = 10^8\,\text{GeV}$. The vertical dashed line corresponds to the time when the Hubble parameter crosses the axion mass, i.e. $m = H(\eta_{\text{osc}})$.
It is also interesting to consider the behavior of the background energy density $\bar{\rho}$. Once the background evolution is known, $\bar{\rho}$ can be obtained from:

$$\bar{\rho} = \frac{1}{2}H^2\bar{\phi}'^2(\eta) + V(\bar{\phi}) = \frac{1}{2}H^2f^2(\theta')^2 + V(f\theta). \tag{2.14}$$

Figure 2.4 shows the evolution of $\bar{\rho}$ normalized by f^2 for different values of θ_0. Early on, $\bar{\rho}$ is constant, as the background field. When the latter starts to oscillate, the energy density begins to decrease in time as a^{-3}, effectively behaving as the energy density of a non-relativistic particle species. This is why axions can serve as dark matter candidates. The dilution takes over later if the initial field value is chosen closer to the hilltop because, as we have seen, the background is stuck by the Hubble friction for longer. This latter observation also explains the behavior in Figure 2.4, where the value of $\bar{\rho}/f^2$ computed at $\eta = 10$ is plotted against the initial displacement angle: since $\bar{\rho}$ begins to dilute at a later time, its value is enhanced approaching the potential hilltop. The value of $\eta = 10$ was chosen with the only criterion of considering a time sufficiently subsequent to the onset of the oscillations during RD. We can further consider the evolution of the equation of state w for the background field, given by:

$$w = \frac{\bar{p}}{\bar{\rho}} = \frac{\frac{1}{2}H^2f^2(\theta')^2 - V(f\theta)}{\frac{1}{2}H^2f^2(\theta')^2 + V(f\theta)}. \tag{2.15}$$

Here, $\bar{p}$ is the pressure of the background field. As we can see from Figure 2.6, when θ is frozen to its initial value, it mimics a cosmological constant, so w is -1. During the oscillations, when $\bar{\rho}$

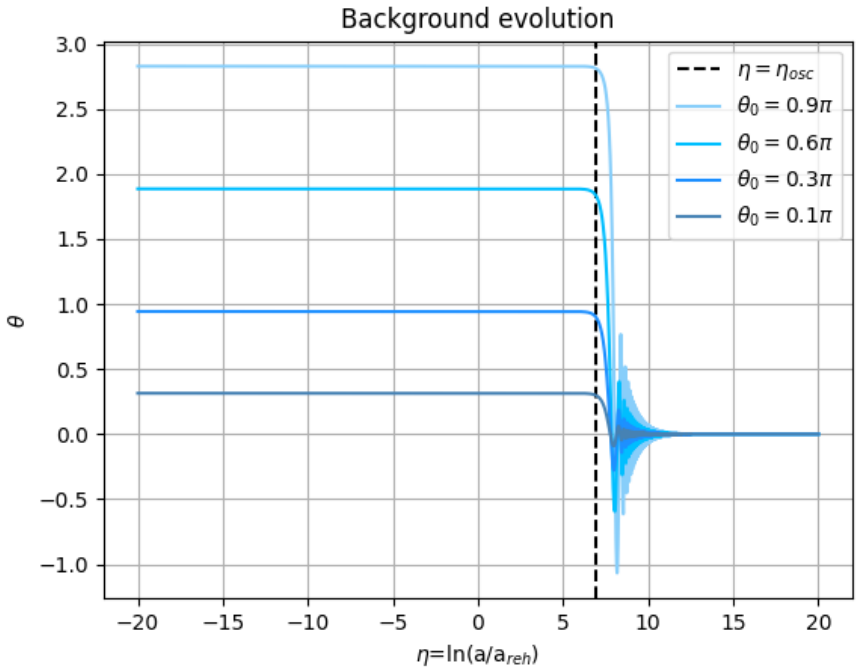

Figure 2.2: Evolution of the background for the initial field values 0.1π, 0.3π, 0.6π and 0.9π.

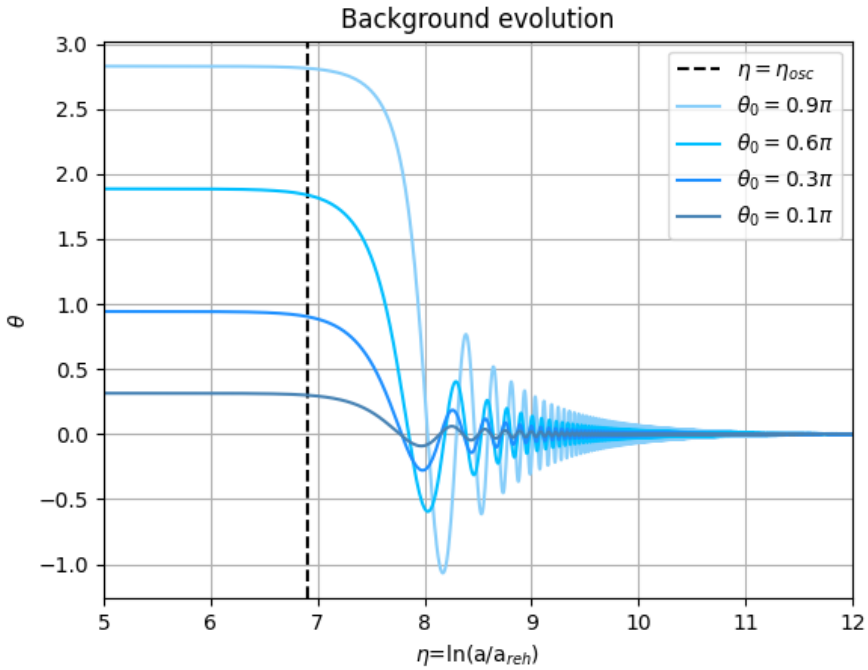

Figure 2.3: Zoomed-in view of the background oscillations for the initial field values 0.1π, 0.3π, 0.6π and 0.9π. The closer θ_0 is to the potential hilltop, the later the onset of the oscillations and the larger their amplitude.

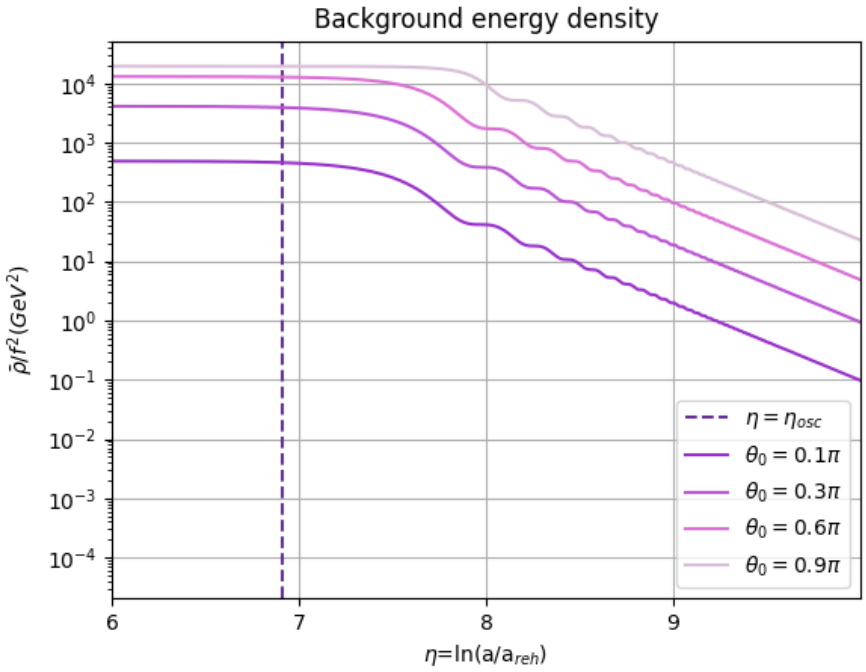

Figure 2.4: Time evolution of $\bar{\rho}/f^2$ for the initial field values 0.1π, 0.3π, 0.6π and 0.9π. The energy density is initially constant, then dilutes as $a^{(-3)}$ during the oscillations. Initial angles closer to π display the decay with a^{-3} later.

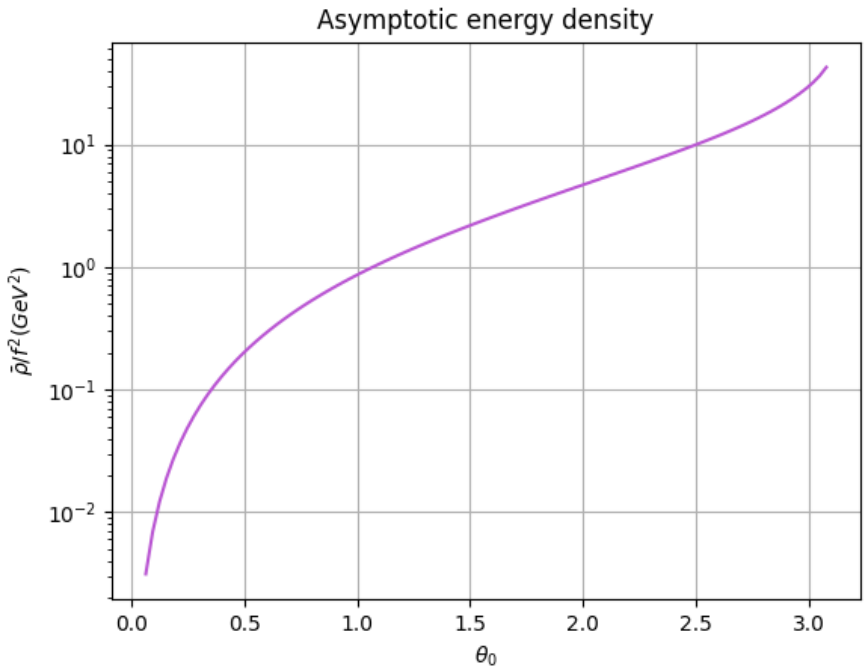

Figure 2.5: Asymptotic value of the background energy density as a function of the initial displacement angle.

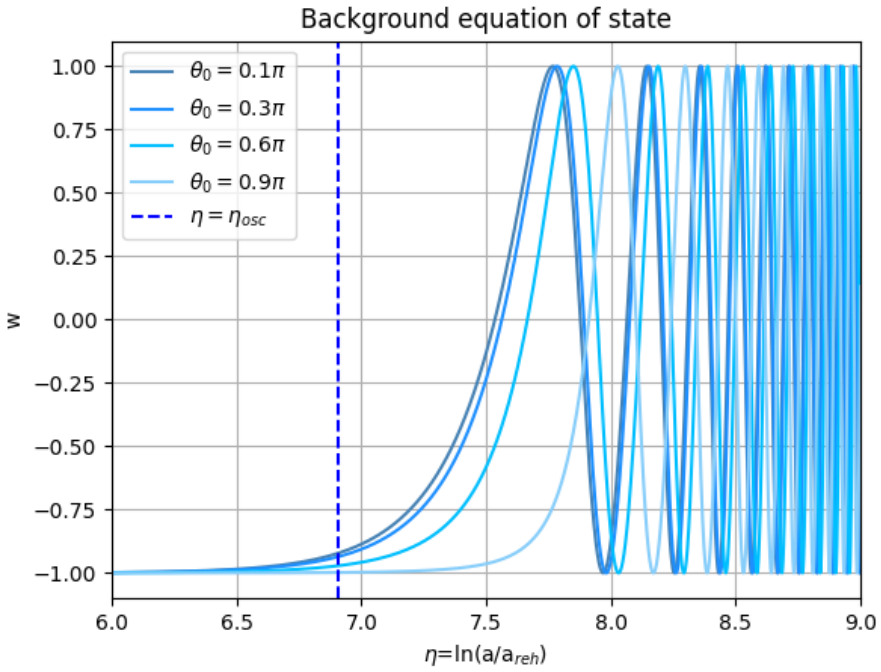

Figure 2.6: Evolution of the equation state for the initial field values 0.1π, 0.3π, 0.6π and 0.9π. In the over-damped regime, $w = -1$, as for a cosmological constant. When $\bar{\rho}$ begins to dilute as a^{-3}, w oscillates around 0.

dilutes as a^{-3}, w oscillates around the equation of state of pressureless matter, i.e. $w = 0$. As for the energy density, the value of θ_0 affects the transition between these two regimes. Now that we have considered the background evolution, we can turn to the equations of motion for the first- and second-order fluctuations.

2.4 First Order Fluctuations

Let us recall the evolution equations we had found for $\delta\phi^{(1)}$ and $\delta\phi^{(2)}$:

$$\delta\ddot{\phi}^{(1)} + 3H\delta\dot{\phi}^{(1)} - \frac{\nabla^2\delta\phi^{(1)}}{a^2} + m^2\cos\left(\frac{\bar{\phi}}{f}\right)\delta\phi^{(1)} = 0, \tag{2.16}$$

$$\delta\ddot{\phi}^{(2)} + 3H\delta\dot{\phi}^{(2)} - \frac{\nabla^2\delta\phi^{(2)}}{a^2} + m^2\cos\left(\frac{\bar{\phi}}{f}\right)\delta\phi^{(2)} = \frac{m^2}{f}\sin\left(\frac{\bar{\phi}}{f}\right)\frac{\left(\delta\phi^{(1)}\right)^2}{2}. \tag{2.17}$$

We will proceed by first solving the equation for $\delta\phi^{(1)}$, noticing in passing that it coincides with the homogeneous version of the second order equation. Hence, we can already remark that $\delta\phi^{(1)}$ will also be the homogeneous part of the solution to the equation for $\delta\phi^{(2)}$.
As observed for the background equation, (2.16) can be derived from the following action:

$$S = \int d^3\vec{x}dta^3(t)\left[\frac{1}{2}(\delta\dot{\phi}^{(1)})^2 - \frac{1}{2a^2(t)}\delta^{ij}\partial_i\delta\phi^{(1)}\partial_j\delta\phi^{(1)} - m^2\cos\left(\frac{\bar{\phi}}{f}\right)\frac{(\delta\phi^{(1)})^2}{2}\right], \tag{2.18}$$

which in conformal time $d\tau = dt/a$ becomes:

$$S = \int d^3\vec{x}d\tau\frac{a^2}{2}\left[(\delta\phi'^{(1)})^2 - \delta^{ij}\partial_i\delta\phi^{(1)}\partial_j\delta\phi^{(1)} - m^2a^2\cos\left(\frac{\bar{\phi}}{f}\right)(\delta\phi^{(1)})^2\right]. \tag{2.19}$$

Notice that we are using the same symbol we had reserved for derivatives with respect to η in the previous section to indicate derivatives with respect to conformal time. In order to reabsorb the overall

a^2 factor in the integrand, we introduce the rescaled perturbation $\delta\chi = a\delta\phi$, in terms of which the action becomes:

$$S = \int d^3\vec{x}d\tau\frac{1}{2}\left[(\delta\chi'^{(1)})^2 - 2\frac{a'}{a}\delta\chi'^{(1)}\delta\chi^{(1)} + \left(\frac{a'}{a}\right)^2(\delta\chi^{(1)})^2 \right.$$
$$\left. -\delta^{ij}\partial_i\delta\chi^{(1)}\partial_j\delta\chi^{(1)} - m^2a^2\cos\left(\frac{\bar{\phi}}{f}\right)(\delta\chi^{(1)})^2\right]. \tag{2.20}$$

The term proportional to $\delta\chi\delta\chi'$ can be removed by noticing that it differs from $\left(-\frac{a''}{a} + \frac{a'^2}{a^2}\right)(\delta\chi^{(1)})^2$ only by a surface term. Dropping the latter we are left with:

$$\begin{aligned} S &= \int d^3\vec{x}d\tau\mathcal{L} \\ &= \int d^3\vec{x}d\tau\frac{1}{2}\left[(\delta\chi'^{(1)})^2 - \delta^{ij}\partial_i\delta\chi^{(1)}\partial_j\delta\chi^{(1)} - \left(m^2a^2\cos\left(\frac{\bar{\phi}}{f}\right) - \frac{a''}{a}\right)(\delta\chi^{(1)})^2\right]. \end{aligned} \tag{2.21}$$

From $\mathcal{L}$, we can compute the conjugate momentum to $\delta\chi^{(1)}$, $p = \frac{\partial\mathcal{L}}{\partial\delta\chi'^{(1)}}$, and proceed to construct the Hamiltonian of the system, given by $H = \int d^3\vec{x}(p\delta\chi'^{(1)} - \mathcal{L})$:

$$H = \int d^3\vec{x}\frac{1}{2}\left[(\delta\chi'^{(1)})^2 + \delta^{ij}\partial_i\delta\chi^{(1)}\partial_j\delta\chi^{(1)} + \left(m^2a^2\cos\left(\frac{\bar{\phi}}{f}\right) - \frac{a''}{a}\right)(\delta\chi^{(1)})^2\right]. \tag{2.22}$$

In preparing to quantize the perturbation $\delta\chi^{(1)}$, let us pass to Fourier space, where the Hamiltonian becomes:

$$H = \frac{1}{2}\int d^3\vec{k}\left[p_kp_k^* + \left(k^2 + m_{eff}^2a^2 - \frac{a''}{a}\right)\delta\chi_k^{(1)}\delta\chi_k^{(1)*}\right]. \tag{2.23}$$

Here, $m_{eff}^2 = m^2\cos\left(\frac{\bar{\phi}}{f}\right)$ and $\delta\chi_k^{(1)}(\tau) = \delta\chi^{(1)}(\tau,\vec{k})$ and $p_k(\tau) = p(\tau,\vec{k})$ are the Fourier transforms of $\delta\chi^{(1)}(\tau,\vec{x})$ and $p(\tau,\vec{x})$ respectively:

$$\delta\chi^{(1)}(\tau,\vec{x}) = \int\frac{d^3\vec{k}}{(2\pi)^3}e^{i\vec{k}\cdot\vec{x}}\delta\chi_k^{(1)}(\tau), \tag{2.24}$$

$$p(\tau,\vec{x}) = \int\frac{d^3\vec{k}}{(2\pi)^3}e^{i\vec{k}\cdot\vec{x}}p_k(\tau). \tag{2.25}$$

Notice that $\delta\chi_k^{(1)}$ and p_k are such that $\delta\chi_k^{(1)*} = \delta\chi_{-k}^{(1)}$ and $p_k^* = p_{-k}$ for their coordinate-space counterparts to be real. It is worth noting that m_{eff}^2 depends on time via the background field $\bar{\phi}$ and can become negative because of the cosine factor. To further simply the expression for H, we introduce the frequency ω_k:

$$\omega_k = k^2 + m_{eff}^2a^2 - \frac{a''}{a}, \tag{2.26}$$

in terms of which:

$$H = \int d^3\vec{k}\frac{1}{2}\left[p_kp_k^* + \omega_k^2\delta\chi_k^{(1)}\delta\chi_k^{(1)*}\right]. \tag{2.27}$$

The next step toward quantising the first order perturbation and its conjugate momentum consists in introducing the time-dependent ladder operators:

$$\delta\chi_k^{(1)}(\tau) = \frac{1}{\sqrt{2|\omega_k(\tau)|}}\left(a_k(\tau) + a_{-k}^\dagger(\tau)\right), \tag{2.28}$$

$$p_k(\tau) = -i\sqrt{\frac{|\omega_k(\tau)|}{2}}\left(a_k(\tau) - a_{-k}^\dagger(\tau)\right). \tag{2.29}$$

The fields $\delta\chi^{(1)}$ and p in coordinate space obey the following canonical commutation relation:

$$\left[\delta\chi^{(1)}(\tau,\vec{x}), p(\tau,\vec{x'})\right] = i(2\pi)^3\delta^{(3)}(\vec{x}-\vec{x'}), \tag{2.30}$$

which yields

$$\left[\delta\chi_k^{(1)}(\tau), p_{k'}^\dagger(\tau)\right] = i(2\pi)^3\delta^{(3)}(\vec{k}-\vec{k'}) \tag{2.31}$$

in Fourier space. To obtain a commutation relation for the ladder operators $a_k(\tau)$ and $a_k^\dagger(\tau)$, we simply invert (2.28) and (2.29), finding:

$$a_k(\tau) = \frac{1}{\sqrt{2}}\left(\sqrt{|\omega_k(\tau)|}\delta\chi_k^{(1)}(\tau) + i\frac{1}{\sqrt{|\omega_k(\tau)|}}p_k(\tau)\right), \tag{2.32}$$

$$a_k^\dagger(\tau) = \frac{1}{\sqrt{2}}\left(\sqrt{|\omega_k(\tau)|}\left(\delta\chi_k^{(1)}(\tau)\right)^\dagger - i\frac{1}{\sqrt{|\omega_k(\tau)|}}p_k^\dagger(\tau)\right), \tag{2.33}$$

and impose (2.31). This returns $\left[a_k(\tau), a_{k'}^\dagger(\tau)\right] = (2\pi)^3\delta^{(3)}(\vec{k}-\vec{k'})$, while all other commutators vanish. In the next section, we will introduce the tool of Bogoliubov transformations to address the time-dependence of the ladder operators.

2.4.1 Bogoliubov Transformations

A Bogoliubov transformation relates two sets of ladder operators. Concretely, if $(a, a^\dagger)$ and $(b, b^\dagger)$ are two sets of time-independent ladder operators, the Bogoliubov transformation linking them is of the form:

$$\begin{aligned} b &= Aa + Ba^\dagger, \\ b^\dagger &= B^*a + A^*a^\dagger. \end{aligned} \tag{2.34}$$

An important remark is due: the a and b operators do not annihilate the same vacuum state. In other words, if $|0\rangle_a$ is the vacuum of a, $b|0\rangle_a \neq 0$. Therefore, the expectation value of the number operator $n_b = b^\dagger b$ on the a-vaccuum, $\langle n_b\rangle_a$, is non-zero and given by:

$$\langle n_b\rangle_a = |B|^2. \tag{2.35}$$

Hence, the a-vacuum is populated by b-particles. If the ladder operators are time-dependent, as in our case, the Bogoliubov transformation involves time-dependent coefficients. Thus, we can express $a_k(\tau)$ and $a_k^\dagger(\tau)$ in terms of fixed-time, and therefore time-independent, ladder operators by means of a Bogoliubov transformation. The advantage is that the time dependence of the operators is transferred to the Bogoliubov coefficients, which are scalars. Let us then fix some initial time τ_0. The ladder operators at any later time τ are related to those at τ_0, by the Bogoliubov transformation:

$$\begin{aligned} a_k(\tau) &= \alpha_k(\tau)a_k(\tau_0) + \beta_k(\tau)a_{-k}^\dagger(\tau_0), \\ a_{-k}^\dagger(\tau) &= \alpha_k^*(\tau)a_{-k}^\dagger(\tau_0) + \beta_k^*(\tau)a_k(\tau_0). \end{aligned} \tag{2.36}$$

Moreover, we know that the instantaneous vacuum defined by $a_k(\tau)$ contains a non-zero average number of particles associated with the initial-time annihilation operator a_k^0. Notice that the Bogoliubov coefficients satisfy

$$|\alpha_k|^2 - |\beta_k|^2 = 1, \tag{2.37}$$

as a consequence of the commutation relation for the ladder operators. Now that we have expressed $a_k(\tau)$ and $a_k^\dagger(\tau)$ in terms of the initial-time ladder operators, we can do the same for the first order perturbation $\delta\chi^{(1)}$ and its conjugate momentum p:

$$\delta\chi^{(1)}(\tau) = u_k(\tau)a_k^0 + u_k^*(\tau)a_{-k}^{\dagger 0}, \tag{2.38}$$

$$p(\tau) = u_k'(\tau)a_k^0 + u_k^{*'}(\tau)a_{-k}^{\dagger 0}, \tag{2.39}$$

where $a_k^0 = a_k(\tau_0)$ for brevity and we have introduced the mode functions $u_k(\tau)$. The commutation relation between $\delta\chi^{(1)}$ and p_k implies the following normalization of the mode functions:

$$u_k(\tau)u_k^{*\prime}(\tau) - u_k'(\tau)u_k^*(\tau) = i. \tag{2.40}$$

The problem of tracking the evolution of $\delta\chi^{(1)}$ reduces to computing the mode functions, which we set out to do in the next section. However, there is one final point to address concerning the initial-time ladder operators. In a curved spacetime, there is no uniquely defined vacuum state, so the choice for a_k^0 and $a_k^{\dagger 0}$ is ambiguous. This is not the case in Minkowski space, where the natural choice falls on the operators that diagonalize the Hamiltonian of the system. Now, if a curved spacetime approaches Minkowski in the asymptotic past and in the asymptotic future, the ambiguity can be circumvented by choosing the sets of ladder operators that diagonalize the Hamiltonian of the system at hand in the far past and future. For the cosmological case, approaching Minkowski space is equivalent to requiring that the system does not feel the effects of the expansion. This is true in the sub-horizon limit and, more in general, when the so-called *adiabaticy conditions* hold:

$$\left|\frac{\omega_k'}{\omega_k^2}\right|^2, \left|\frac{\omega_k''}{\omega_k^3}\right| << 1. \tag{2.41}$$

Here, ω_k is the frequency given by 2.26. If ω_k is real and the adiabaticity conditions are satisfied, the mode functions approach plane waves, the functional form they would take in Minkowski space. Thus, as long as the asymptotic vacua are adiabatic, the initial-time and late-time ladder operators are related by a constant Bogoliubov transformation with coefficients α_k and β_k given by the late-time limit of the time-dependent $\alpha_k(\tau)$ and $\beta_k(\tau)$. The particle interpretation of $|\beta_k|^2$ is then warranted only when the adiabaticity conditions hold. In our case, we considered modes that were deep inside the horizon at the initial time, so up to horizon crossing the effective spacetime is Minkowski. When the modes exit the horizon, adiabaticity is lost but it can be checked numerically that a few e-folds after the onset of the background oscillations the adiabaticity conditions are restored. More details can be found in [9].
In light of what we have seen, $|\beta_k|^2$ is related to the number of particles produced by the expansion of the Universe populating the late-time adiabatic vacuum. Indeed, the expectation value of the late-time number operator $a_k^\dagger a_k$ on the initial-time vacuum, i.e. the state annihilated by a_k^0, can be computed from (2.36) as:

$$\langle a_k^\dagger a_k\rangle = |\beta_k|^2\delta^{(3)}(0). \tag{2.42}$$

The divergent $\delta^{(3)}(0)$ only appears because we are considering an infinite spatial volume, so it should be interpreted as a volume factor:

$$\delta^{(3)}(0)(2\pi)^3 = \int d^3\vec{x} = V, \tag{2.43}$$

where the integral is over comoving coordinates. We therefore have:

$$\langle a_k^\dagger a_k\rangle = |\beta_k|^2\frac{V}{(2\pi)^3}, \tag{2.44}$$

from which we see that $|\beta_k|^2$ corresponds to the expectation value for the number of particles having comoving momentum k created by the expanding background per comoving volume.

2.4.2 Mode Functions Evolution

As anticipated, in this section we analyze the time evolution of the mode functions. We have seen that $\delta\phi^{(1)}$ obeys equation (2.10), which recast in terms of $\delta\chi^{(1)}$ and $\eta = \ln(a/a_{reh})$ becomes:

$$\delta\chi^{(1)\prime\prime} + \left(1 + \frac{H'}{H}\right)\delta\chi^{(1)\prime} + \left[\frac{-\nabla^2}{H^2}e^{-2\eta} - 2 - \frac{H'}{H} + \frac{m^2}{H^2}\cos(\bar{\theta})\right]\delta\chi^{(1)} = 0. \tag{2.45}$$

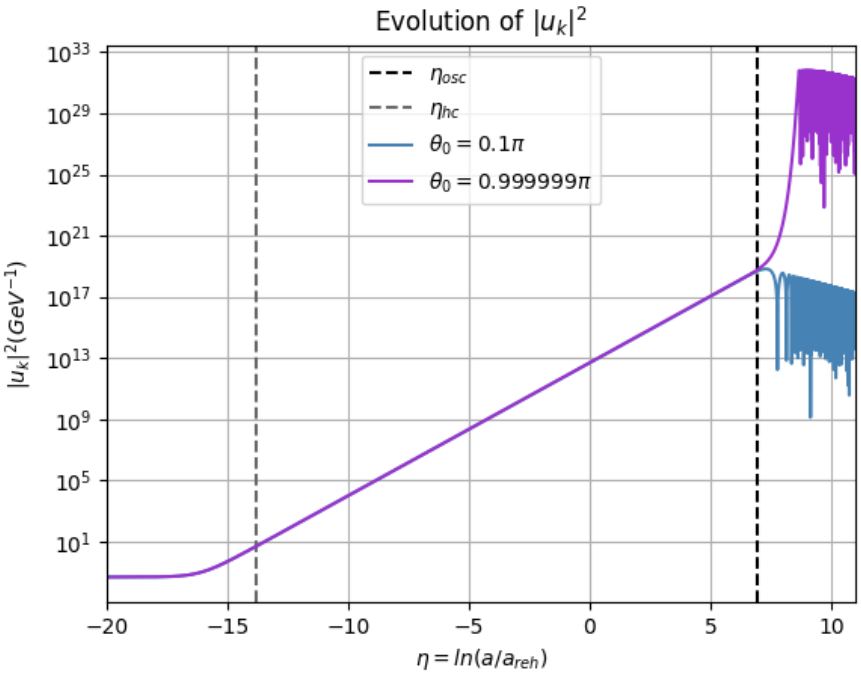

Figure 2.7: Time evolution of $|u_k|^2$. The vertical lines signal the times $\eta_{\rm hc}$, when the mode crosses the horizon to exit it, and $\eta_{\rm osc}$, when the Hubble parameter becomes equal to the mass. The amplitude stays constant until horizon exit, grows in the super-horizon regime and oscillates after $\eta_{\rm osc}$. The amplitude is strongly enhanced near the potential hilltop compared to initial values close to the minimum.

The prime now denotes a derivative with respect to η. The equation of motion for u_k is the Fourier transform of (2.45), given by:

$$u_k'' + \left(1 + \frac{H'}{H}\right) u_k' + \left[\frac{k^2}{H^2} e^{-2\eta} - 2 - \frac{H'}{H} + \frac{m^2}{H^2}\cos(\theta)\right] u_k = 0. \tag{2.46}$$

We have computed numerical solutions for the mode functions, setting $H_{\rm inf} = 10^8\,\text{GeV}$, $m = 100\,\text{GeV}$ and $k/a_{\rm reh} = 100\,\text{GeV}$. For this choice of parameters, the mode is initially sub-horizon, exits the horizon during inflation, and re-enters it after the onset of the oscillations during radiation domination. In fact, small-scale modes that re-enter the horizon when the background field is still over-damped are not affected by the oscillations. Thus, the latter only impact the evolution of perturbations with small enough k. The initial condition for the mode function was set to a positive-frequency WKB solution normalized as in (2.40). Figure 2.7 displays the evolution of $|u_k|^2$ computed numerically for different values of the initial background field θ_0. As we can see, the behavior is independent of θ_0 until the onset of the oscillations: $|u_k|^2$ is constant while inside the horizon, then grows in the super-horizon regime. When the background field begins to oscillate, the amplitude of the mode function also displays oscillations, but values of θ_0 closer to the maximum further enhance it. The enhancement is due to the fact that small fluctuations in the initial field value have a more dramatic effect if θ_0 is closer to the maximum. A larger initial angle always delays the oscillations, but near the minimum the time shift does not lead to sizable differences in the evolution of the field. However, near the maximum, even tiny differences in θ_0 cause significant delays. Thus, patches of the Universe with slightly different initial conditions begin to oscillate at very different times, leading to large fluctuations.

2.5 Second Order Fluctuations

In this section, we solve for the second order perturbation $\delta\chi^{(2)} = a\delta\phi^{(2)}$ using the Green's function method. The equation of motion for $\delta\chi^{(2)}$ reads:

$$\delta\chi^{(2)\prime\prime} + \left(1 + \frac{H'}{H}\right)\delta\chi^{(2)\prime} + \left[\frac{-\nabla^2}{H^2}e^{-2\eta} - 2 - \frac{H'}{H} + \frac{m^2}{H^2}\cos(\bar{\theta})\right]\delta\chi^{(2)} = \\ = \frac{m^2}{2fH^2}\sin(\bar{\theta})e^{-\eta}\left(\delta\chi^{(1)}\right)^2. \tag{2.47}$$

Once again, the prime denotes a derivative with respect to η. Since (2.47) is a nonhomogeneous equation, the solution can be expressed as $\delta\chi^{(2)} = \delta\chi_h^{(2)} + \delta\chi_p^{(2)}$, where $\delta\chi_h^{(2)}$ solves the homogeneous equation and $\delta\chi_p^{(2)}$ is the particular solution. We have already noticed that the homogeneous part of (2.47) is identical to the equation of motion for $\delta\chi^{(1)}$, which we solved in the previous section. Thus, $\delta\chi_h^{(2)} = \delta\chi^{(1)}$. To compute the particular solution, we first Fourier transform the equation of motion for $\delta\chi^{(2)}$. The source term on the right-hand side of (2.47), which is quadratic in $\delta\chi^{(1)}$, can be expressed as:

$$S(\eta,\vec{x}) = \frac{m^2}{2fH^2}\sin(\bar{\theta})e^{-\eta}\int\frac{d^3\vec{k}}{(2\pi)^3}\int\frac{d^3\vec{k'}}{(2\pi)^3}\delta\chi^{(1)}(\eta,\vec{k})\delta\chi^{(1)}(\eta,\vec{k'})e^{i(\vec{k}+\vec{k'})\cdot\vec{x}}. \tag{2.48}$$

Performing the shift $\vec{k} \to \vec{k} - \vec{k'}$ we find:

$$\begin{aligned} S(\eta,\vec{x}) &= \int\frac{d^3\vec{k}}{(2\pi)^3}S(\eta,\vec{k})e^{i\vec{k}\cdot\vec{x}} \\ &= \frac{m^2}{2fH^2}\sin(\bar{\theta})e^{-\eta}\int\frac{d^3\vec{k}}{(2\pi)^3}\int\frac{d^3\vec{k'}}{(2\pi)^3}\delta\chi^{(1)}(\eta,\vec{k}-\vec{k'})\delta\chi^{(1)}(\eta,\vec{k'})e^{i\vec{k}\cdot\vec{x}}, \end{aligned} \tag{2.49}$$

where in the last line we have recognized the source term in Fourier space:

$$S(\eta,\vec{k}) = \frac{m^2}{2H^2}\sin(\bar{\theta})e^{-\eta}\int\frac{d^3\vec{k'}}{(2\pi)^3}\delta\chi^{(1)}(\eta,\vec{k}-\vec{k'})\delta\chi^{(1)}(\eta,\vec{k'}). \tag{2.50}$$

Thus, the Fourier transform of (2.47) is given by:

$$\delta\chi_k^{(2)\prime\prime} + \left(1 + \frac{H'}{H}\right)\delta\chi_k^{(2)\prime} + \left[\frac{k^2}{H^2}e^{-2\eta} - 2 - \frac{H'}{H} + \frac{m^2}{H^2}\cos(\bar{\theta})\right]\delta\chi_k^{(2)} = S(\eta,\vec{k}). \tag{2.51}$$

We proceed with the following Ansatz for the particular solution:

$$\delta\chi_p^{(2)}(\eta,\vec{k}) = c_1(\eta,\vec{k})u_k + c_2(\eta,\vec{k})u_k^*, \tag{2.52}$$

where u_k and u_k^* are the mode functions we computed in the previous section and $c_1(\eta,\vec{k})$ and $c_2(\eta,\vec{k})$ satisfy:

$$c_1'(\eta,\vec{k})u_k + c_2'(\eta,\vec{k})u_k^* = 0. \tag{2.53}$$

Substituting (2.52) into the evolution equation of $\delta\chi^{(2)}$ and using constraint (2.53), we find:

$$c_1'(\vec{k},\eta)u_k' + c_2'(\vec{k},\eta)u_k^{*\prime} = S(\eta,\vec{k}). \tag{2.54}$$

Therefore, $c_1(\eta,\vec{k})$ and $c_2(\eta,\vec{k})$ are formally given by:

$$c_1(\eta,\vec{k}) = \int_{-\infty}^{\eta}d\eta'\frac{-u_k^*(\eta')}{u_k(\eta')u_k^{*\prime}(\eta') - u_k'(\eta')u_k^*(\eta')}S(\eta',\vec{k}), \tag{2.55}$$

$$c_2(\eta,\vec{k}) = \int_{-\infty}^{\eta}d\eta'\frac{u_k(\eta')}{u_k(\eta')u_k^{*\prime}(\eta') - u_k'(\eta')u_k^*(\eta')}S(\eta',\vec{k}), \tag{2.56}$$

and the full perturbation up to second order reads:

$$\delta\chi^{(2)}(\eta,\vec{k}) = u_k a_k^0 + u_k^* a_k^{0\dagger} + \int_{-\infty}^{\eta}d\eta'\frac{-u_k^*(\eta')u_k(\eta) + u_k(\eta')u_k^*(\eta)}{u_k(\eta')u_k^{*\prime}(\eta') - u_k'(\eta')u_k^*(\eta')}S(\eta',\vec{k}). \tag{2.57}$$

Chapter 3

Axion Bispectrum

3.1 Unveiling The Quantumness

In this chapter, we compute the bispectrum of the axion field and energy density perturbations. The upcoming sections describe the calculations in detail; here, we would like to present our motivations. In [12], the authors point out a property of classical bispectra that sets them apart from their quantum counterparts. The quantum bispectrum is associated with the creation of three virtual particles from the vacuum. Instead, classical fluctuations correspond to local variations of the density due to the presence of real particles. If their interactions are governed by causal physics, the presence of particles in the final state implies the decay of a particle in the initial state. When the three momenta considered are such that one is the sum of the other two, as momentum conservation requires for a particle decay, poles analogous to the resonances observed at colliders appear in the bispectrum. As we will see, such a relation between the momenta corresponds to the so-called folded configuration of the bispectrum. The absence of poles in the folded configuration is then a signature of quantum zero-point fluctuations. At the same time, their presence does not prove that the fluctuations are classical because highly excited quantum states can also yield poles.
Let us briefly summarize the main results of [12]. The authors considered an effectively massless scalar field during inflation, which they modeled as a de Sitter expansion. The corresponding adiabatic density fluctuation $\zeta(\vec{x},\tau)$ is given by:

$$\zeta(\vec{x},\tau) = \int \frac{d^3\vec{k}}{(2\pi)^3}\frac{\Delta_\zeta}{\sqrt{k^3}} e^{i\vec{k}\cdot\vec{x}}\left[a_k^\dagger(1-ik\tau)e^{ik\tau} + a_{-k}(1+ik\tau)e^{-ik\tau}\right], \tag{3.1}$$

where the normalization Δ_ζ is fixed based on the observed amplitude. The non-Gaussianity was assumed to arise entirely from non-linear evolution, with the initial state being Gaussian. The quantum commutation relations read:

$$\left[a_k^\dagger, a_{k'}\right] = (2\pi)^3\delta^{(3)}(\vec{k}-\vec{k'}), \tag{3.2}$$

as usual. With the statistics

$$\left\langle a_k a_{-k'}^\dagger \right\rangle_c = \left\langle a_{-k'}^\dagger a_k \right\rangle_c = \frac{1}{2}(2\pi)^3\delta^{(3)}(\vec{k}+\vec{k'}), \tag{3.3}$$

the classical a_k and $a_k^\dagger$ yield the same two-point correlation function as the quantum ladder operators. The bispectrum was computed considering the following interaction Hamiltonian:

$$H_{\text{int}} = -\frac{\lambda}{3!}\dot{\zeta}^3. \tag{3.4}$$

For the quantum case, the in-in formalism returns:

$$\langle\zeta_{k_1}\zeta_{k_2}\zeta_{k_3}\rangle_q = (2\pi)^3\delta^{(3)}(\vec{k}_1+\vec{k}_2+\vec{k}_3)\frac{4\lambda H^{-1}\Delta_\zeta^6}{(k_1+k_2+k_3)^3k_1k_2k_3}. \tag{3.5}$$

As we can see, the only pole is at $k_1 + k_2 + k_3 = 0$. The classical bispectrum was computed by first solving for the fluctuation at second order via the Green's function method, as we did in the previous chapter. Since we will see how to perform this calculation, we only quote the result for now:

$$\langle \zeta_{k_1}\zeta_{k_2}\zeta_{k_3}\rangle_c = (2\pi)^3\delta^{(3)}(\vec{k}_1+\vec{k}_2+\vec{k}_3)\frac{\lambda H^{-1}\Delta_\zeta^6}{3k_1k_2k_3}\left[\frac{3}{(k_1+k_2+k_3)^3}+\frac{1}{(-k_1+k_2+k_3)^3}+\right.$$
$$\left.\frac{1}{(k_1-k_2+k_3)^3}+\frac{1}{(k_1+k_2-k_3)^3}\right]. \quad (3.6)$$

The last three terms in the square brackets are the classical poles we were referring to at the beginning of this section. Their presence can also be explained as follows: since $a_k|0\rangle = 0$, there are no positive frequency modes in the quantum case and only the creation of virtual particles can produce a correlation. Instead, the classical case involves both negative and positive frequency modes because $\left\langle a^\dagger_{-k'}a_k\right\rangle_c \neq 0$. It is precisely the different combinations of $e^{ik\tau}$ and $e^{-ik\tau}$ factors that give rise to the poles. In general, the order of the pole depends on the number of derivatives appearing in the interaction term. In this example, the interaction Hamiltonian entailed three time derivatives, and indeed the poles in 3.6 have order 3. Now, the axion self-interactions do not involve time derivatives, so we do not expect poles in the classical folded bispectrum. Actually, another result from [12] suggests that there should not be any difference at all between the quantum and the classical bispectra if the interaction term does not involve derivatives. The authors show that for a generic cubic interaction of the form $H_{\rm int} = -\frac{\lambda}{3!}\Pi_l(\hat{D}_l\zeta)$, with $l = 1, 2, 3$ and $\hat{D}_l$ some local differential operator, the quantum and the classical three-point functions differ from each other according to:

$$\langle\zeta(\vec{x}_1,\tau)\zeta(\vec{x}_2,\tau)\zeta(\vec{x}_3,\tau)\rangle_q - \langle\zeta(\vec{x}_1,\tau)\zeta(\vec{x}_2,\tau)\zeta(\vec{x}_3,\tau)\rangle_c =$$
$$\frac{i\lambda}{4!}\sum_\sigma\int_{-\infty}^{\tau}d\tau' d^3\vec{x}' a^4(\tau')\left[\zeta(\vec{x}_1,\tau),\hat{D}_{\sigma(1)}\zeta(\vec{x}',\tau')\right]\left[\zeta(\vec{x}_2,\tau),\hat{D}_{\sigma(2)}\zeta(\vec{x}',\tau')\right]\times$$
$$\left[\zeta(\vec{x}_3,\tau),\hat{D}_{\sigma(3)}\zeta(\vec{x}',\tau')\right], \quad (3.7)$$

where σ is a permutation of $(1, 2, 3)$. This result can be generalized to $l > 3$. Notice that the commutators require the presence of at least one time derivative in the interaction Hamiltonian, otherwise they vanish. However, the expansion of the cosine in the axion potential 2.3 can only yield terms of the form $\delta\phi^n$, so by 3.7 we should not observe any difference between the three-point functions. With this mind, we now turn to computing the axion bispectrum.

3.2 Axion Field Bispectrum

3.2.1 Quantum Bispectrum

We begin by computing the quantum bispectrum of the axion field perturbations. The bispectrum is related to the three-point function in Fourier space via:

$$\left\langle\delta\chi(\eta,\vec{k_1})\delta\chi(\eta,\vec{k_2})\delta\chi(\eta,\vec{k_3})\right\rangle = (2\pi)^3\delta^{(3)}(\vec{k}_1+\vec{k}_2+\vec{k}_3)B(k_1,k_2,k_3,\eta), \quad (3.8)$$

where $\delta\chi(\eta,\vec{k})$ is the axion field perturbation and $B(k_1, k_2, k_3, \eta)$ is the bispectrum. In the previous sections, we have decomposed the axion into a homogeneous background and a fluctuation $\delta\chi$ which we have computed up to second order. Indeed, at first order the three-point function vanishes because $\left\langle\delta\chi^{(1)}(\eta,\vec{k_1})\delta\chi^{(1)}(\eta,\vec{k_2})\delta\chi^{(1)}(\eta,\vec{k_3})\right\rangle$ involves the vacuum expectation value of three ladder operators. Thus, the lowest-order contribution to the bispectrum entails a single $\delta\chi^{(2)}$:

$$\left\langle\delta\chi^{(1)}(\eta,\vec{k_1})\delta\chi^{(1)}(\eta,\vec{k_2})\delta\chi^{(2)}(\eta,\vec{k_3})\right\rangle, \quad (3.9)$$

which involves the expectation value of four ladder operators. Using (2.57), we have:

$$\int_{-\infty}^{\eta} d\eta' \frac{-u^*_{k_3}(\eta')u_{k_3}(\eta) + u_{k_3}(\eta')u^*_{k_3}(\eta)}{u_{k_3}(\eta')u^{*\prime}_{k_3}(\eta') - u'_{k_3}(\eta')u^*_{k_3}(\eta')} \frac{m^2 e^{-\eta'}}{2fH^2(\eta')} \sin(\bar{\theta}(\eta')) \times \\ \times \int \frac{d^3\vec{k}}{(2\pi)^3} \left\langle \delta\chi^{(1)}(\eta, \vec{k_1})\delta\chi^{(1)}(\eta, \vec{k_2})\delta\chi^{(1)}(\eta', \vec{k}_3 - \vec{k})\delta\chi^{(1)}(\eta', \vec{k}) \right\rangle . \quad (3.10)$$

The vacuum expectation value (v.e.v.) in equation (3.10) can be evaluated using Wick's theorem. The theorem states that the time-ordered product of a set of operators can be decomposed into a sum of normal-ordered products involving all possible contractions of the operators. Let us unpack this statement. The contraction of two operators is defined as:

$$\mathcal{C}(\hat{A}\hat{B}) = \langle 0|T(\hat{A}\hat{B})|0\rangle, \quad (3.11)$$

where T is the time-ordering operator. T acts on a product of operators by moving those evaluated earlier in time to the right:

$$T(\hat{A}(\eta_A, \vec{x}_A)\hat{B}(\eta_B, \vec{x}_B)) = \begin{cases} \hat{A}(\eta_A, \vec{x}_A)\hat{B}(\eta_B, \vec{x}_B) & \eta_A > \eta_B \\ \pm\hat{B}(\eta_B, \vec{x}_B)\hat{A}(\eta_A, \vec{x}_A) & \eta_A < \eta_B. \end{cases} \quad (3.12)$$

The sign $\pm$ depends on whether the operators considered are bosonic or fermionic. In the latter case, their anti-commuting properties would yield a minus sign. Notice that the four $\delta\chi^{(1)}$'s in (3.10) are time-ordered since η is the upper bound of the integral in η', so $\eta' < \eta$. Finally, the normal ordering acts on a product of ladder operators by moving the annihilation operators to the right. We will denote it with colons, for example:

$$: aa^\dagger a^\dagger a := a^\dagger a^\dagger aa. \quad (3.13)$$

The vacuum expectation value of a normal-ordered product is then, by construction, 0. Therefore, Wick's theorem can be rendered as follows:

$$\begin{aligned} T(\hat{A}\hat{B}\hat{C}...\hat{X}\hat{Y}\hat{Z}) =: \hat{A}\hat{B}\hat{C}...\hat{X}\hat{Y}\hat{Z} : + \\ \mathcal{C}(\hat{A}\hat{B}) : \hat{C}...\hat{X}\hat{Y}\hat{Z} : + \cdots + \\ \mathcal{C}(\hat{A}\hat{B})\mathcal{C}(\hat{C}\hat{D}) : \hat{E}...\hat{X}\hat{Y}\hat{Z} : + \cdots + \\ \mathcal{C}(\hat{A}\hat{B})\mathcal{C}(\hat{C}\hat{D})\mathcal{C}(\hat{E}\hat{F}) : \hat{B}...\hat{X}\hat{Y}\hat{Z} : + \cdots \\ \cdots , \end{aligned} \quad (3.14)$$

where we have listed first the term with no contractions, then the terms involving one contraction, two, three, and so on. Notice that contractions are c-numbers, so they are not affected by the normal ordering and can be pulled out. When computing scattering amplitudes, the bracket with the initial and final states selects the relevant terms from the sum, i.e. the ones involving the appropriate operators to annihilate the initial state and create the final state particles. In the case of a vacuum expectation value, only the terms where all the operators are contracted contribute. Now, the v.e.v. in (3.10) involves four $\delta\chi^{(1)}_k$'s, so there are three ways to form two pairs of contracted fields:

$$\begin{aligned} &\mathcal{C}(\delta\chi_{k_1}(\eta)\delta\chi_{k_2}(\eta))\mathcal{C}(\delta\chi_{k_3-k}(\eta')\delta\chi_k(\eta')), \\ &\mathcal{C}(\delta\chi_{k_1}(\eta)\delta\chi_{k_3-k}(\eta'))\mathcal{C}(\delta\chi_{k_2}(\eta)\delta\chi_k(\eta')), \\ &\mathcal{C}(\delta\chi_{k_1}(\eta)\delta\chi_k(\eta'))\mathcal{C}(\delta\chi_{k_2}(\eta)\delta\chi_{k_3-k}(\eta)). \end{aligned} \quad (3.15)$$

However, the first of these three possibilities corresponds to a disconnected vacuum diagram, while the only meaningful contractions are among fields evaluated at different times.
Thus, $\langle\delta\chi^{(1)}(\eta, \vec{k_1})\delta\chi^{(1)}(\eta, \vec{k_2})\delta\chi^{(1)}(\eta', \vec{k}_3 - \vec{k})\delta\chi^{(1)}(\eta', \vec{k})\rangle$ yields two terms:

$$\left\langle \delta\chi^{(1)}(\eta, \vec{k}_1)\delta\chi^{(1)}(\eta, \vec{k}_2)\delta\chi^{(1)}(\eta', \vec{k}_3 - \vec{k})\delta\chi^{(1)}(\eta', \vec{k}) \right\rangle = u_{k_1}(\eta)u^*_{k_3-k}(\eta')u_{k_2}(\eta)u^*_k(\eta') \\ (2\pi)^6 \left(\delta^{(3)}(\vec{k}_1 + \vec{k}_3 - \vec{k})\delta^{(3)}(\vec{k}_2 + \vec{k}) + \delta^{(3)}(\vec{k}_2 + \vec{k}_3 - \vec{k})\delta^{(3)}(\vec{k}_1 + \vec{k}) \right) . \quad (3.16)$$

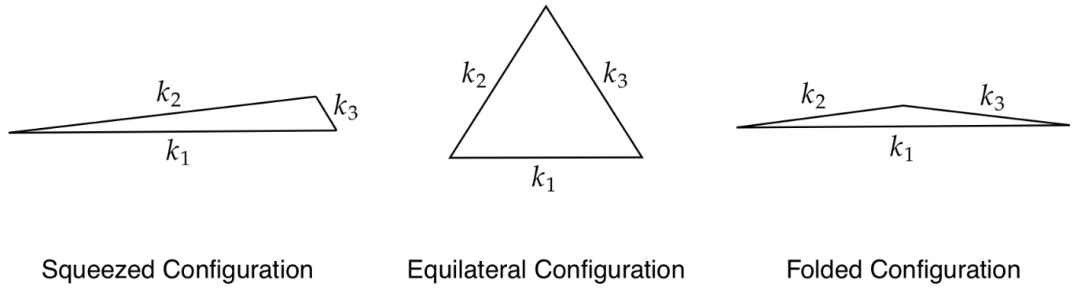

Figure 3.1: Bispectrum triangle configurations. Picture taken from [8].

Enforcing the Dirac delta's using the integration over $d^3\vec{k}$ we obtain an overall momentum-conserving delta $\delta^{(3)}(\vec{k}_1 + \vec{k}_2 + \vec{k}_3)$, so that equation (3.10) now has the standard form (3.8), with $B(k_1, k_2, k_3, \eta)$ given by:

$$B(k_1, k_2, k_3, \eta) = \frac{m^2}{f} \int_{-\infty}^{\eta} d\eta' \frac{-u^*_{k_3}(\eta')u_{k_3}(\eta) + u_{k_3}(\eta')u^*_{k_3}(\eta)}{u_{k_3}(\eta')u^{*\prime}_{k_3}(\eta') - u'_{k_3}(\eta')u^*_{k_3}(\eta')} \frac{e^{-\eta'}}{H^2(\eta')} \sin(\bar{\theta}(\eta')) \times \\ \times u_{k_1}(\eta)u_{k_2}(\eta)u^*_{k_1}(\eta')u^*_{k_2}(\eta'). \quad (3.17)$$

The condition enforced by the Dirac delta, $\vec{k}_1 + \vec{k}_2 + \vec{k}_3 = 0$, has a geometrical interpretation: the three wave vectors form a closed triangle. This constraint gives rise to various possible configurations. Out of the several options, three are particularly significant: *equilateral*, *folded* and *squeezed*. As the name suggests, in the equilateral configuration the three wave vectors all have similar magnitudes, $k_1 \approx k_2 \approx k_3$. The configuration is said to be folded when one of the modes is the sum of the other two, e.g. $k_3 = k_1 + k_2$. Finally, in the squeezed configuration one mode is much smaller than the other two, which in turn are similar, e.g. $k_2 \approx k_3 >> k_1$. A sketch of the three configurations is displayed in Figure 3.1. The numerical results for the axion bispectrum are shown in Figures 3.2 through 3.6. The numerical computation proved really challenging because the η' integral in (3.17) becomes highly oscillatory, especially when considering initial background values close to π. Nonetheless, we can appreciate that the bispectrum is enhanced near the potential hilltop, while the evolution prior to the background oscillations is the same for $\theta_0 = 0.1\pi$ and $\theta_0 = 0.9\pi$. This behavior is observed in all three configurations. However, for the same θ_0, the squeezed one produces the largest bispectrum. This is because in the squeezed configuration, one of the modes is much smaller than the other two. Perturbation modes with smaller k stay outside of the horizon for longer and, as we have seen, the amplitude of the mode functions grows while the corresponding k is super-horizon. Thus, compared to the equilateral and folded configurations, the introduction of a mode much smaller than the other two enhances the bispectrum in the squeezed case. For the same reason, the equilateral configuration produces a slightly larger bispectrum than the folded one because in the latter case one mode is larger than the other two, being their sum. A comparison of the growth of $|u_k|^2$ for $k = 5, 100, 200\,\text{GeV}$ is shown in Figure 3.7. The bispectra shown in Figures 3.2 through 3.6 were obtained setting $k_1 = k_2 = k_3 = 100\,\text{GeV}$ for the equilateral configuration, $k_1 = k_2 + k_3$ with $k_2 = k_3 = 100\,\text{GeV}$ for the folded one and $k_1 = k = 5\,\text{GeV}$ along with $k_2 = k_3 = K = 100\,\text{GeV}$ for the squeezed configuration. The vertical line $\eta = \eta_k$ corresponds to the time when the smallest mode of the squeezed configuration, k, crosses the horizon during inflation, while the line $\eta = \eta_K$ marks the horizon crossing of K. As in previous figures, η_{osc} is the time when $m = H(\eta_{\text{osc}})$.

3.2.2 Classical Bispectrum

The steps that led to equation (3.10) never relied on a_k and $a^\dagger_{-k}$ being non-commuting quantum operators. It is only in the evaluation of the vacuum expectation value

$$\langle \delta\chi^{(1)}(\eta, \vec{k}_1)\delta\chi^{(1)}(\eta, \vec{k}_2)\delta\chi^{(1)}(\eta', \vec{k}_3 - \vec{k})\delta\chi^{(1)}(\eta', \vec{k})\rangle$$

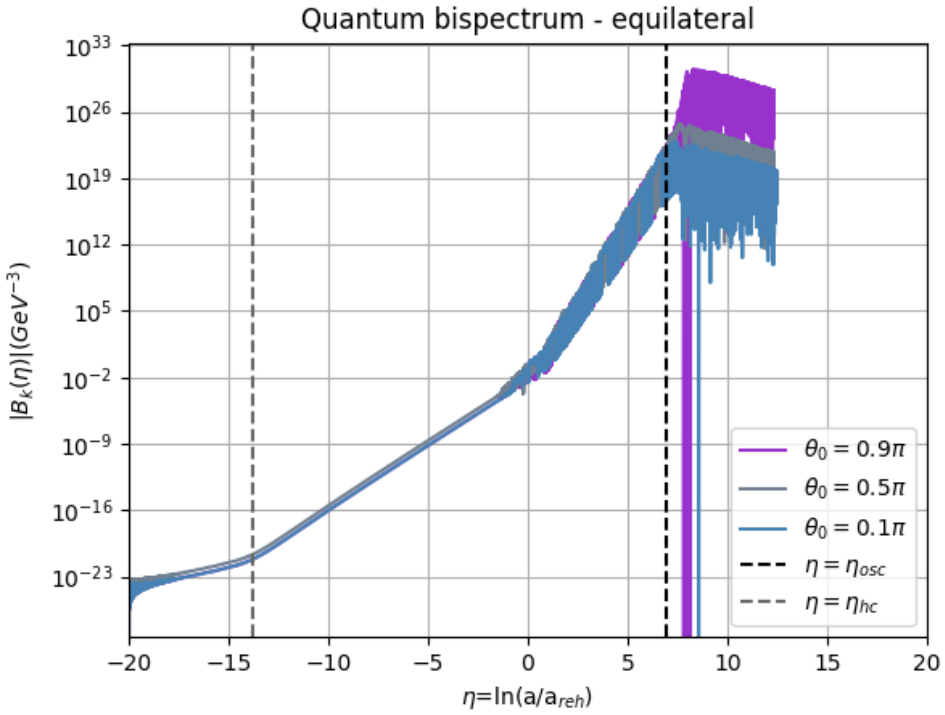

Figure 3.2: Bispectrum of the axion field perturbations in the equilateral configuration for $\theta_0 = 0.1\pi$, $\theta_0 = 0.5\pi$ and $\theta_0 = 0.9\pi$. The bispectrum involves a highly oscillatory integral which becomes harder to compute near the potential hilltop. Nonetheless, we can appreciate that the bispectrum is enhanced approaching the maximum. For the numerical integration the three modes were all set to 100 GeV.

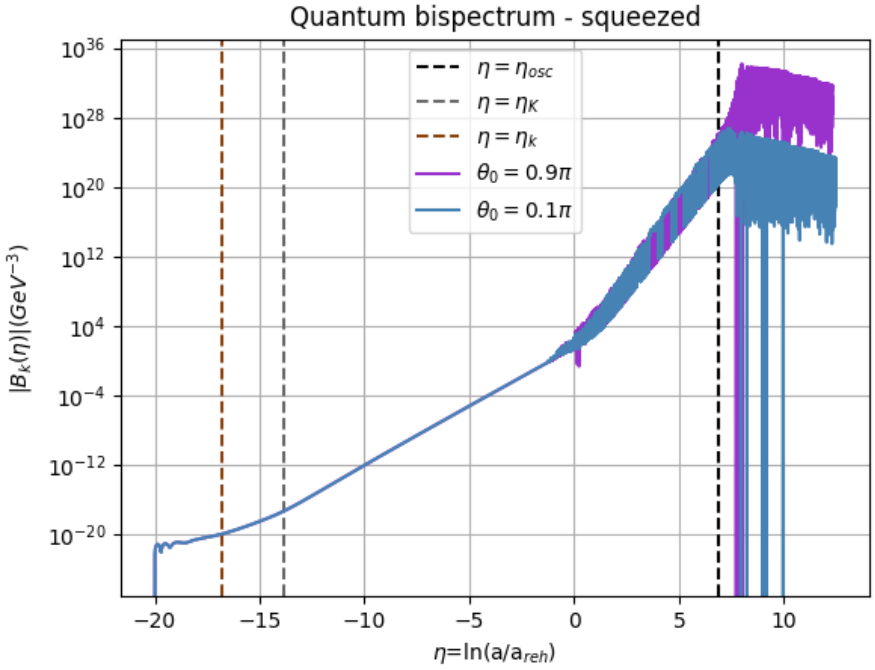

Figure 3.3: Bispectrum of the axion field perturbations in the squeezed configuration for $\theta_0 = 0.1\pi$ and $\theta_0 = 0.9\pi$. As for the equilateral configuration, the bispectrum is enhanced near the potential hilltop. The calculation was performed setting $k_1 = 5\,\text{GeV}$ and $k_2 = k_3 = 100\,\text{GeV}$. The horizon-crossing of k_1 is indicated by the brown dashed line, while the gray line corresponds to the horizon-crossing of k_2 and k_3.

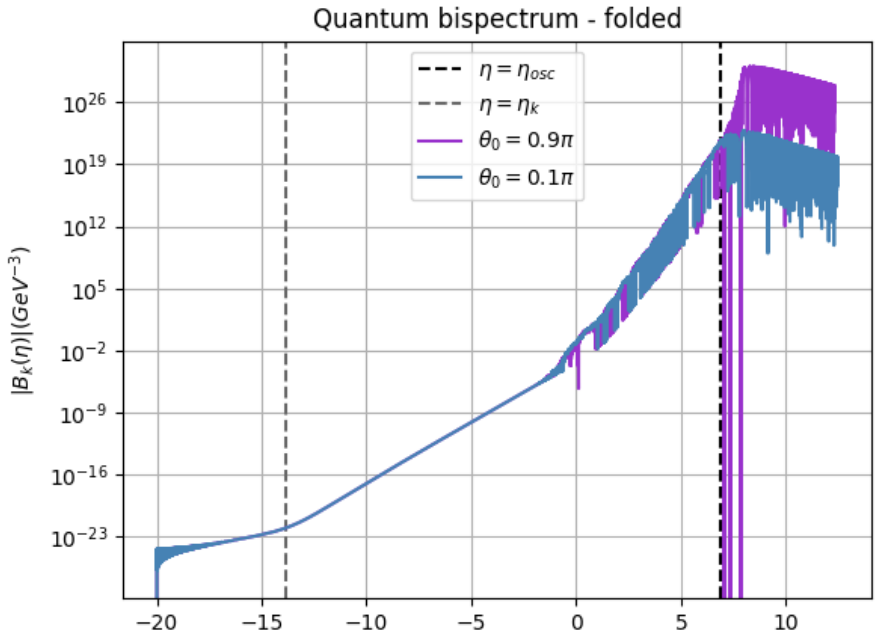

Figure 3.4: Bispectrum of the axion field perturbations in the folded configuration for $\theta_0 = 0.1\pi$ and $\theta_0 = 0.9\pi$. As for the equilateral configuration, the bispectrum is enhanced near the potential hilltop. The calculation was performed setting $k_1 = k_2 + k_3$, with $k_2 = k_3 = 100\,\mathrm{GeV}$.

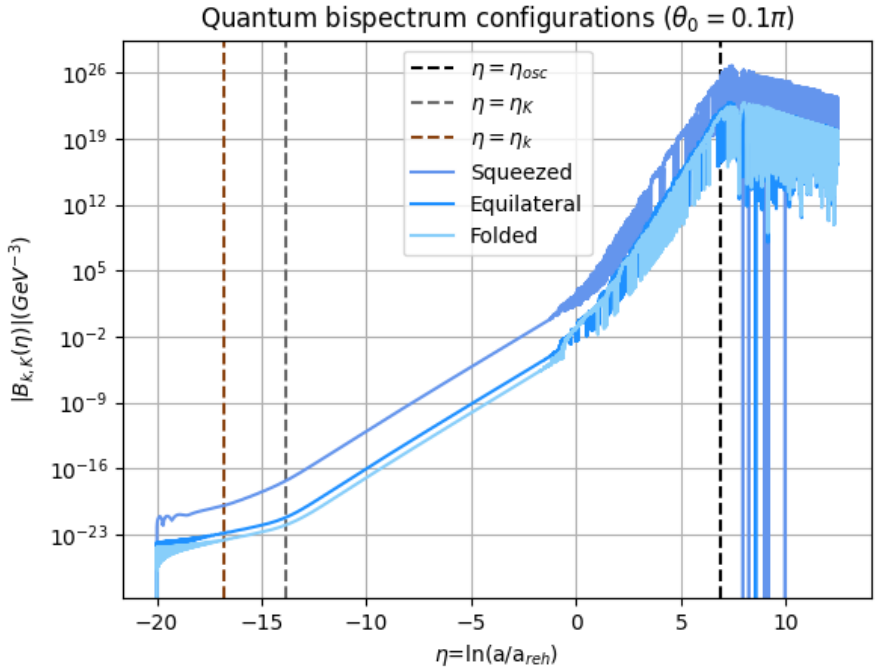

Figure 3.5: Bispectrum of the axion field perturbations for $\theta_0 = 0.1\pi$ in the equilateral, folded and squeezed configurations. The specific instances considered for the folded and squeezed cases were $k_1 = k_2 + k_3$ and $k_1 << k_2 = k_3$ respectively. The squeezed configuration produces the largest bispectrum, while the equilateral and folded configurations yield similar results. This latter fact is due to the enhancement of the mode functions in the super-horizon regime, which is more conspicuous for smaller modes because they stay outside of the horizon for longer. Hence, the squeezed configuration is enhanced because it involves a smaller k. For the same reason, the equilateral bispectrum is slightly larger than the folded one because in the latter case one k is the sum of the other two and is therefore larger.

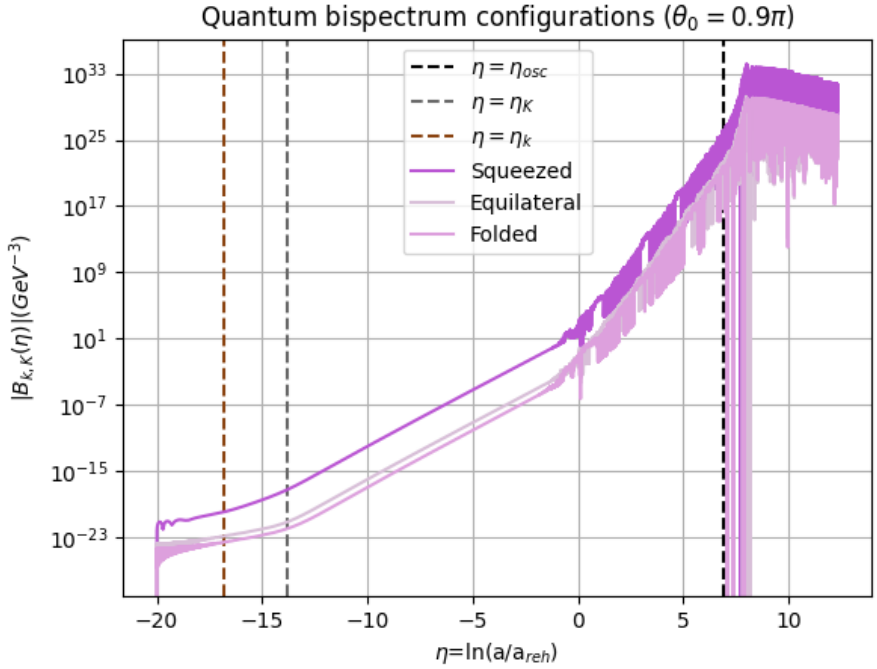

Figure 3.6: Bispectrum of the axion field perturbations for $\theta_0 = 0.9\pi$ in the equilateral, folded and squeezed configurations. The specific instances considered for the folded and squeezed cases were $k_1 = k_2 + k_3$ and $k_1 << k_2 = k_3$ respectively. As observed for the case of $\theta_0 = 0.1\pi$, the bispectrum is enhanced in the squeezed configuration, while the equilateral and folded configurations yield very similar results.

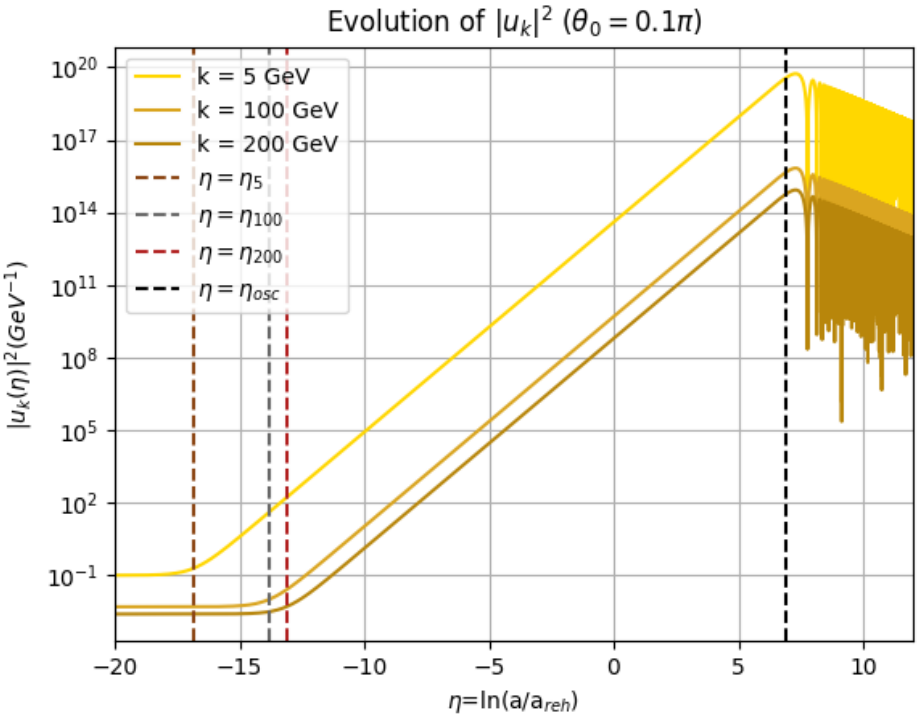

Figure 3.7: Evolution of the amplitude squared of the mode function u_k for $k = 5, 100, 200\,\text{GeV}$ and $\theta_0 = 0.1\pi$. The vertical dashed lines on the left indicate the horizon crossings of the modes considered: the brown one refers to the horizon exit of $k = 5\,\text{GeV}$, the gray one to that of $k = 100\,\text{GeV}$, followed by the horizon exit of the mode $k = 200\,\text{GeV}$ indicated by the red line.

that we leveraged the operator properties of a_k and $a^\dagger_{-k}$. Indeed, the advantage of the Green's function method over the standard in-in computation is that the former is more general and can be applied to both quantum fields and classical variables. In this section, we compute the bispectrum $B(k_1, k_2, k_3, \eta)$ treating a_k and $a^\dagger_{-k}$ as commuting stochastic parameters. In order for the classical set-up to yield the same two-point function as the quantum one, we require:

$$\left\langle a_k a^\dagger_{-k'} \right\rangle_c = \left\langle a^\dagger_{-k'} a_k \right\rangle_c = \frac{1}{2}(2\pi)^3 \delta^{(3)}(\vec{k} + \vec{k'}), \tag{3.18}$$

where the brackets $\langle ... \rangle_c$ now represent an ensemble average and the 1/2 factor appears because a_k and $a^\dagger_{-k}$ commute. Since $\delta\chi^{(1)}_k$ is a Gaussian variable, we can apply Isserlis' theorem. To compute $\langle \delta\chi^{(1)}(\eta, \vec{k}_1)\delta\chi^{(1)}(\eta, \vec{k}_2)\delta\chi^{(1)}(\eta', \vec{k}_3 - \vec{k})\delta\chi^{(1)}(\eta', \vec{k})\rangle_c$, we first substitute the $\delta\chi^{(1)}$'s with their expressions in terms of a_k and $a^\dagger_{-k}$. The product of the four $\delta\chi^{(1)}$'s yields 16 terms but only those with two a_k's and two $a^\dagger_{-k}$'s are non-zero. There are six such terms:

$$\begin{aligned} u_{k_1} u_{k_2} u^*_{k_3-k} u^*_k \left\langle a_{k_1} a_{k_2} a^\dagger_{-k_3+k} a^\dagger_{-k} \right\rangle_c + u_{k_1} u^*_{k_2} u_{k_3-k} u^*_k \left\langle a_{k_1} a^\dagger_{-k_2} a_{k_3-k} a^\dagger_{-k} \right\rangle_c + \\ u_{k_1} u^*_{k_2} u^*_{k_3-k} u_k \left\langle a_{k_1} a^\dagger_{-k_2} a^\dagger_{-k_3+k} a_k \right\rangle_c + u^*_{k_1} u_{k_2} u_{k_3-k} u^*_k \left\langle a^\dagger_{-k_1} a_{k_2} a_{k_3-k} a^\dagger_{-k} \right\rangle_c + \\ u^*_{k_1} u_{k_2} u^*_{k_3-k} u_k \left\langle a^\dagger_{-k_1} a_{k_2} a^\dagger_{-k_3+k} a_k \right\rangle_c + u^*_{k_1} u^*_{k_2} u_{k_3-k} u_k \left\langle a^\dagger_{-k_1} a^\dagger_{-k_2} a_{k_3-k} a_k \right\rangle_c , \end{aligned} \tag{3.19}$$

where the $k_3 - k$ and k mode functions are evaluated at η', while the k_1 and k_2 mode functions at η. As anticipated, these terms can be evaluated using Isserlis' theorem, a useful result for computing the expectation value of a multivariate normal distribution:

$$\langle X_1 ... X_N \rangle = \sum_{p \in P_N} \prod_{(i,j) \in p} \langle X_i X_j \rangle . \tag{3.20}$$

In this notation, p is an element of P_N, the set of all possible pairings of N elements. In other words, $\langle X_1 ... X_N \rangle$ is given by the sum over all pairings of the product of the pair averages $\langle X_i X_j \rangle$. Consider for instance $\left\langle a_{k_1} a_{k_2} a^\dagger_{-k_3+k} a^\dagger_{-k} \right\rangle_c$. Applying Isserlis' theorem we find:

$$\begin{aligned} \left\langle a_{k_1} a_{k_2} a^\dagger_{-k_3+k} a^\dagger_{-k} \right\rangle_c &= \left\langle a_{k_1} a^\dagger_{-k_3+k} \right\rangle_c \left\langle a_{k_2} a^\dagger_{-k} \right\rangle_c + \left\langle a_{k_1} a^\dagger_{-k} \right\rangle_c \left\langle a_{k_2} a^\dagger_{-k_3+k} \right\rangle_c \\ &= \frac{(2\pi)^6}{4} \left(\delta^{(3)}(\vec{k}_1 + \vec{k}_3 - \vec{k}) \delta^{(3)}(\vec{k}_2 + \vec{k}) + \delta^{(3)}(\vec{k}_1 + \vec{k}) \delta^{(3)}(\vec{k}_2 + \vec{k}_3 - \vec{k}) \right) . \end{aligned} \tag{3.21}$$

Because of (3.18), $\left\langle a^\dagger_{-k_1} a^\dagger_{-k_2} a_{k_3-k} a_k \right\rangle_c$ evaluates to the same combination of delta functions. Integrating over $d^3\vec{k}$, the first and last term in (3.19) yield

$$\Re \left(u_{k_1}(\eta) u_{k_2}(\eta) u^*_{k_1}(\eta') u^*_{k_2}(\eta') \right) \delta^{(3)}(\vec{k}_1 + \vec{k}_2 + \vec{k}_3).$$

The terms from the second to the fifth also involve the ensemble averages:

$$\left\langle a_{k_1} a^\dagger_{-k_2} \right\rangle_c = \left\langle a^\dagger_{-k_1} a_{k_2} \right\rangle_c , \tag{3.22}$$

$$\left\langle a_{k_3-k} a^\dagger_{-k} \right\rangle_c = \left\langle a^\dagger_{-k_3+k} a_k \right\rangle_c , \tag{3.23}$$

which are proportional to $\delta^{(3)}(\vec{k}_1 + \vec{k}_2)\delta^{(3)}(\vec{k}_3)$. Since $\vec{k}_3 = 0$ cannot correspond to a fluctuation, these terms do not contribute, as in the quantum calculation. Thus, the classical bispectrum $B_c(k_1, k_2, k_3, \eta)$ reads:

$$\begin{aligned} B_c(k_1, k_2, k_3, \eta) = \int_{-\infty}^{\eta} d\eta' \frac{-u^*_{k_3}(\eta') u_{k_3}(\eta) + u_{k_3}(\eta') u^*_{k_3}(\eta)}{u_{k_3}(\eta') u^*_{k_3}(\eta') - u'_{k_3}(\eta') u^*_{k_3}(\eta')} \frac{m^2 e^{-\eta'}}{2fH^2(\eta')} \sin(\bar{\theta}(\eta')) \times \\ \times \left[\Re \left(u_{k_1}(\eta) u_{k_2}(\eta) u^*_{k_1}(\eta') u^*_{k_2}(\eta') \right) + \Re \left(u_{k_1}(\eta) u^*_{k_2}(\eta) u^*_{k_1}(\eta') u_{k_2}(\eta') \right) \right] . \end{aligned} \tag{3.24}$$

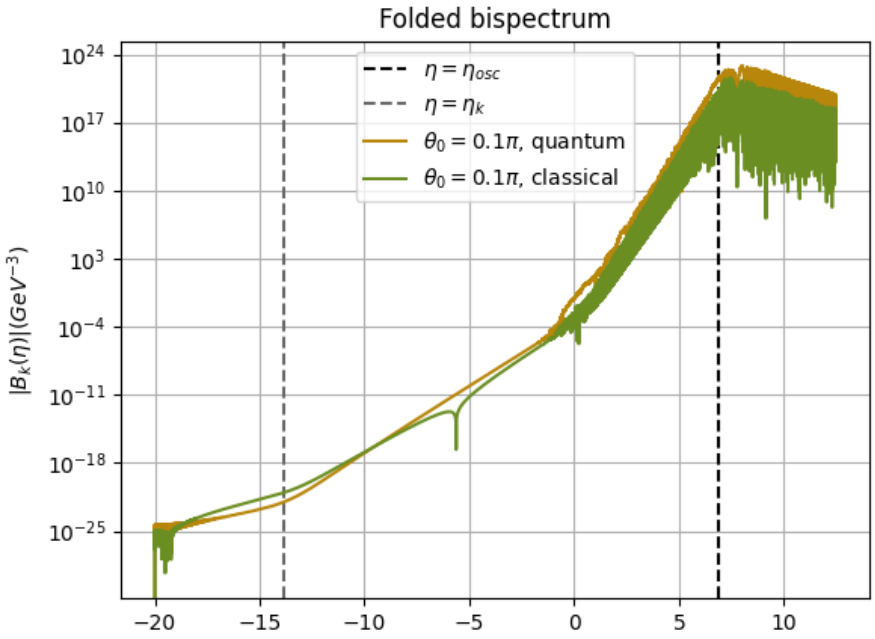

Figure 3.8: Comparison between the quantum and the classical bispectrum in the folded configuration for $\theta_0 = 0.1\pi$. Once again, the classical and the quantum result are very similar. To perform the numerical integration we set $k_1 = k_2 + k_3$ with $k_2 = k_3 = 100\,\text{GeV}$.

$$B_c(k_1,k_2,k_3,\eta) = \frac{B_q(k_1,k_2,k_3,\eta)}{4} + \int_{-\infty}^{\eta} d\eta' \frac{-u^*_{k_3}(\eta')u_{k_3}(\eta) + u_{k_3}(\eta')u^*_{k_3}(\eta)}{u_{k_3}(\eta')u^*_{k_3}(\eta') - u'_{k_3}(\eta')u^*_{k_3}(\eta')} \frac{m^2 e^{-\eta'}}{2fH^2(\eta')} \times$$
$$\times \sin(\bar{\theta}(\eta')) \left[\frac{1}{2}u^*_{k_1}(\eta)u^*_{k_2}(\eta)u_{k_1}(\eta')u_{k_2}(\eta') + \Re\left(u_{k_1}(\eta)u^*_{k_2}(\eta)u^*_{k_1}(\eta')u_{k_2}(\eta')\right)\right]. \tag{3.25}$$

Let us examine this expression and attempt to understand how it differs from the quantum result. By writing $\Re\left(u_{k_1}(\eta)u_{k_2}(\eta)u^*_{k_1}(\eta')u^*_{k_2}(\eta')\right)$ as

$$\frac{1}{2}\left(u_{k_1}(\eta)u_{k_2}(\eta)u^*_{k_1}(\eta')u^*_{k_2}(\eta') + u^*_{k_1}(\eta)u^*_{k_2}(\eta)u_{k_1}(\eta')u_{k_2}(\eta')\right), \tag{3.26}$$

we can express the classical bispectrum in terms of the quantum one, which we denote with $B_q(k_1,k_2,k_3,\eta)$: The 1/4 multiplying $B_q(k_1,k_2,k_3,\eta)$ is simply due to the 1/2 in (3.18), while the two terms in the square brackets stem from the commutativity of the classical a_k and $a^\dagger_k$. In quantum mechanics $\langle\delta\chi_{k_1}(\eta)\delta\chi_{k_3-k}(\eta')\rangle\ \langle\delta\chi_{k_2}(\eta)\delta\chi_k(\eta')\rangle$ and $\langle\delta\chi_{k_1}(\eta)\delta\chi_k(\eta')\rangle\ \langle\delta\chi_{k_2}(\eta)\delta\chi_{3-k}(\eta')\rangle$ result only in a term proportional to $u_{k_1}(\eta)u_{k_2}(\eta)u^*_{k_3-k}(\eta')u^*_k(\eta')$ because $a_k|0\rangle = \langle 0|a^\dagger_{-k'} = 0$. However, in this classical set-up $\langle a^\dagger_{-k'}a_k\rangle \neq 0$, so, for instance, $\langle\delta\chi_{k_1}(\eta)\delta\chi_{k_3-k}(\eta')\rangle\ \langle\delta\chi_{k_2}(\eta)\delta\chi_k(\eta')\rangle$ involves also the products $u^*_{k_1}(\eta)u^*_{k_2}(\eta)u_{k_3-k}(\eta')u_k(\eta')$, $u_{k_1}(\eta)u^*_{k_2}(\eta)u^*_{k_3-k}(\eta')u_k(\eta')$ and $u^*_{k_1}(\eta)u_{k_2}(\eta)u_{k_3-k}(\eta')u^*_k(\eta')$.
The numerical results for (3.24) in the folded configuration are shown in Figures 3.8 and 3.9. The integration was performed setting $k_1 = k_2 + k_3$ with $k_2 = k_3 = 100\,\text{GeV}$. We find that the classical bispectrum is very similar to the quantum result rather than enhanced. The figures show the comparison only for $\theta_0 = 0.1\pi$, but the agreement is also observed for $\theta_0 = 0.9\pi$. The absence of the poles aligns with our expectations from the discussion at the beginning of this chapter. However, we also notice a small enhancement of the quantum bispectrum during the background oscillations. Whether this difference is an artifact of the numerical integration or a genuine effect could not be determined because the computation was fully numerical.

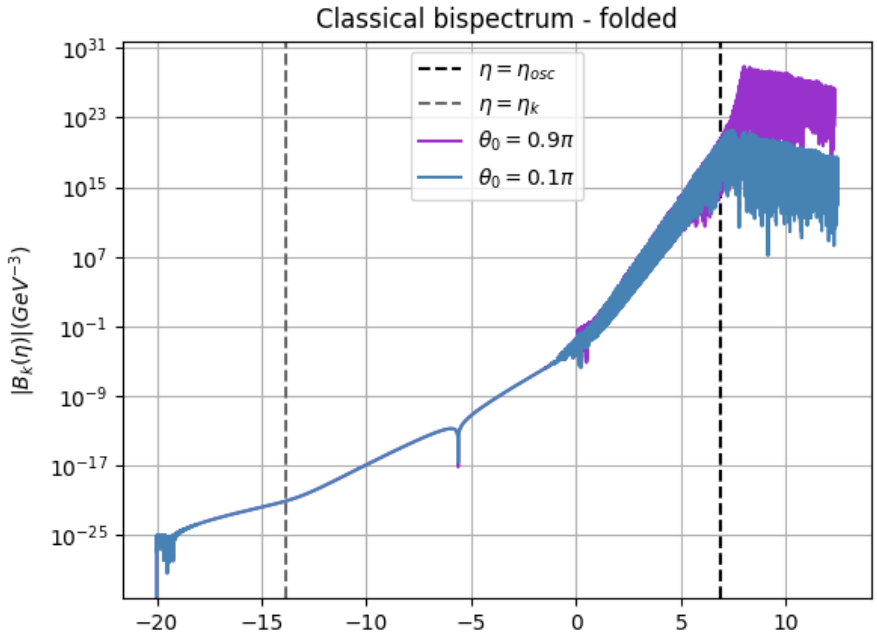

Figure 3.9: Classical bispectrum of the axion field perturbations in the folded configuration for $\theta_0 = 0.1\pi$ and $\theta_0 = 0.9\pi$. As in the quantum result, initial displacement angles closer to the maximum of the potential enhance the bispectrum. For the computation the modes were set to $k_1 = 200\,\text{GeV}$ and $k_2 = k_3 = 100\,\text{GeV}$.

3.3 Axion Energy Density Bispectrum

In this section we compute the quantum bispectrum of the axion energy density perturbations, $B_{\delta\rho_k}(k_1, k_2, k_3, \eta)$, defined analogously to the bispectrum of the field fluctuations:

$$\langle \delta\rho_{k_1}(\eta)\delta\rho_{k_2}(\eta)\delta\rho_{k_3}(\eta)\rangle = \delta^{(3)}(\vec{k}_1 + \vec{k}_2 + \vec{k}_3) B_{\delta\rho_k}(k_1, k_2, k_3, \eta). \tag{3.27}$$

We begin by deriving an expression for the density perturbation $\delta\rho$. The energy density ρ is given by:

$$\rho = \frac{1}{2}H^2\phi'^2(\eta, \vec{x}) + \frac{1}{2e^{2\eta}}\delta^{ij}\partial_i\phi(\eta, \vec{x})\partial_j\phi(\eta, \vec{x}) + V(\phi), \tag{3.28}$$

where $\phi(\eta, \vec{x}) = \bar{\phi}(\eta) + \delta\phi(\eta, \vec{x})$ and $\delta\phi(\eta, \vec{x}) = \delta\phi^{(1)}(\eta, \vec{x}) + \delta\phi^{(2)}(\eta, \vec{x})$. By expanding equation (3.28) up to second order in the field perturbations we find:

$$\rho = \bar{\rho} + \delta\rho = \bar{\rho} + H^2\bar{\phi}'\left(\delta\phi^{(1)}\right)' + \frac{dV}{d\bar{\phi}}\delta\phi^{(1)} + H^2\bar{\phi}'\left(\delta\phi^{(2)}\right)' + \frac{dV}{d\bar{\phi}}\delta\phi^{(2)} + \frac{1}{2}H^2\left(\delta\phi^{(1)\prime}\right)^2 + \frac{1}{2e^{2\eta}}\left(\partial_i\delta\phi^{(1)}\right)^2 + \frac{1}{2}\frac{d^2V}{d\bar{\phi}^2}\left(\delta\phi^{(1)}\right)^2 + ..., \tag{3.29}$$

with $\bar{\rho} = \frac{1}{2}H^2\bar{\phi}'^2(\eta) + V(\bar{\phi})$. The energy density perturbation in momentum space is therefore:

$$\delta\rho_k = H^2\bar{\phi}'\left(\delta\phi_k^{(1)}\right)' + \frac{dV}{d\bar{\phi}}\delta\phi_k^{(1)} + H^2\bar{\phi}'\left(\delta\phi_k^{(2)}\right)' + \frac{dV}{d\bar{\phi}}\delta\phi_k^{(2)} + \int \frac{d^3\vec{k}'}{(2\pi)^3}\frac{1}{2}\left[\left(\frac{-(k-k')_i k'^i}{e^{2\eta}} + \frac{d^2V}{d\bar{\phi}^2}\right)\delta\phi^{(1)}_{k-k'}\delta\phi^{(1)}_{k'} + H^2\delta\phi^{(1)\prime}_{k-k'}\delta\phi^{(1)\prime}_{k'}\right] + \cdots, \tag{3.30}$$

where, again, we are considering contributions up to second order in $\delta\phi^{(1)}$ and linear in $\delta\phi^{(2)}$. We can recognize a first-order contribution, given by the first two terms in (3.30), and a second-order one, given by the terms proportional to $(\delta\phi^{(1)})^2$ and $\delta\phi^{(2)}$. For convenience, we therefore write $\delta\rho_k = \delta\rho_k^{(I)} + \delta\rho_k^{(II)}$,

in analogy with the decomposition of $\delta\phi$. As for the field bispectrum, the lowest-order contribution to $\langle\delta\rho_{k_1}\delta\rho_{k_2}\delta\rho_{k_3}\rangle$ will be of the form $\left\langle\delta\rho^{(I)}_{k_1}\delta\rho^{(I)}_{k_2}\delta\rho^{(II)}_{k_3}\right\rangle$, since $\left\langle\delta\rho^{(I)}_{k_1}\delta\rho^{(I)}_{k_2}\delta\rho^{(I)}_{k_3}\right\rangle$ involves the v.e.v. of three ladder operators. In particular, we have:

$$\begin{aligned}
&\left\langle\delta\rho^{(I)}_{k_1}(\eta)\delta\rho^{(I)}_{k_2}(\eta)\delta\rho^{(II)}_{k_3}(\eta)\right\rangle = \\
&\quad\left\langle\left(H^2\bar{\phi}'(\delta\phi^{(1)}_{k_1})'+\frac{dV}{d\bar{\phi}}\delta\phi^{(1)}_{k_1}\right)\left(H^2\bar{\phi}'(\delta\phi^{(1)}_{k_2})'+\frac{dV}{d\bar{\phi}}\delta\phi^{(1)}_{k_2}\right)\left(H^2\bar{\phi}'(\delta\phi^{(2)}_{k_3})'+\frac{dV}{d\bar{\phi}}\delta\phi^{(2)}_{k_3}\right)\right\rangle \\
&\qquad+\int\frac{d^3\vec{k}'}{(2\pi)^3}\frac{1}{2}\left\langle\left(H^2\bar{\phi}'(\delta\phi^{(1)}_{k_1})'+\frac{dV}{d\bar{\phi}}\delta\phi^{(1)}_{k_1}\right)\left(H^2\bar{\phi}'(\delta\phi^{(1)}_{k_2})'+\frac{dV}{d\bar{\phi}}\delta\phi^{(1)}_{k_2}\right)\right. \\
&\qquad\left.\left(\left[\frac{-(k_{3\,i}-k'_i)k'^i}{e^{2\eta}}+\frac{d^2V}{d\bar{\phi}^2}\right]\delta\phi^{(1)}_{k_3-k'}\delta\phi^{(1)}_{k'}+H^2\delta\phi^{(1)'}_{k_3-k'}\delta\phi^{(1)'}_{k'}\right)\right\rangle. \quad (3.31)
\end{aligned}$$

Let us focus on the first term in (3.31):

$$\begin{aligned}
&\left\langle\left(H^2\bar{\phi}'(\delta\phi^{(1)}_{k_1})'+\frac{dV}{d\bar{\phi}}\delta\phi^{(1)}_{k_1}\right)\left(H^2\bar{\phi}'(\delta\phi^{(1)}_{k_2})'+\frac{dV}{d\bar{\phi}}\delta\phi^{(1)}_{k_2}\right)\left(H^2\bar{\phi}'(\delta\phi^{(2)}_{k_3})'+\frac{dV}{d\bar{\phi}}\delta\phi^{(2)}_{k_3}\right)\right\rangle = \\
&\qquad(H^2\bar{\phi}')^3\left\langle\delta\phi^{(1)'}_{k_1}\delta\phi^{(1)'}_{k_2}\delta\phi^{(2)'}_{k_3}\right\rangle+\left(\frac{dV}{d\bar{\phi}}\right)^3\left\langle\delta\phi^{(1)}_{k_1}\delta\phi^{(1)}_{k_2}\delta\phi^{(2)}_{k_3}\right\rangle+ \\
&\quad(H^2\bar{\phi}')^2\left(\frac{dV}{d\bar{\phi}}\right)\left(\left\langle\delta\phi^{(1)'}_{k_1}\delta\phi^{(1)'}_{k_2}\delta\phi^{(2)}_{k_3}\right\rangle+\left\langle\delta\phi^{(1)'}_{k_1}\delta\phi^{(1)}_{k_2}\delta\phi^{(2)'}_{k_3}\right\rangle+\left\langle\delta\phi^{(1)}_{k_1}\delta\phi^{(1)'}_{k_2}\delta\phi^{(2)'}_{k_3}\right\rangle\right)+ \\
&\qquad(H^2\bar{\phi}')\left(\frac{dV}{d\bar{\phi}}\right)^2\left(\left\langle\delta\phi^{(1)'}_{k_1}\delta\phi^{(1)}_{k_2}\delta\phi^{(2)}_{k_3}\right\rangle+\left\langle\delta\phi^{(1)}_{k_1}\delta\phi^{(1)'}_{k_2}\delta\phi^{(2)}_{k_3}\right\rangle+\left\langle\delta\phi^{(1)}_{k_1}\delta\phi^{(1)}_{k_2}\delta\phi^{(2)'}_{k_3}\right\rangle\right). \quad (3.32)
\end{aligned}$$

Since $c_1(\eta,\vec{k})$ and $c_2(\eta,\vec{k})$ satisfy (2.53), these v.e.v.'s will yield expressions similar to the bispectrum (3.17) but involving the mode functions for $\delta\phi$, rather than those of the rescaled perturbation $\delta\chi$, and their time derivatives where $\delta\phi'$ appears. Calling $v_k(\eta)$ the mode functions for $\delta\phi$, we have $v_k(\eta)=e^{-\eta}u_k(\eta)$. Therefore, we can compute the v.e.v.'s in (3.32) one by one:[1]

$$\begin{aligned}
&(H^2\bar{\phi}')^3\left\langle\delta\phi^{(1)'}_{k_1}\delta\phi^{(1)'}_{k_2}\delta\phi^{(2)'}_{k_3}\right\rangle^{"} = (H^2\bar{\phi}')^3 \\
&\qquad\int_{-\infty}^{\eta}d\eta'\frac{-v^*_{k_3}(\eta')v'_{k_3}(\eta)+v_{k_3}(\eta')v'^*_{k_3}(\eta)}{v_{k_3}(\eta')v^{*'}_{k_3}(\eta')-v'_{k_3}(\eta')v^*_{k_3}(\eta')}\frac{m^2}{fH^2(\eta')}\sin(\bar{\theta}(\eta'))v'_{k_1}(\eta)v'_{k_2}(\eta)v^*_{k_1}(\eta')v^*_{k_2}(\eta'), \quad (3.33)
\end{aligned}$$

$$\begin{aligned}
&\left(\frac{dV}{d\phi}\right)^3\left\langle\delta\phi^{(1)}_{k_1}\delta\phi^{(1)}_{k_2}\delta\phi^{(2)}_{k_3}\right\rangle^{"} = \left(\frac{dV}{d\phi}\right)^3 \\
&\qquad\int_{-\infty}^{\eta}d\eta'\frac{-v^*_{k_3}(\eta')v_{k_3}(\eta)+v_{k_3}(\eta')v^*_{k_3}(\eta)}{v_{k_3}(\eta')v^{*'}_{k_3}(\eta')-v'_{k_3}(\eta')v^*_{k_3}(\eta')}\frac{m^2}{fH^2(\eta')}\sin(\bar{\theta}(\eta'))v_{k_1}(\eta)v_{k_2}(\eta)v^*_{k_1}(\eta')v^*_{k_2}(\eta'), \quad (3.34)
\end{aligned}$$

$$\begin{aligned}
&(H^2\bar{\phi}')^2\left(\frac{dV}{d\phi}\right)\left(\left\langle\delta\phi^{(1)'}_{k_1}\delta\phi^{(1)'}_{k_2}\delta\phi^{(2)}_{k_3}\right\rangle^{"}+\left\langle\delta\phi^{(1)'}_{k_1}\delta\phi^{(1)}_{k_2}\delta\phi^{(2)'}_{k_3}\right\rangle^{"}+\left\langle\delta\phi^{(1)}_{k_1}\delta\phi^{(1)'}_{k_2}\delta\phi^{(2)'}_{k_3}\right\rangle^{"}\right) = \\
&(H^2\bar{\phi}')^2\left(\frac{dV}{d\phi}\right)\left(\int_{-\infty}^{\eta}d\eta'\frac{-v^*_{k_3}(\eta')v_{k_3}(\eta)+v_{k_3}(\eta')v^*_{k_3}(\eta)}{v_{k_3}(\eta')v^{*'}_{k_3}(\eta')-v'_{k_3}(\eta')v^*_{k_3}(\eta')}\frac{m^2}{fH^2(\eta')}\sin(\bar{\theta}(\eta'))v'_{k_1}(\eta)v'_{k_2}(\eta)v^*_{k_1}(\eta')v^*_{k_2}(\eta')\right. \\
&\qquad+\int_{-\infty}^{\eta}d\eta'\frac{-v^*_{k_3}(\eta')v'_{k_3}(\eta)+v_{k_3}(\eta')v^{*'}_{k_3}(\eta)}{v_{k_3}(\eta')v^{*'}_{k_3}(\eta')-v'_{k_3}(\eta')v^*_{k_3}(\eta')}\frac{m^2}{fH^2(\eta')}\sin(\bar{\theta}(\eta'))v'_{k_1}(\eta)v_{k_2}(\eta)v^*_{k_1}(\eta')v^*_{k_2}(\eta') \\
&\qquad\left.+\int_{-\infty}^{\eta}d\eta'\frac{-v^*_{k_3}(\eta')v'_{k_3}(\eta)+v_{k_3}(\eta')v^{*'}_{k_3}(\eta)}{v_{k_3}(\eta')v^{*'}_{k_3}(\eta')-v'_{k_3}(\eta')v^*_{k_3}(\eta')}\frac{m^2}{fH^2(\eta')}\sin(\bar{\theta}(\eta'))v_{k_1}(\eta)v'_{k_2}(\eta)v^*_{k_1}(\eta')v^*_{k_2}(\eta')\right), \quad (3.35)
\end{aligned}$$

[1] The notation $\langle\ldots\rangle^{"}$ means that there is a factor $(2\pi)^3\delta^{(3)}(\vec{k}_1+\vec{k}_2+\vec{k}_3)$ multiplying the right-hand side which we omit for brevity.

$$(H^2\bar{\phi}')\left(\frac{dV}{d\phi}\right)^2\left(\left\langle\delta\phi^{(1)\prime}_{k_1}\delta\phi^{(1)}_{k_2}\delta\phi^{(2)}_{k_3}\right\rangle''+\left\langle\delta\phi^{(1)}_{k_1}\delta\phi^{(1)\prime}_{k_2}\delta\phi^{(2)}_{k_3}\right\rangle''+\left\langle\delta\phi^{(1)}_{k_1}\delta\phi^{(1)}_{k_2}\delta\phi^{(2)\prime}_{k_3}\right\rangle''\right)=$$
$$(H^2\bar{\phi}')\left(\frac{dV}{d\phi}\right)^2\left(\int_{-\infty}^{\eta}d\eta'\frac{-v^*_{k_3}(\eta')v_{k_3}(\eta)+v_{k_3}(\eta')v^*_{k_3}(\eta)}{v_{k_3}(\eta')v^{*\prime}_{k_3}(\eta')-v'_{k_3}(\eta')v^*_{k_3}(\eta')}\frac{m^2}{fH^2(\eta')}\sin(\bar{\theta}(\eta'))v'_{k_1}(\eta)v_{k_2}(\eta)v^*_{k_1}(\eta')v^*_{k_2}(\eta')\right.$$
$$+\int_{-\infty}^{\eta}d\eta'\frac{-v^*_{k_3}(\eta')v_{k_3}(\eta)+v_{k_3}(\eta')v^*_{k_3}(\eta)}{v_{k_3}(\eta')v^{*\prime}_{k_3}(\eta')-v'_{k_3}(\eta')v^*_{k_3}(\eta')}\frac{m^2}{fH^2(\eta')}\sin(\bar{\theta}(\eta'))v_{k_1}(\eta)v'_{k_2}(\eta)v^*_{k_1}(\eta')v^*_{k_2}(\eta')$$
$$\left.+\int_{-\infty}^{\eta}d\eta'\frac{-v^*_{k_3}(\eta')v'_{k_3}(\eta)+v_{k_3}(\eta')v^{*\prime}_{k_3}(\eta)}{v_{k_3}(\eta')v^{*\prime}_{k_3}(\eta')-v'_{k_3}(\eta')v^*_{k_3}(\eta')}\frac{m^2}{fH^2(\eta')}\sin(\bar{\theta}(\eta'))v_{k_1}(\eta)v_{k_2}(\eta)v^*_{k_1}(\eta')v^*_{k_2}(\eta')\right). \quad (3.36)$$

The second term in (3.31) yields:

$$\int\frac{d^3\vec{k'}}{(2\pi)^3}\frac{1}{2}\left\langle\left(H^2\bar{\phi}'(\delta\phi^{(1)}_{k_1})'+\frac{dV}{d\phi}\delta\phi^{(1)}_{k_1}\right)\left(H^2\bar{\phi}'(\delta\phi^{(1)}_{k_2})'+\frac{dV}{d\phi}\delta\phi^{(1)}_{k_2}\right)\right.$$
$$\left.\left(\left[\frac{-(k_{3\,i}-k'_i)k'^i}{e^{2\eta}}+\frac{d^2V}{d\phi^2}\right]\delta\phi^{(1)}_{k_3-k'}\delta\phi^{(1)}_{k'}+H^2\delta\phi^{(1)\prime}_{k_3-k'}\delta\phi^{(1)\prime}_{k'}\right)\right\rangle=$$
$$(H^2\bar{\phi}')^2\int\frac{d^3\vec{k'}}{(2\pi)^3}\frac{1}{2}\left[\frac{-(k_{3\,i}-k'_i)k'^i}{e^{2\eta}}+\frac{d^2V}{d\phi^2}\right]\left\langle\delta\phi^{(1)\prime}_{k_1}\delta\phi^{(1)\prime}_{k_2}\delta\phi^{(1)}_{k_3-k'}\delta\phi^{(1)}_{k'}\right\rangle''+$$
$$(H^2\bar{\phi}')^2\int\frac{d^3\vec{k'}}{(2\pi)^3}\frac{1}{2}H^2\left\langle\delta\phi^{(1)\prime}_{k_1}\delta\phi^{(1)\prime}_{k_2}\delta\phi^{(1)\prime}_{k_3-k'}\delta\phi^{(1)\prime}_{k'}\right\rangle''+$$
$$(H^2\bar{\phi}')\frac{dV}{d\phi}\int\frac{d^3\vec{k'}}{(2\pi)^3}\frac{1}{2}\left[\frac{-(k_{3\,i}-k'_i)k'^i}{e^{2\eta}}+\frac{d^2V}{d\phi^2}\right]\left\langle\delta\phi^{(1)\prime}_{k_1}\delta\phi^{(1)}_{k_2}\delta\phi^{(1)}_{k_3-k'}\delta\phi^{(1)}_{k'}\right\rangle''+$$
$$(H^2\bar{\phi}')\frac{dV}{d\phi}\int\frac{d^3\vec{k'}}{(2\pi)^3}\frac{1}{2}H^2\left\langle\delta\phi^{(1)\prime}_{k_1}\delta\phi^{(1)}_{k_2}\delta\phi^{(1)\prime}_{k_3-k'}\delta\phi^{(1)\prime}_{k'}\right\rangle''+$$
$$(H^2\bar{\phi}')\frac{dV}{d\phi}\int\frac{d^3\vec{k'}}{(2\pi)^3}\frac{1}{2}\left[\frac{-(k_{3\,i}-k'_i)k'^i}{e^{2\eta}}+\frac{d^2V}{d\phi^2}\right]\left\langle\delta\phi^{(1)}_{k_1}\delta\phi^{(1)\prime}_{k_2}\delta\phi^{(1)}_{k_3-k'}\delta\phi^{(1)}_{k'}\right\rangle''+$$
$$(H^2\bar{\phi}')\frac{dV}{d\phi}\int\frac{d^3\vec{k'}}{(2\pi)^3}\frac{1}{2}H^2\left\langle\delta\phi^{(1)}_{k_1}\delta\phi^{(1)\prime}_{k_2}\delta\phi^{(1)\prime}_{k_3-k'}\delta\phi^{(1)\prime}_{k'}\right\rangle''+$$
$$\left(\frac{dV}{d\phi}\right)^2\int\frac{d^3\vec{k'}}{(2\pi)^3}\frac{1}{2}\left[\frac{-(k_{3\,i}-k'_i)k'^i}{e^{2\eta}}+\frac{d^2V}{d\phi^2}\right]\left\langle\delta\phi^{(1)}_{k_1}\delta\phi^{(1)}_{k_2}\delta\phi^{(1)}_{k_3-k'}\delta\phi^{(1)}_{k'}\right\rangle''+$$
$$\left(\frac{dV}{d\phi}\right)^2\int\frac{d^3\vec{k'}}{(2\pi)^3}\frac{1}{2}H^2\left\langle\delta\phi^{(1)}_{k_1}\delta\phi^{(1)}_{k_2}\delta\phi^{(1)\prime}_{k_3-k'}\delta\phi^{(1)\prime}_{k'}\right\rangle''=$$
$$(H^2\bar{\phi}')^2\left[\frac{-k_{1_i}k_2^i}{e^{2\eta}}+\frac{d^2V}{d\phi^2}\right]v'_{k_1}v'_{k_2}v^*_{k_1}v^*_{k_2}+(H^2\bar{\phi}')^2H^2v'_{k_1}v'_{k_2}v'^*_{k_1}v'^*_{k_2}+$$
$$(H^2\bar{\phi}')\frac{dV}{d\phi}\left[\frac{-k_{1_i}k_2^i}{e^{2\eta}}+\frac{d^2V}{d\phi^2}\right]v'_{k_1}v_{k_2}v^*_{k_1}v^*_{k_2}+(H^2\bar{\phi}')\frac{dV}{d\phi}H^2v'_{k_1}v_{k_2}v'^*_{k_1}v'^*_{k_2}+$$
$$(H^2\bar{\phi}')\frac{dV}{d\phi}\left[\frac{-k_{1_i}k_2^i}{e^{2\eta}}+\frac{d^2V}{d\phi^2}\right]v_{k_1}v'_{k_2}v^*_{k_1}v^*_{k_2}+(H^2\bar{\phi}')\frac{dV}{d\phi}H^2v_{k_1}v'_{k_2}v'^*_{k_1}v'^*_{k_2}+$$
$$\left(\frac{dV}{d\phi}\right)^2\left[\frac{-k_{1_i}k_2^i}{e^{2\eta}}+\frac{d^2V}{d\phi^2}\right]v_{k_1}v_{k_2}v^*_{k_1}v^*_{k_2}+\left(\frac{dV}{d\phi}\right)^2H^2v_{k_1}v_{k_2}v'^*_{k_1}v'^*_{k_2}, \quad (3.37)$$

where the time dependence of the mode functions has been omitted for brevity. The classical bispectrum can be computed through similar steps, with the only difference that the expectation values are to be evaluated using the statistics 3.18. The numerical results of the energy density bispectrum are shown in Figures 3.10 through 3.16, where we compare the bispectrum for $\theta_0 = 0.1\pi$ and $\theta_0 = 0.9\pi$ in

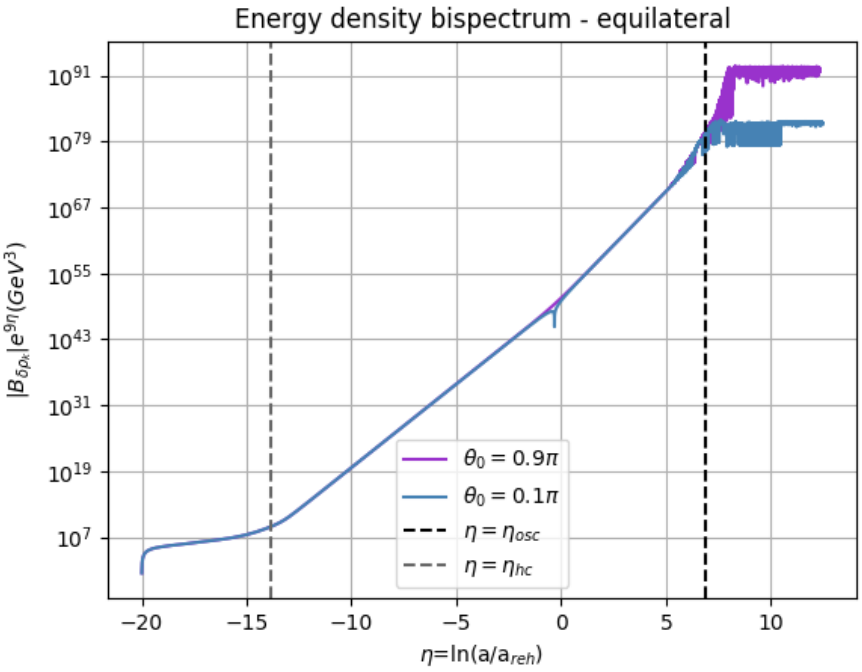

Figure 3.10: Bispectrum of the axion energy density for $\theta_0 = 0.1\pi$ and $\theta_0 = 0.9\pi$ in the equilateral configuration multiplied by $(a/a_{reh})^9 = e^{9\eta}$.

the three configurations divided by the cubed background energy density The modes were set to the same values considered for the bispectrum of the field fluctuations, namely $k_1 = k_2 = k_3 = 100\,\text{GeV}$ in the equilateral configuration, $k_1 = 5\,\text{GeV}$ and $k_2 = k_3 = 100\,\text{GeV}$ for the squeezed one, and $k_1 = k_2 + k_3$ with $k_2 = k_3 = 100\,\text{GeV}$ in the folded case. As for the bispectrum of the axion field, we observe an enhancement near the potential hilltop and a larger bispectrum in the squeezed configuration. Notice that, before the background starts to oscillate, the purple line in Figures 3.11 through 3.13, corresponding to $\theta_0 = 0.9\pi$ is below the blue line, which shows the bispectrum for $\theta_0 = 0.1\pi$. This is due to the fact that we are dividing $|B_{\delta\rho}|$ by the background energy density cubed, $\bar{\rho}^3$. The latter is larger near the potential hilltop, whereas the time evolution of $|B_{\delta\rho}|$ prior to the oscillations is not affected by θ_0. This is better appreciated in Figure 3.10, which compares the equilateral bispectrum multiplied by $(a/a_{\text{reh}})^9 = e^{9\eta}$ for $\theta_0 = 0.1\pi$ and $\theta_0 = 0.9\pi$. As we have seen, the background energy density is constant while θ is overdamped and decreases as a^{-3} during the oscillations. When this happens, the same scaling is also observed in the fluctuation $\delta\rho$. Thus, both $|B_{\delta\rho}|/\bar{\rho}^3$ and $|B_{\delta\rho}|e^{9\eta}$ become constant after $m = H(\eta_{\text{osc}})$. Finally, Figure 3.16 compares the quantum and classical energy density bispectrum in the folded configuration. The classical result shows no enhancement, and the bispectra are very similar up to the onset of the oscillations. From that point on, the quantum bispectrum becomes larger. We noticed a similar behavior in the bispectrum of the field fluctuations and, as in that case, we could not determine whether the enhancement of the quantum result is genuine or due to the numerical integration, which becomes especially challenging in the oscillatory regime.

3.4 Field Dynamics Bispectrum

In this section, we present an alternative computation of the axion bispectrum and compare it with the Green's function method. Since the initial conditions completely determine the evolution of ϕ, we can ascribe the fluctuation $\delta\phi$ to a difference in the initial conditions. In other words, we can think of $\delta\phi$ as the difference in the field evolution due to different initial conditions:

$$\delta\phi = \phi(\bar{\phi}_0 + \delta\phi_0) - \phi(\bar{\phi}_0). \tag{3.38}$$

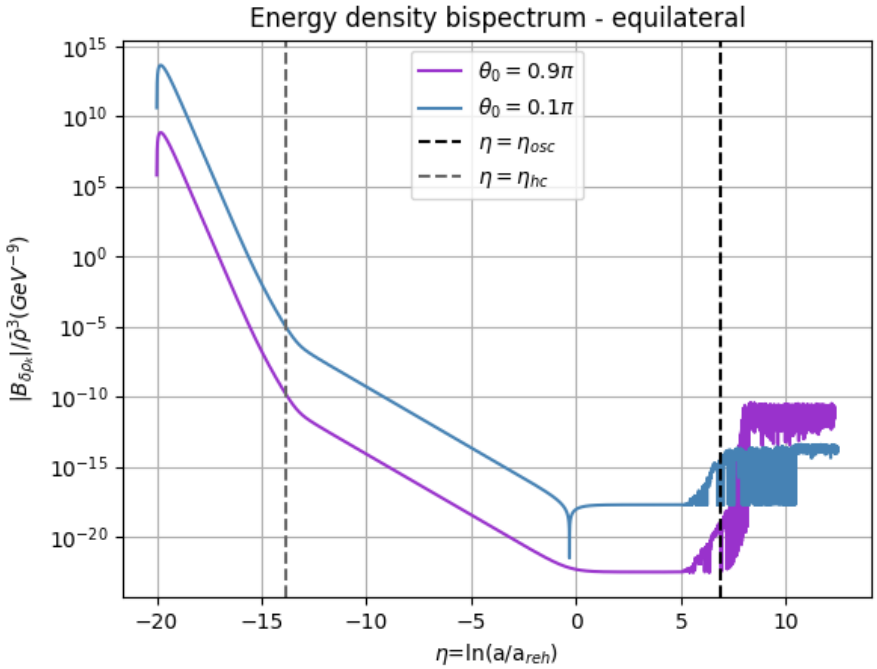

Figure 3.11: Bispectrum of the axion energy density for $\theta_0 = 0.1\pi$ and $\theta_0 = 0.9\pi$ in the equilateral configuration. The modulus of the bispectrum has been divided by the background energy density, which is larger near the potential hilltop. This is why the bispectrum with $\theta_0 = 0.1\pi$ is initially larger even though the time evolution prior to the background oscillations is the same regardless of the initial displacement angle.

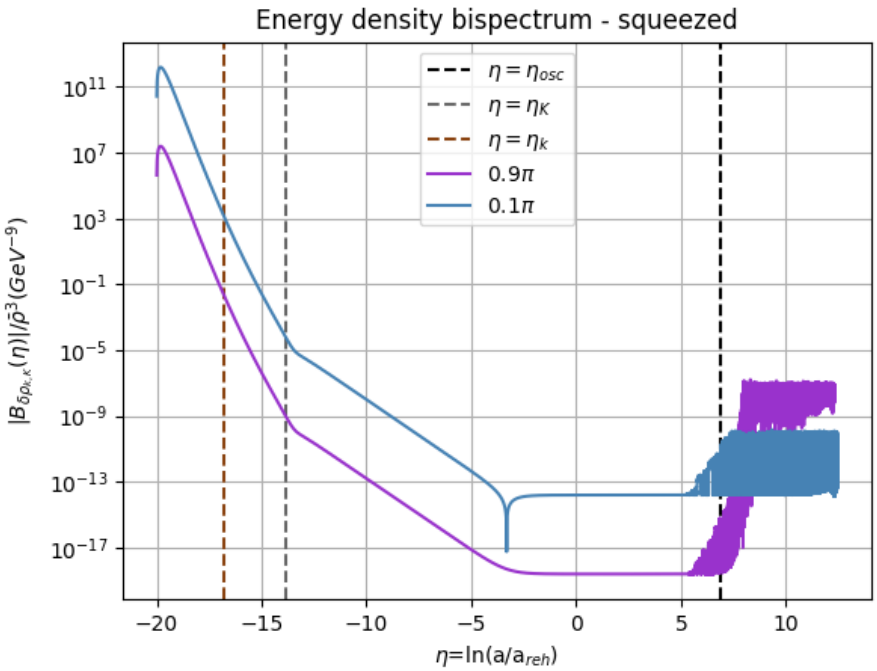

Figure 3.12: Bispectrum of the axion energy density for $\theta_0 = 0.1\pi$ and $\theta_0 = 0.9\pi$ in the squeezed configuration divided by the background energy density.

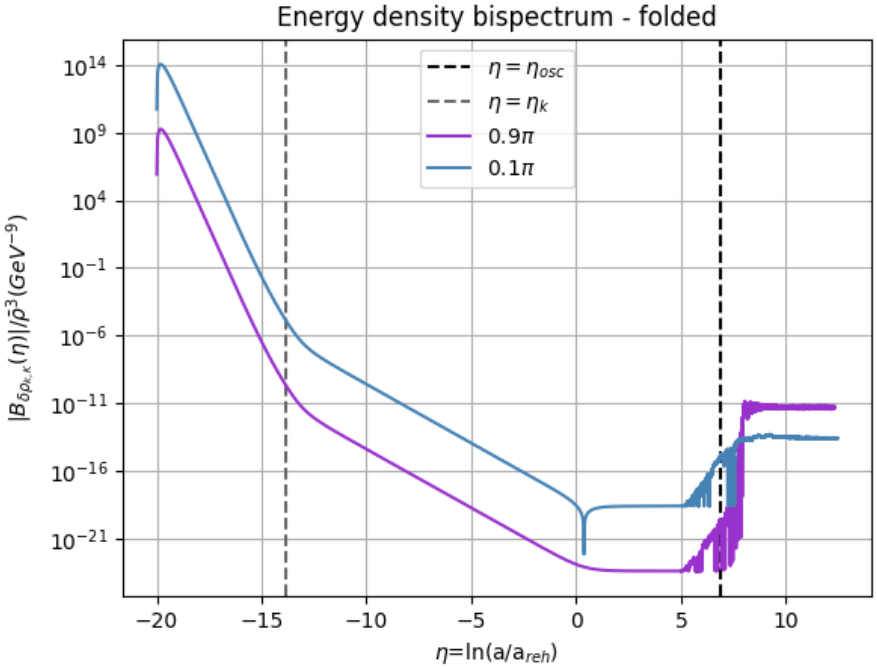

Figure 3.13: Bispectrum of the axion energy density for $\theta_0 = 0.1\pi$ and $\theta_0 = 0.9\pi$ in the folded configuration divided by the background energy density.

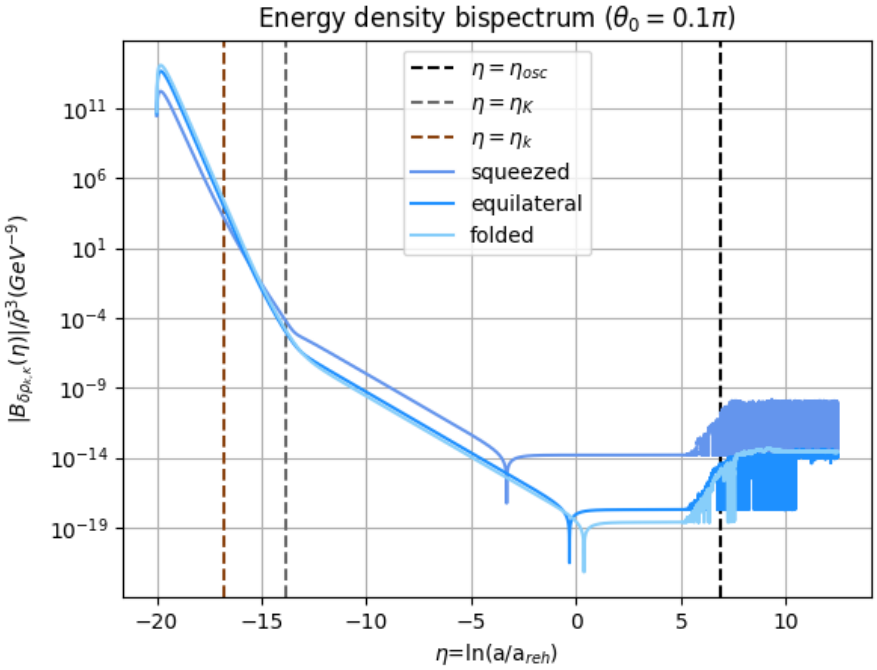

Figure 3.14: Bispectrum of the axion energy density in the equilateral, folded, and squeezed configurations for $\theta_0 = 0.1\pi$. As for the bispectrum of the field, the equilateral configuration yields a result similar to the folded one with $k_1 = k_2 + k_3$, while the squeezed configuration $k_1 << k_2 \approx k_3$ produces a larger bispectrum.

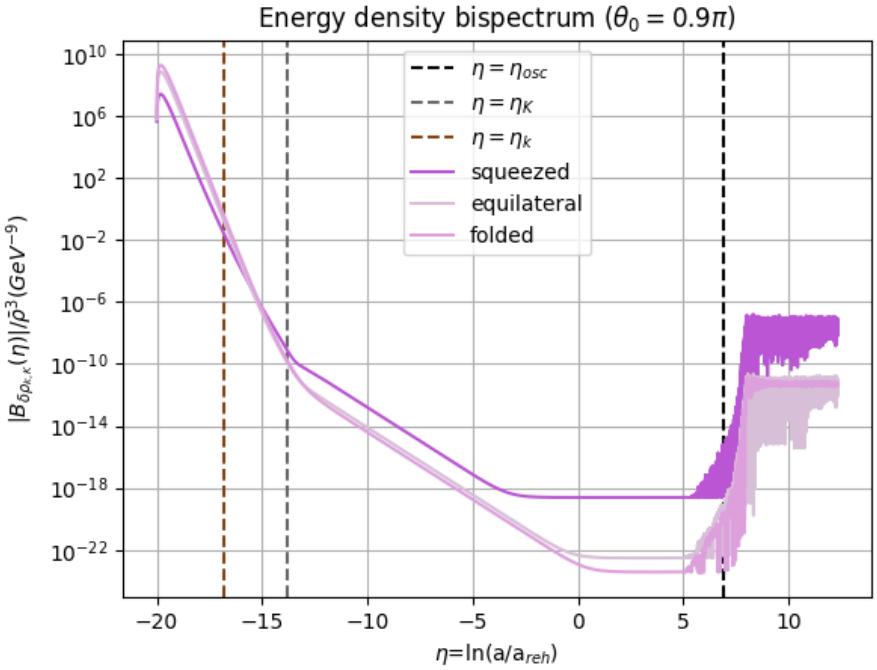

Figure 3.15: Bispectrum of the axion energy density in the equilateral, folded, and squeezed configurations for $\theta_0 = 0.9\pi$. As for the bispectrum of the field, the equilateral configuration yields a result similar to the folded one with $k_1 = k_2 + k_3$, while the squeezed configuration $k_1 << k_2 \approx k_3$ produces a larger bispectrum.

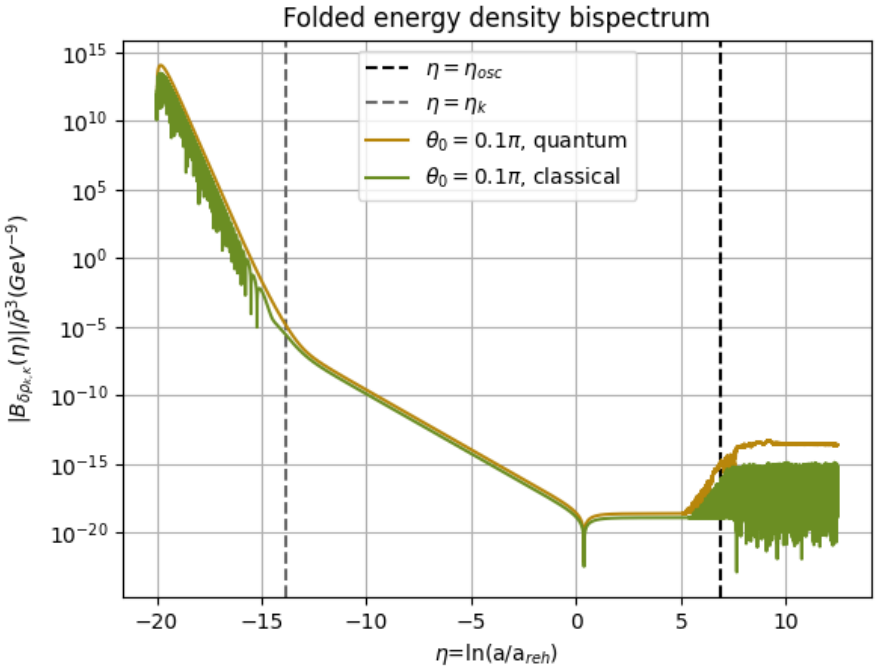

Figure 3.16: Comparison between the quantum and the classical energy density bispectrum in the folded configuration for $\theta_0 = 0.1\pi$. As expected, there is no enhancement of the classical bispectrum over the quantum result. The two are very similar up to the background oscillations, when the quantum bispectrum begins to grow slightly more than the classical one. To perform the numerical integration we set $k_1 = k_2 + k_3$ with $k_2 = k_3 = 100\,\text{GeV}$.

Here $\delta\phi_0$ is the fluctuation $\delta\phi(\eta_0, \vec{x})$ evaluated at some initial time η_0 during inflation. Expanding $\delta\phi$ in $\delta\phi_0$, we have:

$$\delta\phi = \delta\phi_0 \left.\frac{\partial\phi}{\partial\phi_0}\right|_{\phi_0=\bar{\phi}_0} + \frac{\delta\phi_0^2}{2} \left.\frac{\partial^2\phi}{\partial\phi_0^2}\right|_{\phi_0=\bar{\phi}_0} + \frac{\delta\phi_0^3}{6}\frac{\partial^3\phi}{\partial\phi_0^3} + \cdots, \tag{3.39}$$

from which we can single out the perturbation up to second order:

$$\delta\phi = \delta\phi_0 \frac{\partial\bar{\phi}}{\partial\bar{\phi}_0} + \frac{\delta\phi_0^2}{2}\frac{\partial^2\bar{\phi}}{\partial\bar{\phi}_0^2}. \tag{3.40}$$

In terms of $\delta\chi = e^{\eta}\delta\phi$ and passing to Fourier space, (3.40) becomes:

$$\delta\chi_k(\eta) = e^{\eta}\left[e^{-\eta_0}\delta\chi_k(\eta_0)\frac{\partial\bar{\phi}}{\partial\bar{\phi}_0} + \int\frac{d^3\vec{k}'}{(2\pi)^3}\frac{1}{2}\frac{\partial^2\bar{\phi}}{\partial\bar{\phi}_0^2}e^{-2\eta_0}\delta\chi_{k-k'}(\eta_0)\delta\chi_{k'}(\eta_0)\right]. \tag{3.41}$$

We would like to compute the bispectrum yielded by this approximation for $\delta\chi_k$ and compare it with the bispectrum we computed in the previous section. The lowest-order contribution to $\langle\delta\chi_{k_1}(\eta)\delta\chi_{k_2}(\eta)\delta\chi_{k_3}(\eta)\rangle$ reads:

$$\begin{aligned}\langle\delta\chi_{k_1}(\eta)\delta\chi_{k_2}(\eta)\delta\chi_{k_3}(\eta)\rangle = e^{3\eta}\left(\frac{\partial\bar{\phi}}{\partial\bar{\phi}_0}\right)^3 e^{-3\eta_0}\langle\delta\chi_{k_1}(\eta_0)\delta\chi_{k_2}(\eta_0)\delta\chi_{k_3}(\eta_0)\rangle + \\ \frac{e^{3\eta}}{2}\left(\left.\frac{\partial\bar{\phi}}{\partial\phi_0}\right|_{\phi_0=\bar{\phi}_0}\right)^2 \left.\frac{\partial^2\phi}{\partial\phi_0^2}\right|_{\phi_0=\bar{\phi}_0}\int\frac{d^3\vec{k}}{(2\pi)^3}e^{-4\eta_0}\langle\delta\chi_{k_1}(\eta_0)\delta\chi_{k_2}(\eta_0)\delta\chi_{k_3-k}(\eta_0)\delta\chi_k(\eta_0)\rangle.\end{aligned} \tag{3.42}$$

The first term in (3.42) arises if the fluctuations have some intrinsic non-Gaussianity present at the initial time and is usually neglected. We will not consider it as well. To compute the second term we first need to determine $\partial\bar{\phi}/\partial\bar{\phi}_0$ as a function of time. Let us differentiate the background equation of motion (2.13), where $\theta = \phi/f$, with respect to $\bar{\phi}_0$:

$$\left(\frac{\partial\bar{\phi}}{\partial\bar{\phi}_0}\right)'' + \left(3 + \frac{H'}{H}\right)\left(\frac{\partial\bar{\phi}}{\partial\bar{\phi}_0}\right)' + \frac{m^2}{H^2}f\cos\left(\frac{\bar{\phi}}{f}\right)\frac{1}{f}\left(\frac{\partial\bar{\phi}}{\partial\bar{\phi}_0}\right) = 0. \tag{3.43}$$

Calling $\gamma = \partial\bar{\phi}/\partial\bar{\phi}_0$ for a more compact notation, we have:

$$\gamma'' + \left(3 + \frac{H'}{H}\right)\gamma' + \frac{m^2}{H^2}\cos\left(\frac{\bar{\phi}}{f}\right)\gamma = 0, \tag{3.44}$$

which can be solved numerically with the initial conditions $\gamma(\eta_0) = 1$ and $\gamma'(\eta_0) = 0$. In fact, prior to the oscillations, θ is frozen to its initial value by the Hubble friction, so $\theta = \theta_0$ and $\gamma = 1$. Since we also need the second derivative of $\bar{\phi}$ with respect to $\bar{\phi}_0$, we take a further derivative of (3.43) and introduce $\xi = \partial^2\bar{\phi}/\partial\bar{\phi}_0^2$. The equation for ξ then reads:

$$\xi'' + \left(3 + \frac{H'}{H}\right)\xi' + \frac{m^2}{H^2}\left[-\frac{1}{f}\sin\left(\frac{\bar{\phi}}{f}\right)\gamma^2 + \cos\left(\frac{\bar{\phi}}{f}\right)\xi\right] = 0. \tag{3.45}$$

In this case, the appropriate initial conditions are $\xi(\eta_0) = 0$ and $\xi'(\eta_0) = 0$, since the background is initially a linear function of θ_0. Finally, the lowest-order contribution to the bispectrum is given by:

$$\begin{aligned}&\langle\delta\chi_{k_1}(\eta)\delta\chi_{k_2}(\eta)\delta\chi_{k_3}(\eta)\rangle = \\ &\quad= \frac{e^{3\eta}e^{-4\eta_0}}{2}\gamma^2(\eta)\xi(\eta)\int\frac{d^3\vec{k}}{(2\pi)^3}\langle\delta\chi_{k_1}(\eta_0)\delta\chi_{k_2}(\eta_0)\delta\chi_{k_3-k}(\eta_0)\delta\chi_k(\eta_0)\rangle \\ &\quad= \delta^{(3)}(\vec{k}_1 + \vec{k}_2 + \vec{k}_3)e^{3\eta}\gamma^2(\eta)\xi(\eta)e^{-4\eta_0}u_{k_1}(\eta_0)u_{k_2}(\eta_0)u_{k_1}^*(\eta_0)u_{k_2}^*(\eta_0).\end{aligned} \tag{3.46}$$

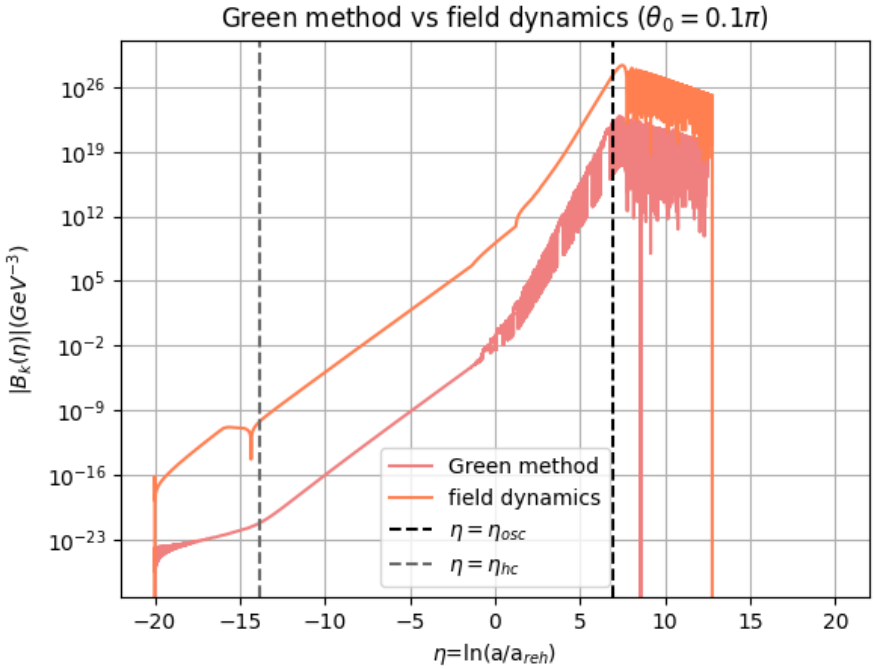

Figure 3.17: Comparison between the bispectrum computed by means of the Green's function method and the bispectrum found assuming $\delta\phi$ is entirely accounted for by the difference in the field evolution brought about by different initial conditions. The bispectra were computed setting $\theta_0 = 0.1\pi$ and in the equilateral configuration.

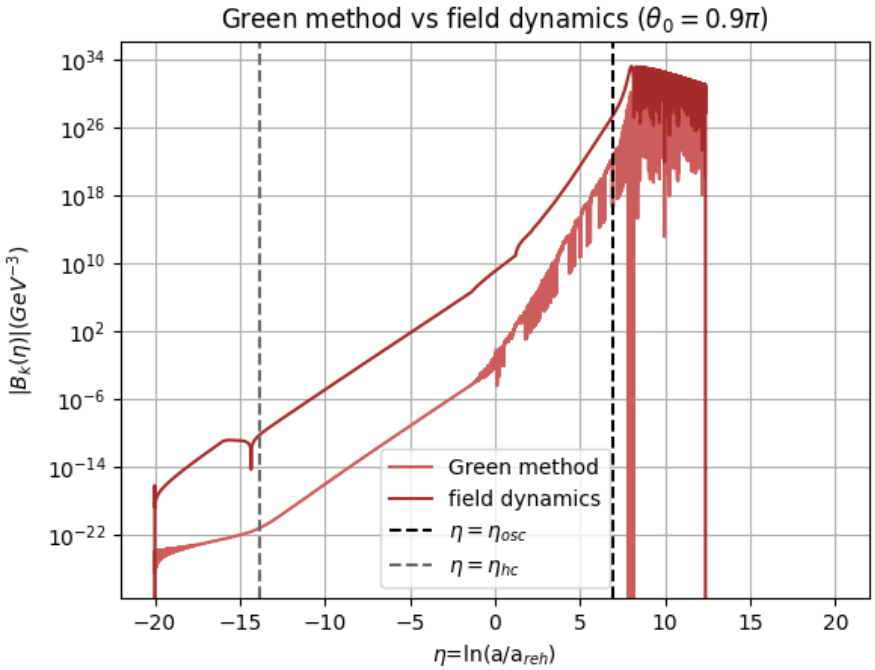

Figure 3.18: Comparison between the bispectrum computed by means of the Green's function method and the bispectrum found assuming $\delta\phi$ is entirely accounted for by the difference in the field evolution brought about by different initial conditions. The bispectra were computed setting $\theta_0 = 0.9\pi$ and in the equilateral configuration.

Let us apply this expansion to the axion energy density (3.28) as well:

$$\rho = \bar{\rho} + \delta\rho = \frac{1}{2}H^2\bar{\phi}'^2 + V(\bar{\phi}) + \delta\phi_0\left(H^2\bar{\phi}'\gamma' + \frac{\partial V}{\partial\phi_0}\right) + \frac{\delta\phi_0^2}{2}\left(H^2\gamma'^2 + H^2\bar{\phi}'\xi' + \frac{\partial^2 V}{\partial\phi_0^2}\right) + \frac{\gamma^2\delta^{ij}}{2e^{2\eta}}\partial_i\delta\phi_0\partial_j\delta\phi_0 + \cdots, \tag{3.47}$$

where we have highlighted only the first- and second-order contributions. The energy density perturbation in momentum space reads:

$$\delta\rho_k = \delta\phi_k(\eta_0)\left(H^2\bar{\phi}'\gamma' + \frac{\partial V}{\partial\phi_0}\right) + \int\frac{d^3\vec{k'}}{(2\pi)^3}\frac{1}{2}\left(H^2\gamma'^2 + H^2\bar{\phi}'\xi' + \frac{\partial^2 V}{\partial\phi_0^2} - \frac{\gamma^2}{e^{2\eta}}(k-k')_i k'^i\right)\delta\phi_{k-k'}(\eta_0)\delta\phi_k(\eta_0). \tag{3.48}$$

The derivatives of the potential in terms of γ and ξ are given by:

$$\left.\frac{\partial V}{\partial\phi_0}\right|_{\phi_0=\bar{\phi}_0} = m^2 f\sin\left(\frac{\bar{\phi}}{f}\right)\gamma, \tag{3.49}$$

$$\left.\frac{\partial^2 V}{\partial\phi_0^2}\right|_{\phi_0=\bar{\phi}_0} = m^2\cos\left(\frac{\bar{\phi}}{f}\right)\gamma^2 + m^2 f\sin\left(\frac{\bar{\phi}}{f}\right)\xi. \tag{3.50}$$

Finally, the lowest-order contribution to $\langle\delta\rho_{k_1}\delta\rho_{k_2}\delta\rho_{k_3}\rangle$ reads:

$$\langle\delta\rho_{k_1}\delta\rho_{k_2}\delta\rho_{k_3}\rangle = \left(H^2\bar{\phi}'\gamma' + \frac{\partial V}{\partial\phi_0}\right)^2\int\frac{d^3\vec{k}}{(2\pi)^3}\frac{1}{2}\left(H^2\gamma'^2 + H^2\bar{\phi}'\xi' + \frac{\partial^2 V}{\partial\phi_0^2} - \frac{\gamma^2}{e^{2\eta}}(k_3-k)_i k^i\right)\times$$

$$\langle\delta\phi_{k_1}(\eta_0)\delta\phi_{k_2}(\eta_0)\delta\phi_{k_3-k}(\eta_0)\delta\phi_k(\eta_0)\rangle = \left(H^2\bar{\phi}'\gamma' + \frac{\partial V}{\partial\phi_0}\right)^2\left(H^2\gamma'^2 + H^2\bar{\phi}'\xi' + \frac{\partial^2 V}{\partial\phi_0^2} - \frac{\gamma^2}{e^{2\eta}}k_{1_i}k_2^i\right)\times$$
$$e^{-4\eta_0}u_{k_1}(\eta_0)u_{k_2}(\eta_0)u^*_{k_1}(\eta_0)u^*_{k_2}(\eta_0). \tag{3.51}$$

The numerical results for (3.46) and (3.51) are shown in Figures 3.17 through 3.20, where they are also compared with the bispectra we computed in the previous sections. As we can see, the two calculations differ by several orders of magnitude, and this regardless of the initial background value. The discrepancy is due to the fact that we considered a mode which was still deep inside the horizon at the initial time η_0. The formalism we adopted in this section is not able to capture possible effects appearing at horizon-crossing. This is because interpreting $\delta\phi$ as the difference in the field evolution due to different initial conditions presupposes super-horizon scales. In fact, patches of the Universe separated by a distance larger than the horizon are not in causal contact and, to a first approximation, evolve independently of each other. Hence, the fluctuation of the field across such distances can really be ascribed to different initial field values.

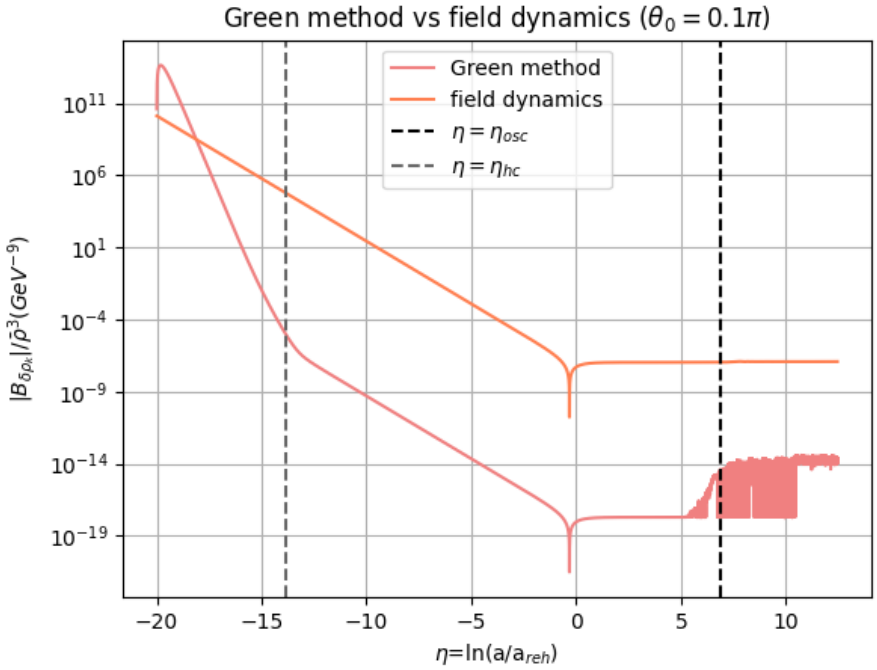

Figure 3.19: Comparison between the energy density bispectrum computed by means of the Green's function method and the bispectrum found assuming $\delta\phi$ is entirely accounted for by the difference in the field evolution brought about by different initial conditions. The bispectra were computed setting $\theta_0 = 0.1\pi$ and in the equilateral configuration.

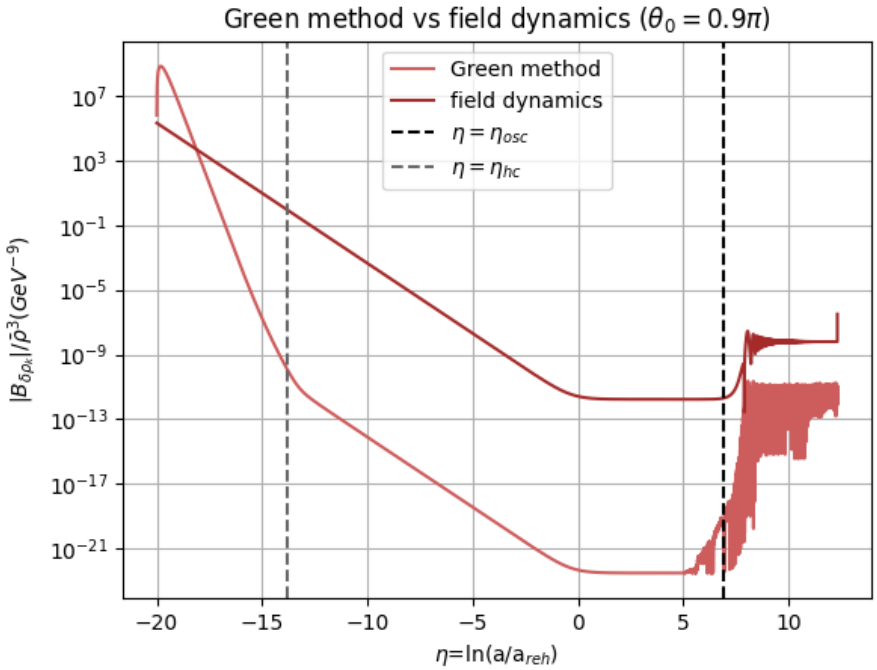

Figure 3.20: Comparison between the energy density bispectrum computed by means of the Green's function method and the bispectrum found assuming $\delta\phi$ is entirely accounted for by the difference in the field evolution brought about by different initial conditions. The bispectra were computed setting $\theta_0 = 0.9\pi$ and in the equilateral configuration.

Chapter 4

Conclusions

The aim of this thesis was twofold: to compute the bispectrum of the axion field and energy density perturbations and to investigate possible signatures that can prove the quantum nature of the correlations. The advantages of considering axions are related in particular to the second point: axions are self-interacting fields and can be produced non-thermally. Fluctuations of free quantum fields appear classical, but interactions and the associated non-Gaussianity might remove the ambiguity. Moreover, inflation squeezes the axion fluctuations, placing them in highly quantum states. Interactions with the thermal bath would erase the quantumness through decoherence but the non-thermal production mechanism and the absence of interactions with other fields might preserve the quantum features. All these properties make axions uniquely suited to our purposes.

In the first chapter, we reviewed the inflationary paradigm. After going over essential concepts from the study of the early universe, we presented the historical motivations for the introduction of inflation. An early period of quasi-exponential expansion is able to explain why the Universe looks so homogeneous and isotropic over scales that in the standard cosmological history have always lain outside the range of causal interactions. Since the Hubble radius decreases during inflation, a region the size of the observable universe today could have been causally connected at the beginning of the expansion. Moreover, inflation can account for the smallness of the curvature parameter. This observational fact is puzzling from the standpoint of the Big Bang model and requires highly fine-tuned initial conditions. In fact, unless the curvature is exactly 0, the standard evolution of the Universe unfolds in the direction of Ω_k increasingly different from 0. Instead, the dynamics of inflation is able to drive Ω_k very close to 0 from a general initial value. It is also able to dilute the energy density of any particle species present at the beginning of the expansion very efficiently. This solves a third shortcoming of the Big Bang model, the problem of unwanted relics. These are very heavy particles predicted by extensions of the Standard Model whose production in the early universe is unavoidable but at variance with observations. In fact, they would contribute to the matter and energy budget of the Universe with a density parameter much greater than one. We have also outlined how a simple scalar field can realize inflation through slow-roll dynamics. If the field is endowed with a sufficiently flat potential along which it can roll with a slowly changing velocity, it effectively behaves as a cosmological constant and can drive an accelerated expansion of the Universe. Once the slope of the potential is no longer negligible, inflation ends: the inflaton rolls toward the minimum and enters a regime of damped oscillations. At the same time, it decays into ordinary matter leaving behind a bath of relativistic particles. The last feature of inflation we reviewed is how it connects primordial density perturbations to quantum fluctuations of the inflaton field.

The second chapter was devoted to analyzing the evolution of the axion field. We considered axions from the misalignment mechanism and assumed that the Peccei-Quinn symmetry was broken before inflation. We followed the axion evolution through inflation, modeled as a de Sitter expansion, and radiation domination, assuming an instantaneous reheating. We decomposed the field into a homogeneous background and a fluctuation involving contributions up to second-order, and derived the corresponding equations of motion. These were solved numerically for different values of the initial displacement angle. The evolution of the background is determined by the competition between the

potential force $dV/d\phi$ and the Hubble friction. Since the Hubble parameter decreases in time, it dominates early on and keeps the background frozen to its initial value. After H crosses the axion mass, the potential takes over and the axion enters a regime of damped oscillations. Exactly when this happens is highly dependent on the initial background value. In particular, the onset of the oscillations is delayed approaching the potential hilltop. Moreover, initial angles closer to the maximum enhance the amplitude of the oscillations. We have also computed the evolution of the background energy density and found that it remains constant as long as the axion is overdamped, and red-shifts as a^{-3} in the oscillatory regime. The energy density is enhanced near the potential hilltop, both because the initial constant value is larger and because the dilution sets in later. In the last two sections, we turned to the evolution of axion perturbations. To study the effects of the oscillations on the perturbations, we considered modes that exit the horizon during inflation and re-enter it after the background has started oscillating. We began by quantizing the fluctuation at first order using the Bogoliubov formalism. This allowed us to express the fluctuation and its conjugate momentum in terms of time-independent ladder operators and mode functions, which encode the time evolution. We solved the equation of motion for the mode functions numerically and considered the effect of different initial background values on their evolution. We found that the behavior of the solutions only starts to differ after the background oscillations begin: the amplitude of the mode functions is constant in the sub-horizon regime and grows while the mode is super-horizon. When the background begins to oscillate, the amplitude of the mode functions also displays oscillations but we observe an additional enhancement approaching the potential hilltop. This is because near the maximum even tiny differences in the initial field value cause significant delays in the onset of the oscillations. Thus, patches of the universe with slightly different initial conditions begin to oscillate at vastly different times, sourcing large fluctuations. Finally, in the last section, we computed the perturbation at second order using the Green's function method. Going to second order in the perturbations is necessary to compute the bispectrum because the fluctuation at first order is Gaussian.

In the third chapter, we computed the bispectrum of the axion field and energy density. For both quantities, we compared the bispectrum found assuming the canonical commutation relations of quantum mechanics with the bispectrum yielded by commuting stochastic parameters a_k and $a_k^\dagger$ whose statistical properties return the same two-point function of the quantum ladder operators. This comparison was motivated by the findings in [12]. The authors show that the bispectrum of classical fluctuations must display poles in the folded configuration corresponding to physical decay processes. The absence of these poles is a signature of quantum zero-point fluctuations. Since the order of the poles is related to the number of time derivatives in the interaction Hamiltonian, this effect should not hold for the axion, whose self-interactions do not involve time derivatives. Indeed, we found that neither the field classical bispectrum nor that of the energy density are enhanced compared to the quantum bispectrum in the folded configuration. The only difference we observe is a slight enhancement of the quantum folded bispectrum during the background oscillations. Since the numerical integration is especially challenging in the oscillatory regime and no analytical results can be used for comparison, we could not determine whether the difference is genuine or an artifact of the numerical solution. We have also computed the quantum bispectrum in the equilateral and squeezed configurations and for different initial background values in the same configuration. We found that the squeezed configuration produces the largest bispectrum because it involves one mode that is much smaller than the other two. Smaller modes stay outside of the horizon for longer and the amplitude of the mode functions grows in the super-horizon regime. For the same reason, the equilateral configuration yields a larger bispectrum than the folded one: in the folded configuration, one of the three modes is larger than the other two, being their sum, so it grows less. For all three configurations, initial displacement angles closer to the maximum enhance the bispectrum. This is because near the potential hilltop the fluctuations themselves are larger. In the last section, we presented an alternative computation of the bispectrum based on an expansion of the field in powers of the initial time fluctuation $\delta\phi_0$. The idea underlying this formalism is that, since the initial conditions completely determine the evolution of ϕ, the fluctuation $\delta\phi$ measures the difference in the field evolution due to different initial conditions. We found that the bispectrum yielded by the $\delta\phi_0$ expansion does not approximate well the result of the Green's function method when the mode is initially sub-horizon. This is because the premise that $\delta\phi$

is entirely due to the field evolving from different initial conditions is a good approximation only on super-horizon scales.
In closing, we thank the reader for their interest in this work.

Not fare well,
But fare forward, voyagers.

- *The Dry Salvages*, T. S. Eliot

References

[1] N. Aghanim et al. Planck2018 results: Viii. gravitational lensing. *Astronomy & Astrophysics*, 641:A8, September 2020.

[2] Andreas Albrecht, Paul J. Steinhardt, Michael S. Turner, and Frank Wilczek. Reheating an inflationary universe. *Phys. Rev. Lett.*, 48:1437–1440, May 1982.

[3] Kenta Ando and Vincent Vennin. Bipartite temporal bell inequalities for two-mode squeezed states. *Phys. Rev. A*, 102:052213, Nov 2020.

[4] C. P. Burgess, R. Holman, and D. Hoover. Decoherence of inflationary primordial fluctuations. *Physical Review D*, 77(6), March 2008.

[5] David Campo and Renaud Parentani. Decoherence and entropy of primordial fluctuations. i. formalism and interpretation. *Physical Review D*, 78(6), September 2008.

[6] David Campo and Renaud Parentani. Decoherence and entropy of primordial fluctuations. ii. the entropy budget. *Physical Review D*, 78(6), September 2008.

[7] Aoumeur Daddi Hammou and Nicola Bartolo. Cosmic decoherence: primordial power spectra and non-Gaussianities. *JCAP*, 04:055, 2023.

[8] Valentina Danieli. *Quantum Effects in Cosmology: Unveiling the Quantum Nature of the Primordial Fluctuations*. PhD thesis, SISSA, Trieste, 2024.

[9] Valentina Danieli, Takeshi Kobayashi, Nicola Bartolo, Sabino Matarrese, and Matteo Viel. Anharmonic effects on the squeezing of axion perturbations. *Journal of Cosmology and Astroparticle Physics*, 2024(04):058, April 2024.

[10] Jessie de Kruijf and Nicola Bartolo. The effect of quantum decoherence on inflationary gravitational waves. *JCAP*, 11:041, 2024.

[11] Scott Dodelson. *Modern Cosmology*. Academic Press, Amsterdam, 2003.

[12] Daniel Green and Rafael A. Porto. Signals of a quantum universe. *Physical Review Letters*, 124(25), June 2020.

[13] Alan H. Guth. Inflationary universe: A possible solution to the horizon and flatness problems. *Phys. Rev. D*, 23:347–356, Jan 1981.

[14] Edward W. Kolb and Michael S. Turner. *The Early Universe*, volume 69. Taylor and Francis, 5 2019.

[15] Andrew Liddle. *An introduction to modern cosmology / Andrew Liddle*. Wiley, Chichester, 3. ed edition, 2015.

[16] Andrew R. Liddle and David H. Lyth. *Cosmological inflation and large-scale structure / Andrew R. Liddle, David H. Lyth*. Cambridge university press, Cambridge [etc, c2000.

[17] Fernando C. Lombardo and Diana López Nacir. Decoherence during inflation: The generation of classical inhomogeneities. *Physical Review D*, 72(6), September 2005.

[18] D. H. (David Hilary) Lyth and Andrew R. Liddle. *The primordial density perturbation : cosmology, inflation and the origin of structure*. Cambridge University Press, Cambridge, U.K. ;, 2009.

[19] David J.E. Marsh. Axion cosmology. *Physics Reports*, 643:1–79, July 2016.

[20] Jérôme Martin and Vincent Vennin. Non Gaussianities from Quantum Decoherence during Inflation. *JCAP*, 06:037, 2018.

[21] Jerome Martin and Vincent Vennin. Observational constraints on quantum decoherence during inflation. *JCAP*, 05:063, 2018.

[22] Jérôme Martin and Vincent Vennin. Bell inequalities for continuous-variable systems in generic squeezed states. *Physical Review A*, 93(6), June 2016.

[23] Jérôme Martin and Vincent Vennin. Leggett-garg inequalities for squeezed states. *Physical Review A*, 94(5), November 2016.

[24] Jérôme Martin and Vincent Vennin. Obstructions to bell cmb experiments. *Physical Review D*, 96(6), September 2017.

[25] P Martineau. On the decoherence of primordial fluctuations during inflation. *Classical and Quantum Gravity*, 24(23):5817–5834, November 2007.

[26] Michael Edward Peskin and Daniel V. Schroeder. *An Introduction to Quantum Field Theory*. Westview Press, 1995. Reading, USA: Addison-Wesley (1995) 842 p.

[27] Héctor Ramírez. Noncanonical approaches to inflation, 2019.

[28] Valery A. Rubakov and Dmitry S. Gorbunov. *Introduction to the theory of the early universe : hot Big Bang theory / Valry A. Rubakov, Dmitri S. Gorbunov*. World Scientific, New Jersey, 2. ed edition, c2018.

[29] C. A. Wuensche and T. Villela. 25 years of cosmic microwave background research at inpe, 2010.